Optimal Sizing of Stand-Alone Renewable Energy Systems for Electricity & Fresh Water Supply

Elisabeth Insam

Master of Science Thesis

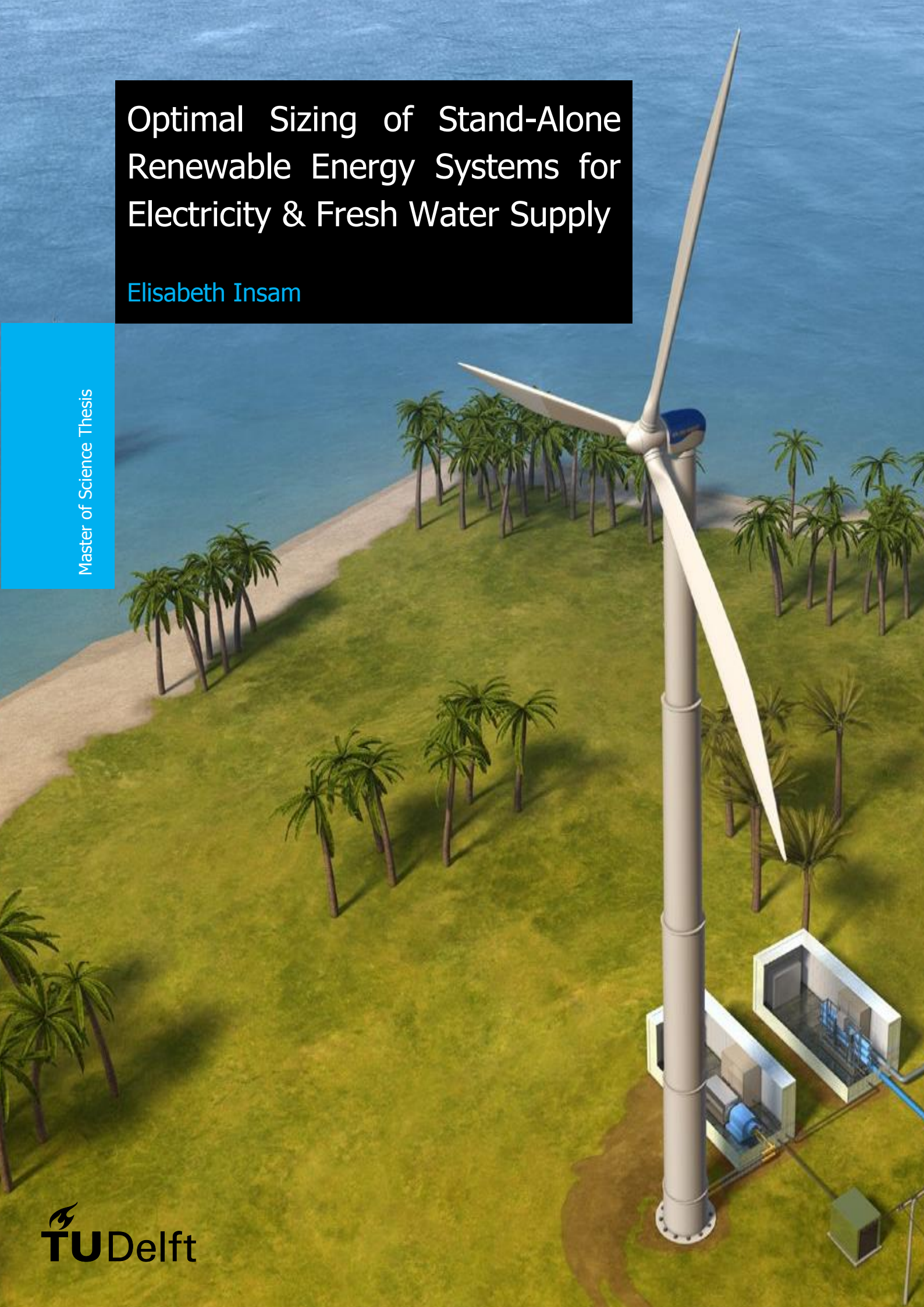

TU Delft

Optimal Sizing of Stand-Alone Renewable Energy Systems for Electricity and Fresh Water Supply

MASTER OF SCIENCE THESIS

For the degree of Master of Science in Sustainable Energy Technology (SET)

at the Delft University of Technology

Elisabeth Insam

Submitted: *16th October, 2017*
Defended: *23rd October, 2017*

Student number: 4421884

Thesis committee: Prof. dr. Peter Palensky
Dr.ir. Jose L. Rueda Torres
Dr. ir. Bas Heijman

Faculty of Electrical Engineering, Mathematics and Computer Science

Delft University of Technology

TU Delft

Acknowledgments

I would like to thank my supervisors José Luis Rueda Torres and Bas Heijman for the knowledge and guidance I have received for my Master thesis with respect to their area of expertise. The fields of modelling, optimisation and reverse osmosis were for the most part new to me and I am most contented for the skills and the know-how I have acquired and developed during this time.

I would also like to extend thanks to Herre Rost van Tonningen of *SolteQ Energy B.V.* for his input, ideas and information as well as for having me provided with the context of a real hands-on project which makes it more tangible and exciting to work on. Providing remote communities in less developed countries with both drinking water and electricity in a sustainable way have always been two topics of great interest to me. This project gave me the opportunity to combine them in my thesis and hence work on matters that I do feel strongly about.

Finally, I want to express my sincere gratitude to my family and friends for their support and encouragement, but most importantly, for putting matters into perspective when it was necessary. A special thank you shall also be given to my lovely (former) roommates and study peers who have made my stay in Holland an enjoyable and extraordinary experience full of PVT which I will always carry in my heart.

Last, but most definitely not least, 'my' mountains…What sense of elation, ease and support they have been giving me and what mighty ways they have to bring about humility as well as respect and appreciation for nature, life and our planet. So, let's please stop violating and contaminating the Earth, which is also the source of all our nourishment, and jointly embark on the journey of becoming truly sustainable and more conscious in the way we live and think.

Delft University of Technology *Elisabeth Insam*

4th October, 2017

Abstract

Remote areas throughout the world often face great difficulties with regards to a cost-effective production of electricity and drinking water. To date, it is mostly done by means of diesel generators which are however subject to volatile market prices, high operational cost, logistical supply problems and environmental concerns. Stand-alone microgrids powered by renewable energy sources have the potential to overcome these drawbacks. In this context, *SolteQ Energy* has developed the FreshWaterMill system (FWM) which can provide an isolated community with both electricity and fresh water. It involves a wind turbine with a hydraulic transmission system for water desalination via the process of reverse osmosis (RO) in addition to a generator which is placed in parallel to the RO plant. The generator is seconded by a PV system and a battery bank for electricity production. The main constraints for the implementation of renewable energy systems are the high initial cost, a problem especially faced by developing countries. However, in contrast to developed countries, their system reliability requirements for power system design are less strict which allows for more freedom in finding an optimal compromise between system cost and reliability. This trade-off approach has the potential to substantially lower the overall cost as stand-alone renewable energy systems tend to be oversized due to the fluctuating and unpredictable nature of solar and wind and the lack of controllable energy sources.

This thesis aims at optimally sizing the bespoke FWM system for specific locations by searching for a best compromise point between the conflicting objectives, cost and system reliability. For this purpose, a model of the FWM system and a suitable operation strategy has been developed and the triple-objective optimisation problem was defined which simultaneously minimises the net present cost (NPC) as well as the loss of power and water supply probability. The optimal sizing procedure is performed by means of the Pareto-based multi-objective genetic algorithm (GA) solver ‘gamultiobj’ part of the Matlab Optimisation Toolbox. The Pareto-based multi-objective method provides the system designers with numerous FWM system configurations along with the optimal size of each component allowing them to find one or more appropriate solutions from a set of alternatives based on specific requirements of the location. GA has been chosen because compared to classical optimisation techniques it is highly applicable to complex and multi-modal problems with a large search space and is able to tackle these with little computational effort. The simulations of the FWM system are run for an entire year and require the input of hourly solar radiation, wind speed, ambient temperature, electricity and fresh water demand of the location under study as well as technical and economic specifications for each component. The simulation and optimisation procedure has been applied to a real case study of a remote Colombian island in the Caribbean Sea with a yearly average wind speed of 7 m/s.

Results demonstrate that for the case study of Johnny Cay a substantial cost decrease of 26% could be achieved if the system reliability is to be reduced to 99%. Further reducing the reliability

of the FWM system no longer yields major cost gains. The lower NPC is mainly a result of considerably smaller capacity ratings of the PV system and the battery bank which decrease by 28% and 55%, respectively, for the solution presented above. For lower wind speeds, i.e. 4 m/s and 5 m/s, the cost decrease merely amounted to about 17% with respect to a system reliability of 99%. In these cases, a higher portion of PV energy throughout the year is necessary due to lower wind speeds and hence the need of a bigger battery system in order to store the increased electricity produced during the day. Furthermore, compared to the current FWM design, the use of the extended FWM design, which includes an electric drive for the RO unit, shows a meaningful cost decrease only for water supply reliabilities close to 100%. However, for lower wind speeds, especially for 4 m/s, the electric drive becomes an overall quintessential component for all reliability values. Finally, results were compared for different reliability indices showing that a deliberate choice with respect to a suitable index is of high importance and that each reliability index has its shortcomings. Hence, in order to gain extensive information regarding the number, magnitude and type of outages, a comparison of the individual results is highly advisable.

Table of Contents

Acronyms

ACS…annualised cost of system

BWRO…Brackish water reverse osmosis

CST…Concentrated solar thermal

DC…direct current

DOD…depth of discharge

ED…Electrodialysis

FWM…FreshWaterMill

GA…genetic algorithm

HPP…High-pressure pump

IDA…International Desalination Association

LCE…levelised cost of energy

LLP …loss of load probability

LPSP…loss of power supply probability

LWSP…loss of water supply probability

MED…Multi-effect distillation

MPPT…Maximum Power Point Tracking

MSF…Multi-stage flash

MVC…Mechanical vapour compression

NOCT…Nominal Operating Cell Temperature

NPV…Net Present Value

NSGA… Non-dominated Sorting Genetic Algorithm

Psi…pounds per square inch

PSO…Particle Swarm Optimisation

PV…photovoltaics

RES…Renewable energy sources

RE…Renewable energies

RO…Reverse osmosis

SEC…Specific energy consumption

SOC…State of charge

STC…Standard Test Conditions

SWRO…Seawater reverse osmosis

TVC…Thermal vapour compression

VC…Vapour compression

VSD…Variable speed drive

WHO…World Health Organization

List of figures

List of tables

Nomenclature

$\Delta\pi$	Osmotic pressure differential across the membrane [bar]
ΔC	Salt concentration differential across the membrane [g/m^3]
ΔP	Hydraulic pressure differential across the membrane [bar]
η_{bat}	Round-trip efficiency of battery bank [-]
η_{ch}	Efficiency of the charge controller [-]
η_{EM}	Efficiency of electric motor [-]
η_{gen}	Total efficiency of generator unit [-]
η_{HM}	Efficiency of hydraulic motor [-]
η_{HPP}	Efficiency of high-pressure pump [-]
η_{inv}	Inverter efficiency [-]
a_i	Component-specific annuity [-]
a_{tot}	Annuity factor of FWM system lifetime [-]
c_p	Salt concentration of the membrane [g/m^3]
C_{bat}^{nom}	Nominal capacity of each battery [Ah]
C_{bb}^{min}	Minimum allowed battery bank's capacity level [Ah]
C_{bb}^{nom}	Nominal capacity of battery bank [Ah]
$C_{bb,soc}$	Battery bank's capacity level [Ah]
C_i	Capital costs of component i [€]
DOD	Depth of discharge [-]
FF	Fill factor [-]
G	Global solar radiation [W/m^2]
h_{ref}	Reference height [m]
I_{ch}^{max}	Charge controller's maximum input current [A]

I_{sc}	PV module's short circuit current [A]
I_{sc}^{STC}	PV module's short circuit current at STC [A]
K_V	Open-circuit voltage temperature coefficient [V/°C]
K_I	Short circuit temperature coefficient [A/°C]
L_i	Lifetime of component i [-]
$LPSP_{sev}$	Loss of power supply probability including severity factor [-]
$LWSP_{sev}$	Loss of power supply probability including severity factor [-]
m_i	Maintenance costs as percentage of capital costs of component i [-]
NDP	Net driving pressure [bar]
NPC_i	Net present cost of component i [€]
$NOCT$	Nominal Operating Cell Temperature [°C]
N_{bat}	Total number of batteries [-]
N_{bat}^{p}	Number of batteries connected in parallel [-]
N_{bat}^{s}	Number of batteries connected in series [-]
N_{ch}	Number of charge controllers [-]
N_{pv}	Total number of PV modules [-]
N_{pv}^{max}	Maximum allowed number of PV panels [-]
N_{pv}^{p}	Number of PV modules connected in parallel [-]
N_{pv}^{s}	Number of PV modules connected in series [-]
N_{RO}	Number of RO vessels [-]
P_c	Concentrate pressure [bar]
P_f	Feed pressure [bar]
P_p	Permeate pressure [bar]
$P_{bb,flow}$	Battery bank's power flow [W]
P_{demand}	AC power output from inverter [W]

P_{demand}^{avg}	Average yearly electricity demand [W]
P_{EM}	Power output from electric motor [W]
P_{EM}^{nom}	Nominal power of electric motor [W]
P_{gen}	Power output from generator [W]
P_{gen}^{nom}	Nominal power of generator [W]
P_{HM}	Power output from hydraulic motor [W]
P_{HM}^{nom}	Nominal power of hydraulic motor [W]
P_{HPP}	Power input into high-pressure pump [W]
P_{load}	DC power input into inverter [W]
Pm_{unit}	Power output of each power unit [W]
Ppv_{tot}	Total PV power output [W]
Ppv_{unit}	Charge controller's power output of each power unit [W]
P_{RO}	Power output of high-pressure pump [W]
P_{RO}^{min}	Total minimum power requirement of RO plant [W]
P_{RO}^{max}	Total maximum power requirement of RO plant [W]
$P_{RO,unit}^{max}$	Minimum power requirement of RO unit [W]
$P_{RO,unit}^{min}$	Maximum power requirement of RO unit [W]
P_{supply}	Available power from wind generator, PV system and battery [W]
$Pwind$	Wind power output [W]
$Pwind_{el}$	Wind power for electricity generation [W]
$Pwind_{w}$	Wind power for water production [W]
Q_c	Concentrate flow [m^3/h]
Q_f	Feed flow [m^3/h]
Q_p	Permeate flow [m^3/h]
Q_s	Salt flow [m^3/h]

R	Recovery factor [-]
r	Discount rate [-]
S	Membrane surface area [m^2]
sf_{el}	Severity factor for electricity outage [-]
sf_w	Severity factor for fresh water outage [-]
T_a	Ambient temperature [°C]
T_c	Cell temperature [°C]
TMP	Transmembrane pressure [bar]
v	Wind speed [m/s]
v_{cut-in}	Cut-in wind speed [m/s]
$v_{cut-out}$	Cut-out wind speed [m/s]
v_{ref}	Reference wind speed [m/s]
V_{bat}	Nominal battery voltage [V]
V_{bus}	Nominal bus voltage [V]
V_{ch}^{max}	Charge controller's maximum input voltage [V]
V_{oc}	PV module's open-circuit voltage [V]
V_{oc}^{STC}	PV module's open-circuit voltage at STC [V]
W_{demand}	Water demand [m^3]
w_{el}	Electricity demand priority weighting factor [-]
W_{RO}	Total fresh water production [m^3]
$W_{RO,unit}$	Fresh water production volume of one RO unit [m^3]
W_{SOC}	Water tank volume [m^3]
W_{SOC}^{min}	Minimum water tank volume [m^3]
W_{SOC}^{max}	Maximum water tank volume [m^3]
W_{tank}	Fresh water tank volume [m^3]
w_w	Water demand priority weighting factor [-]

Y_i	Number of replacements of component i [-]
z_0	Surface roughness[m]

1

Introduction

The first chapter aims at defining the main motivation and the underlying problem presented in this thesis. On this basis, the objectives and research questions are formulated followed by an overview of the proposed methodology including the structure of the thesis and the content of each chapter are addressed.

1.1 Background and motivation

The world's rapid economic development in the past decades as well as the rising water scarcity and the decrease in ground water reservoirs largely drive the growing demand in electricity and clean water. These two elements are pivotal for every human being in order to ensure good living standards and sustainable economic growth for the society. Water is an abundant natural resource that covers three quarters of the earth's surface. However, less than 3% of it can be regarded as drinking water of which 2.5% is locked up in the Arctic and in glaciers in the form of ice [1]. About a quarter of the world's population does not have access to a satisfactory quality and/or quantity of drinking water [1]. In fact, in some remote areas around the world, people are used to drinking slightly brackish water which has damaging effects on the digestive tract and skin [2]. Worldwide drought and desertification, inter alia due to the impacts of climate change, are expected to sharpen the problem in the near future especially in semi-arid and costal as well as island areas. According to the Worldwatch Institute, two thirds of the world's population is anticipated to encounter some sort of water scarcity by 2025 [3].

About 40% of the world's population lives at a distance of less than 100 km from the sea which makes water desalination an applicable technology [4]. Desalination is commonly defined as the process of removing dissolved salts from saline or brackish water in order to make it usable for human consumption for domestic, agricultural and industrial purposes. Many water-stressed areas are expanding their supply with desalinated water in order to meet the growing demand [5].

In numerous arid or semi-arid regions as it is the case in the Middle East and North Africa (MENA) region or the Caribbean islands, conventional water supply alternatives are not or scarcely available. Here, the process of desalination has become one of the most significant sources for drinking water [6]. Qatar and Kuwait, for instance, already fully rely on desalinated water for domestic as well as industrial use, making desalination no longer a marginal or supplemental water resource [4].

Water desalination is an energy intensive process and as a result the energy consumption represents a significant cost in the economics. The primary energy source for driving desalination plants are conventional fossil fuels. However, recent environmental concerns regarding greenhouse gas emissions and the associated global warming have fostered the utilization of cleaner energy supplies. Renewable energy resources are ubiquitous and present a huge potential for achieving diversity in energy production technologies as well as seconding the transformation towards clean energy sources and thus balancing the use of fossil fuels associated with the reduction of emissions. While desalination is still expensive, renewable energy technology deployment costs are expected to lower in the near future [6]. This is of particular interest to remote arid regions and islands with small populations and poor infrastructure for fresh water and electricity transmission and distribution. These regions are often vested with high renewable energy potential thus making these resources a suitable energy supply alternative for the local and sustainable generation of electricity and the production of drinking water in areas near waterbodies such as lakes, estuaries or coastal areas [7].

1.2 Problem definition

In many areas in the world the connection to the main electricity grid is not readily feasible due to their remoteness and scarce population. Expanding the grid a long way into far-off and rural regions in order to power desalination plants and to provide a community with electricity is usually associated with high costs. Stand-alone diesel generator sets are the incumbent technology to date in order to produce electricity in isolated communities. These systems fully rely on diesel, a fuel which is subject to volatile market prices, logistical supply problems and environmental concerns [2]. Autonomous water desalination and electricity generation systems driven by renewable energy sources have the potential to overcome the drawbacks that diesel generators have. In this context, small isolated communities such as islands represent unique challenges as the majority is almost exclusively dependent on fossil fuels and the high costs of electricity production they face gives them incentives to look for alternatives. Many locations worldwide feature an abundant potential of renewable energies and as a matter of fact, fresh water scarcity co-exists in most cases with ample occurrence of renewables, especially solar energy [8]. Generally, the individual use of wind or solar energy can lead to substantial oversizing due to the fluctuating nature of these sources, thus increasing the operating and life cycle costs [9]. For this reason, integrated hybrid systems comprising more than one renewable energy source and/or

batteries can be more reliable and cost-efficient. Indeed, in many regions wind and solar energy have a countervailing effect making them suitable for being used in a hybrid energy system.

In this context, *SolteQ Energy B.V.* has developed the *FreshWaterMill* (FWM), a stand-alone system which is capable of providing a remote community with both fresh water and electricity, produced exclusively by renewable energies. This new, innovative concept is based on a hydraulic windmill that converts wind energy into high pressure which is used as prime energy for a RO water purification system. The FWM concept uses the two-bladed Lagerwey 18/80 wind turbine with a nominal rating of 80 kW. However, according to *SolteQ Energy B.V.*, by employing a hydraulic transmission system rather than a more typical electromechanical one, the wind turbine can reach up to about 100 kW as the losses in the gear and the generator can be eliminated. In order to produce electricity, a hydraulic generator is placed in parallel to the RO system which is assisted by a PV system and a battery bank. With the current design of the FWM system, the RO unit can only be powered by wind energy. However, an extended version is intended to be developed in which electricity from the PV array or the battery bank can assist with the production of fresh water via an electric motor.

One of the drawbacks of some renewable energy sources is their intermittency paired with low predictability. Also, the variations of solar and wind energy may not match with the time distribution of the load demand. As a result, stand-alone power systems such as the FWM system, which are based on wind and solar technologies and do not include controllable sources, face a greater design challenge than other conventional energy sources, which can operate continuously. As more components and supplies are involved in such plants, the optimal sizing of the sub-systems such as wind turbine, PV array, battery bank, RO unit is no longer a simple task due to the amount of design variables and their interdependency. Moreover, the fact that two different loads, i.e. water as well as electricity demand, are covered at the same time within one system, adds a further degree of complexity. In this case, manual trial-and-error techniques considering the fluctuating nature of renewable energies can be cumbersome. Computer programs and optimization algorithms are then required in order to search for the optimal solution within a sensible timeframe.

As no controllable energy source is used in stand-alone renewable energy systems such as the FWM and due to the fluctuating character of solar radiation and wind speed which highly influence the resulting energy production, power reliability analysis is regarded as an essential step in any system design process. A stand-alone power system is considered to be reliable if it has sufficient power to meet the load during a certain time period. Different methods and indices exist in order to assess the reliability of the power system.

In contrast to diesel generator sets for which the operational costs are high compared to the capital costs, renewable based generation systems show increased initial costs combined with low running costs. Suitable sizing of the renewable energy microgrid highly influences the up-front

system cost and is thus pivotal. In addition, designing stand-alone systems for 100% power and water supply reliability can result in exceedingly high system costs as under such criteria even short duration peak demands must be met although the likelihood for them to occur is rare. In many parts of the world, as it is the case for less developed countries, this is not always the most cost-efficient approach because their main limitation is the lack of financial resources and hence the reliability requirements of power systems is less strict than in developed countries [10]. Hence, finding an optimal trade-off between system costs and reliability can further promote the use of renewable energies for electricity generation and fresh water production in less developed and off-grid areas.

1.3 Objectives and research questions

The main objective of this thesis is to find the optimal size of the FWM system components in order to satisfy the requirements for a specific fresh water and electricity load distribution assumed to be installed at the selected location. The optimal sizing procedure is based on a trade-off between cost and system reliability, an approach that is assumed to considerably lower the overall cost of the FWM system, especially for less developed countries. It should be noted at this point that the system reliability only refers to outages incurred by insufficient power supply by the renewable energy sources and the storage systems; it does not include outages due to a failure of the system components or maintenance activities.

In order to reach this objective, a model of the FWM system is first created in Matlab. Also, a suitable operation strategy needs to be developed in order to achieve the optimal combined output since fresh water and electricity are produced within the same system and hence their controls are interdependent. The model of the FWM system is the basis of the simulation and optimal sizing procedure. Following the model set-up and the optimisation problem formulation, a number of cost-efficient FWM system configurations and the optimal size of each sub-system can be calculated for any given location with the input of real climate and load data as well as technical and economic specifications of the chosen components. The thesis does not aim at a detailed analysis on smart power control; it rather focuses on results on a system level by looking into the technical and economic potential of the innovative FWM system which this study is based on. The small Colombian island of Johnny Cay, which is part of the archipelago of San Andrés, has been selected as a case study since interest was recently expressed by governmental authorities to implement a sustainable island project [11].

Based on the problem definition and the objectives posed in the framework of this thesis the following main and sub-research questions are explored:

How can the stand-alone FWM system be optimally designed and sized in order to substantially reduce its overall costs and still maintain a high system reliability in terms of fresh water and electricity supply?

- What is an appropriate metric for assessing the FWM system reliability in terms of fresh water and electricity supply?
- What type of format of the optimisation problem is suitable and which of the existing optimisation solvers are attractive to tackle the computational complexities?
- How do cost and configurations of the FWM system vary with decreasing power system reliability and what insights can be gained from it?
- Does the FWM system benefit from the addition of an electric drive which assists with the production of fresh water?

1.4 Thesis methodology and outline

An overview of the proposed thesis methodology and the individual steps are illustrated in Figure 1. The positioning of this thesis with respect to the relevant literature and its gaps is explained in section 3.3 at the end of the literature review.

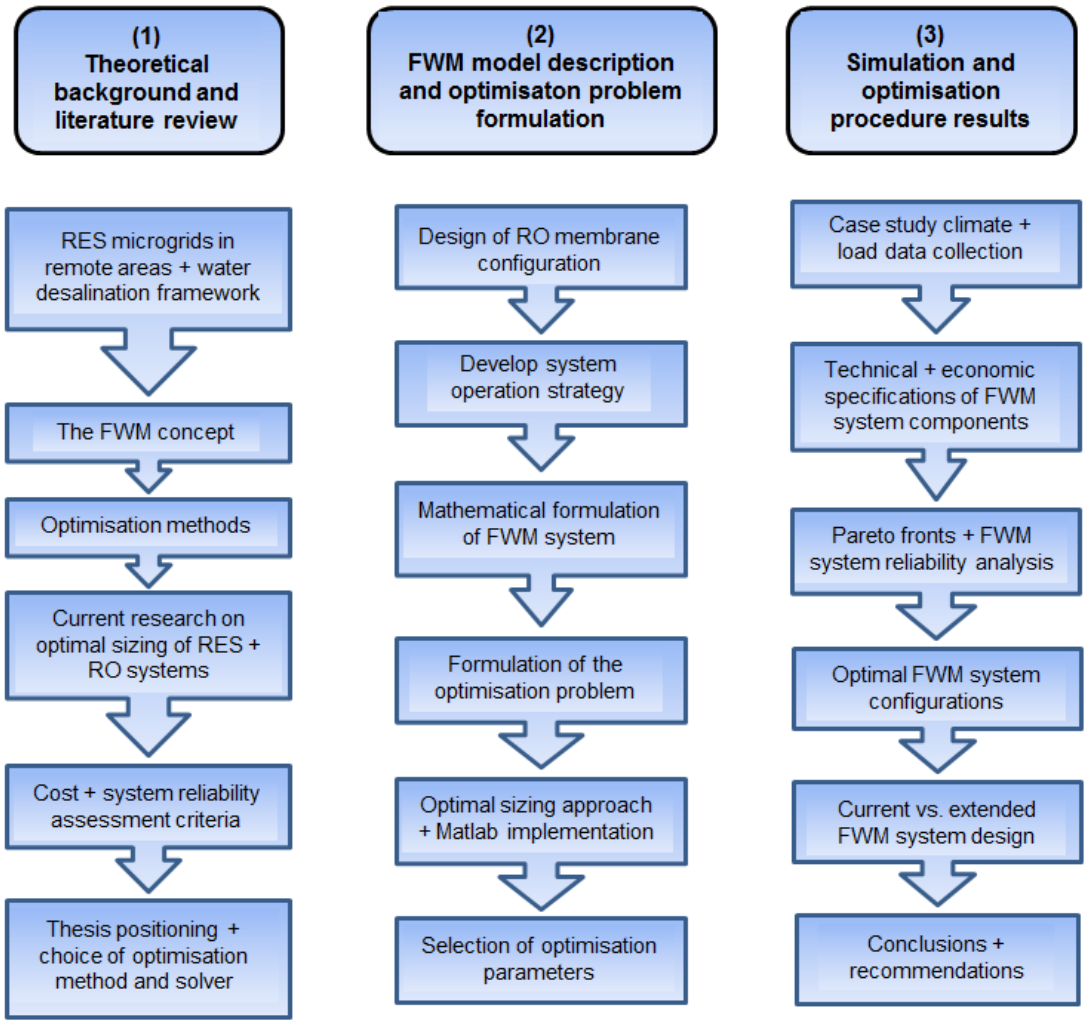

Figure 1. Proposed thesis methodology.

The thesis is divided into eight chapters which aim at answering the research questions step-by-step.

In chapter 1 the motivation for the thesis has been explained and appropriate objectives and research questions were deduced followed by an overview of the proposed thesis approach.

Chapter 2 provides background information on stand-alone renewable energy microgrids including major design challenges and storage technologies. Next, the context of water desalination is addressed by giving an overview of different desalination methods, their energy consumption and cost. The main focus is set on the RO process which is explained in more detail. Lastly, the innovative *FreshWaterMill* system, which is the basis of this study, is discussed.

In chapter 3 an overview of optimisation techniques is given followed by a literature study which reviews different optimisation algorithms and procedures employed to date for the design and sizing of small-scale stand-alone water purification and electricity generation systems in remote areas. Also, the most important economic and technical assessment criteria of stand-alone RES-based microgrids are introduced and explained. Finally, the positioning and contribution of this thesis with respect to prior art is discussed and the selection of the optimisation algorithm and solver is explained.

Chapter 4 describes the modelling of the FWM system. First, the extended and further improved configuration of the hybrid FWM system is discussed. Next, the design of the RO unit which is the basis of the optimal sizing procedure is envisaged. Consequently, all components of the microgrid are modelled and integrated into one system. As a last step, the proposed operation strategy is introduced where the interaction between the different sub-systems can be viewed.

Chapter 5 aims at providing an overview of the optimisation framework. First, the optimisation problem is set up for which the decision variables and constraints are identified and suitable objective functions are chosen. Second, the chosen optimisation algorithm is explained in detail and an overview of the simulation and optimisation procedure is given.

In Chapter 6 background information of the chosen case study location is given and the simulation parameters such as load profiles, climatic conditions and costs, lifetime and technical specification of the components are envisaged.

Chapter 7 presents the optimal sizing results obtained through simulations carried along a complete year. The Pareto fronts are presented and the optimal system configurations are analysed based on different reliabilities. Consequently, a sensitivity analysis with respect to different wind speeds is conducted. Next, a comparison is made between the current and future design of the FWM system for different average wind speeds and ultimately the main findings of the research are discussed. The model is explored for a real case study of a remote island community in the Caribbean Sea.

Chapter 8 draws conclusions based on the previous chapters and gives suggestions for further research.

Two main software packages are used in the framework of this thesis. For the development of the simulation-based optimisation model the Global Optimization Toolbox within the Matlab environment (Matlab version 2016b) is employed. With regards to the design of the RO membrane configuration, the latest version, ROSA 9.1 (Reverse Osmosis System Analysis) design software by DOW is used. It is a sophisticated RO design program that predicts the performance of membranes in user-specified systems. Furthermore, in order to retrieve the climate data for the case study, Meteonorm software is consulted which has access to a database of meteorological data from all sites around the world.

2

Theoretical background

In this chapter, the reader is provided with essential background information regarding microgrids and water purification technologies and systems. Firstly, the application purpose of stand-alone power systems and their development is explained which is followed by an overview of the most common microgrid configurations using renewable energy sources. In this framework, the main shortcomings related to such systems are also addressed. The second part makes the reader acquainted with the topic of water desalination and water quality. It introduces the technologies used for producing drinking water, the respective energy consumption, cost and system configuration based on renewable energy sources. The focus is primarily set on the reverse osmosis technique which is explained more thoroughly in section 2.3. Lastly, a new concept for electricity generation and fresh water production in off-grid areas, the *FreshWaterMill* system, is described which is the basis of the simulation and optimal sizing procedure in the following chapters.

2.1 Microgrids in remote areas

In most places of the world, electricity is supplied by national grids which usually extend throughout the whole country as well as being interconnected with cross-border regions. In remote and rural places however, the traditional approach of serving communities through a centralised grid system is not always feasible due to a combination of lack of financial resources, insufficient energy service, reduced grid reliability, extended building times and construction challenges to connect far-off regions. As a result, autonomous microgrids are often built in these areas which generate power locally and serve a relatively small number of customers who are interconnected via a shared distribution system. The term ‘microgrid’ is not universally defined which is why ‘minigrids’, ‘nanogrids’ or ‘picogrids’ are often used interchangeably in literature [12]. According to the grid categorisation proposed by IRENA in 2015, microgrids are in the capacity range of 5-100 kW [13].

Stand-alone energy systems are designed for the generation of electricity using a single power source or a number of power generation devices such as photovoltaics, wind turbines, micro hydro, biomass gasifiers and conventional fossil fuel generators. The capacity can range from providing a single household with electricity to large microgrids which power an entire village or island. To date, many islands still rely on diesel or gasoline generator sets for their electricity production and thus have to spend a substantial amount of their gross domestic product on the import of fuels [13]. Also, diesel fuel is subject to volatile market prices as well as logistical supply problems for remote regions and its use creates dependency. In recent years, the development of local power generation systems based on renewable energies has drastically increased due to a constant reduction in cost regarding sustainable energy technologies, especially PV and wind, lower operational cost compared to conventional power systems and environmental concerns regarding the use of fossil fuels [14]. In addition, remote regions are often vested with high renewable energy potential thus making these resources a suitable energy supply alternative for the local and sustainable generation of electricity [7]. Some renewable energy sources like wind and solar are however characterised by intermittency and unpredictability. The stochastic behaviour of solar and wind energy may not match with the time distribution of load demand making them unreliable for off-grid applications. Especially the independent use of these energy sources reveal low reliability and consequently these power systems tend to be oversized leading to an increase in capital costs [15]. As a result, storage, intelligent control and/or conventional back-up systems like diesel generators are often required. Another approach which can substantially decrease the need for storage or back-up systems is the combination of different renewable energy sources that are capable to counter-balance each other. The integration of solar and wind energy, which in many locations display complementary characteristics, has proven to be a particularly successful and cost-efficient option for the supply of electricity to remote sites like islands where no central grid is available. On the other hand, systems running on biomass energy are suitable for forest regions whereas micro hydro power is often employed in remote hilly sites and integrated with other renewable technologies into hybrid microgrids [16]. Although the integrated use of different renewable energy sources which complement each other minimises storage requirements and increases power supply reliability, in the majority of cases stand-alone microgrids do still require some sort of storage device in order to smoothen the mismatch between power generation and demand [14]. Figure 2 illustrates a basic autonomous hybrid solar-wind system consisting of wind and solar energy generators, a controller, an inverter and a battery bank.

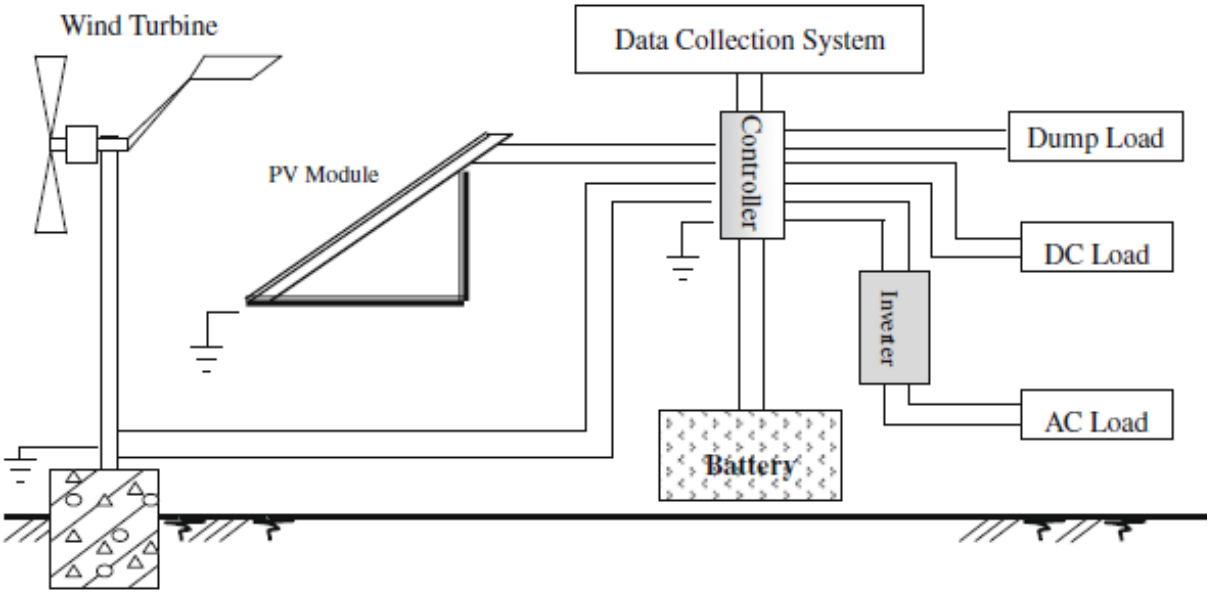

Figure 2. Stand-alone hybrid renewable energy micro grid [15]**.**

The PV panels and the wind turbine are combined and integrated in a power system in order to satisfy load demand. The wind turbines as well as the PV array are often connected to a common DC bus through a regulator in order to match it with the required DC bus voltage of the installed battery bank. DC as well as AC loads can be accommodated in such systems with the use of proper power conversion devices [15]. The storage systems are connected to the renewable technologies using suitable power electronics circuits that control the flow of energy into and out of the storage system. The control system is the central part of stand-alone microgrids as it enables communication between the different components. It administers the energy output of the various sources, transmits the required amount of energy to the sinks and regulates the operation of the storage system in due form including protection from overcharging and deep discharging [16].

Storage technologies help in peak shaving and levelling out load fluctuations to achieve an efficient energy management. During peak power demand when more energy than the base generation is required, storage devices supply the surplus whereas in times where demand is low these devices are charged for later use. Figure 3 provides a typical generation and load profile demonstrating the positive impact storage systems can have on autonomous energy generation systems. It clearly shows that in case no storage system is used, the power generators need to be sized in a way to accommodate peak load resulting in a capacity that is only proper for a limited amount of hours per day whereas for the remaining time frame the system is substantially oversized.

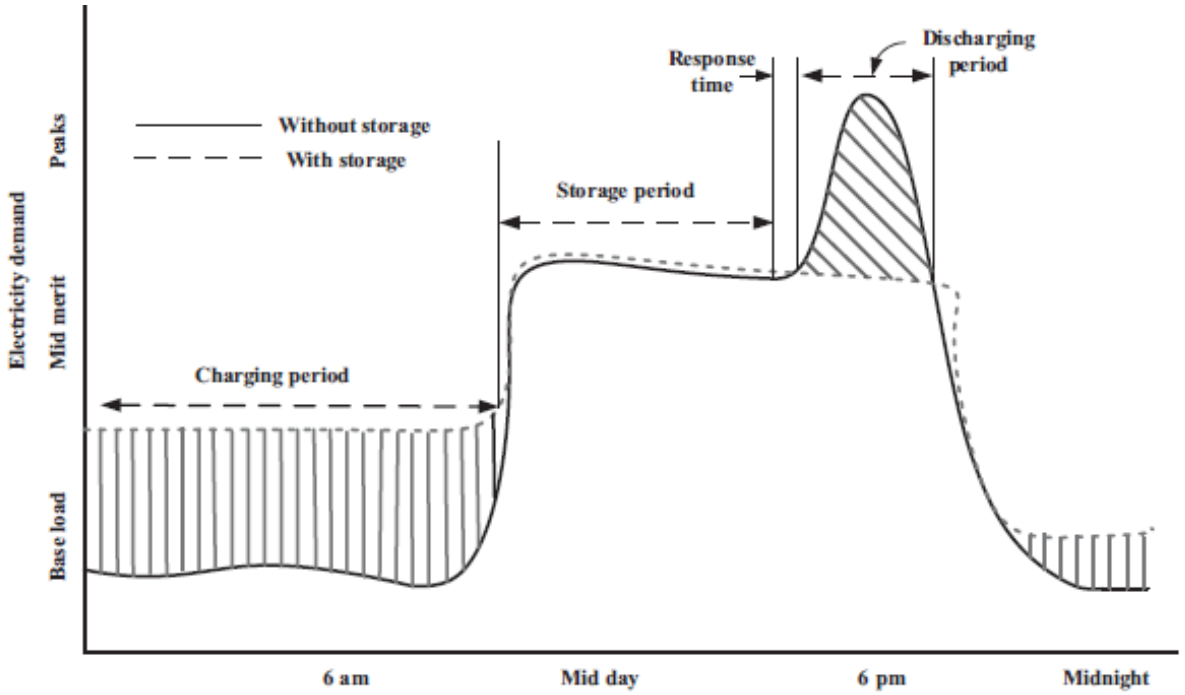

Figure 3. Energy generation management for stand-alone microgrids with energy storage [16]**.**

To date, a great variety of energy storage technologies aimed at particular areas of application is available. Depending on the duration of their storage capabilities, storage technologies can be divided into short-term, medium-term and long-term. Short-term storage devices include (super-) capacitors and flywheels. For a medium time frame, fuel cells, hydrogen storage, compressed air energy storage and batteries are mostly used while for long-term storage pumped hydro storage is employed. When compared to other storage systems, batteries are the most flexible, responsive and reliable ones. They can react within 20 ms in order to respond to generation and load changes making them highly suitable for autonomous electricity generation systems [16]. Many different types of batteries are used today such as lead-acid, nickel-cadmium, vanadium redox or lithium ion. Each type is characterised by a certain number of life cycles, reliability, depth of discharge, energy density and cost which is why a choice for a certain type should be carefully made based on the necessities and applications. Stationary batteries are almost always of the lead-acid type. Lead-acid batteries are well-proven technologies as they have been around for a long time, display high reliability, low self-discharge, low cost and low maintenance making them suitable for applications in remote and developing regions. However, this type of batteries are of low energy density, are characterised by limited cycle life in addition to being sensitive to deep discharge. Low energy density does not present a major limitation since space restrictions rarely exist in remote places. Also, the limited cycle count does not pose a major problem because the batteries are seldom deep discharged when used in autonomous renewable power systems. Lead-acid batteries should nevertheless be replaced every 2-3 years and a proper control strategy should be in place to avoid deep discharge [17].

In contrast to diesel generator systems, microgrids based on renewable energy technologies show higher up-front cost combined with low running costs as the fuel does not have to be purchased. The high initial cost is a major drawback of renewable-based power systems since financial resources are scarcely available, especially in less developed countries. Because the design of stand-alone renewable energy systems highly influences the cost, suitable sizing and optimisation of its components and the system as a whole is pivotal. Numerous components and supplies are involved in such power plants and thus the sizing and control of the sub-systems like wind turbine, PV array and battery bank is no longer a simple task due to the amount of design variables and their interdependency. In chapter 3 a literature review is performed and different optimisation methods and approaches for this purpose are discussed.

2.2 Water desalination framework

Water consumption and water quality

Water need has increased drastically in the past years due to population growth, increase of per capita water demand, industrial expansion, tourism, agricultural development and contamination of existing water resources which has led to severe water shortage problems [4]. To date, according to the United Nations World Water Development Report, 8% of fresh water supply is used for domestic, 22% for industrial and 70% for agricultural purposes on a global scale [18]. These numbers certainly diverge when developed and less developed countries are compared since generally the latter strongly rely on agriculture whereas the former show higher domestic as well as industrial water consumption. To put it into context, an average person in the U.S. consumes close to 600 litres of fresh water a day, whereas in Kenya, daily water use amounts to about 50 litres with rural and remote areas consuming yet less [18]. As a matter of fact, most of the available water resources on Earth, i.e. more than 99%, cannot be used for domestic, industrial or agricultural purposes due to high salinity levels or because it is trapped in the form of ice on glaciers or in the Arctic [1]. For this reason, the water industry has become increasingly reliant upon water desalination, a process which involves separating dissolved salts and other minerals from the water source in order to turn it into fresh water. The International Desalination Association (IDA) reported that in 2015 more than 18 000 desalination plants existed worldwide with a global capacity of 86.8 million m^3 a day [19]. The number represents about 0.6% of the global water supply, of which the MENA region, being very arid, possess close to 40% of the total installed capacity. In this region, a big number of large desalination plants can be found which produce 800.000 m^3 a day and more [6].

The chemical quality of water is usually expressed as total dissolved solids (TDS) in part per million (ppm) or its equivalent milligrams per litre (mg/L). TDS comprise inorganic salts such as calcium, magnesium or chlorides and small amounts of organic matter that are dissolved in water. Different purposes require different water quality standards. Irrigation for instance, should not use water which exceeds 2 000 ppm of TDS, whereas drinking water requires a concentration lower

than 1 000 ppm in order to be considered potable. However, the World Health Organisation strongly suggests drinking water to hold no more than 500 ppm of TDS [20]. Brackish water, usually from underground, lies in the range of 1 000 ppm to 10 000 ppm whereas it is termed salty water when the concentration exceeds 10 000 ppm. Finally, seawater is characterised by its concentration being between 30 000 to 45 000 ppm. Typical seawater as it is found in most oceans amounts to about 35 000 ppm while concentrations of 45 000 ppm are measured in the region of the Arabian Gulf [21].

Desalination methods and energy requirements

There are two broad categories of desalination technologies which can be classified as membrane-based using electricity or heat-based using thermal energy and electricity. The water streams are similar for all desalination methods: feed water in the form of brackish or seawater taken from waterbodies such as the ocean or in the form of wastewater, is used as water source for the desalination plant. Once the specific purification process has been applied, the feed water is turned into product water (also called permeate or fresh water) and concentrate (also called brine or reject water) with the latter featuring a high level of salinity. Thermal desalination methods mimic the natural water cycle by producing water vapour through the usage of heat which is then condensed to form fresh water. The three major types of thermal desalination are multi-stage flash distillation (MSF), multi-effect distillation (MED) and vapour compression distillation (VC). Thermal technologies are mostly used by countries rich in oil where the prices of thermal energy are very low. These methods predominantly treat highly saline waters and are built to obtain large volumes of product water. Membrane technologies on the other hand, do not involve phase changes; they only need electricity or shaft power in order to produce high pressures which isolate fresh water from salty water by making use of a membrane that is only permeable to water. The most common processes for membrane-based methods are RO and electrodialysis (ED). Regions lacking domestic fossil fuels are more prone to using membrane-based desalination plants which are powered by electricity and require less energy and lower flow rates. RO can be used for the desalination of brackish waters (BWRO) as well as seawater (SWRO) whereas ED is mostly employed for low saline waters. To date, in terms of total installed desalination capacity, RO is the incumbent technology which accounts for 60%, followed by multi-stage flash (MSF) with a share of about 27% [6].

Desalination plants are highly energy intensive and thus the energy consumption is a major driving factor for the economic feasibility. Energy requirement in the form of thermal as well as electrical energy can make up between 50% and 70% of the total operating cost [22]. As a consequence, a multitude of large-scale water purification plants are situated close to power stations or industries with thermal process energy waste. The typical specific energy consumption (SEC) for seawater desalination using heat as their main source is in the order of 7-14 kWh/m^3 compared to 3-8 kWh/m^3 for membrane-based technologies. However, numbers can differ

substantially dependent on the plant capacity, among others. Specific energy consumption may exceed 15 kWh/m^3 for very small sizes units [23]. As far as water purification via the RO process is concerned, desalinating brackish water requires considerably less energy compared to seawater as it is already of higher purity in the first place. Table 1 illustrates representative SECs for the major water purification technologies. The energy requirements are separated into thermal energy which is used to heat the seawater and electricity which is used to drive pumps, compressors and auxiliary equipment.

Table 1. Specific energy consumption for the major water desalination techniques [24].

Technology	Thermal energy consumption [kWh/m³]	Electrical energy consumption [kWh/m³]	Total energy consumption [kWh/m³]
MSF	7-10	3-5	10-15
MED	4.5-6.5	2.5-3	7-9.5
VC	N/A	8-15	8-15
BWRO	N/A	1-4	1-4
SWRO	N/A	3-9	3-9
ED	N/A	1.5-4	1.5-4

The RO process is momentarily the technology that requires the least amount of energy, especially when energy recovery devices are employed. Energy recovery devices make use of the energy contained in the reject water exiting the RO modules at high pressures which are only slightly below those of the feed water. This pressure energy, amounting to about two thirds of the total hydraulic power originally supplied by the HPP, can be recovered and returned to the shaft of the main pump resulting in substantial energy savings [25]. Although the energy usage for RO processes are lower compared to thermal methods it still represents the greatest share in operational costs as brackish or salty water has to be pumped through the membranes with pressures up to 80 bar.

Renewable energy technologies for water desalination

As discussed in the previous section, desalination plants are mainly powered by fossil fuels which produce the required thermal and/or electrical energy. In recent years, however, the usage of renewable energy technologies has experienced a rapid growth, mainly due to environmental reasons, decreasing costs of RES technologies and dependency on oil imports and the volatile market prices thereof. Nevertheless, as of now, the global overall capacity of sustainable desalination plants accounts for less than 1% of the total installation capacity [6]. Renewable energies can be highly suitable for powering desalination plants if the location allows for it. The renewable energy technologies mostly employed so far include concentrated solar thermal (CST), PV energy, wind energy and geothermal energy. The feasibility of each technology is specific to

the location in question and depends upon available renewable energy sources, desalination method, energy price, water quality, costs of land and labour as wells as taxes and permits, plant capacity, brine disposal and technical resources of the area [2]. In arid regions, for instance, such as the MENA region with high insolation levels, solar energy in the form of CST for thermal desalination as well as PV or CST for membrane desalination offers great potential. For coastal and island communities, on the other hand, wind energy coupled with membrane-based techniques is of great interest [6]. Figure 4 presents an overview of the possible technological combinations of different RES coupled with the most common desalination methods.

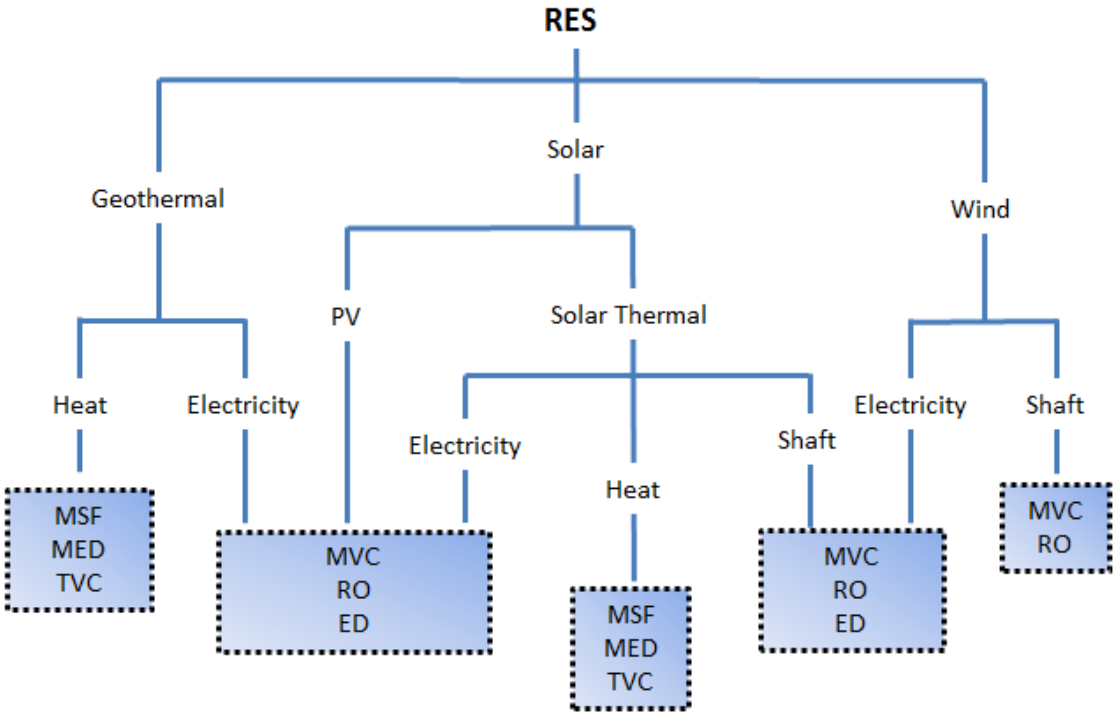

Figure 4. Possible technological combinations of RES and desalination methods [24]**.**

In remote arid regions where there is no connection to the electricity grid, the employment of autonomous systems for the provision of fresh water is common. The market for such stand-alone plants is mainly found in areas which suffer from a lack of or difficulties in energy supply resulting in high energy costs. The majority of autonomous desalination units built in remote and off-grid areas run on diesel generator sets [2]. However in recent years, RES/diesel hybrid systems as well as water purification units driven exclusively by renewable energies have become more popular. The most prevalent and feasible autonomous desalination system practices are solar or geothermal energy in connection with thermal desalination as well as PV and wind turbines combined with RO units [2]. RO desalination systems coupled with renewable energies have the highest share of the total installed desalination plants capacity driven by renewable energy sources. The suitability of RES technologies, especially wind turbines and photovoltaic arrays, for RO desalination systems is due to the capability of such units to desalinate small quantities of water for remote and isolated areas with low energy consumption

and little need for maintenance. RO is indeed a widely scalable technology; it can produce huge amounts of fresh water to a couple of m^3 a day [26].

The fluctuating character and unpredictability of renewable energy sources is a major restriction to a wider implementation of RES-based water purification units for off-grid applications. The majority of desalination methods are not adequate for working at oscillating as well as discontinuous availability of energy supply [7]. RO systems, for instance, require a rather constant flow of energy and if the energy supply to the RO unit is interrupted, at each stop, a part of the produced fresh water has to be used to clean the membranes before it can start running again. As a consequence, desalination systems tend to be either oversized in order to produce larger quantities of fresh water in a limited time window or be equipped with energy storage devices such as batteries or thermal storage in order to accumulate energy surpluses for the long-term or smooth out short-term changes in the energy supply [27]. Further, stand-alone applications are often equipped with big water tanks in order to store the product water for a continuous supply even when no electricity is produced [28]. Another practice commonly applied is the use of diesel generator units in hybrid systems which are switched on when required [27].

Fresh water costs

Water desalination costs have declined during the last years to a number of USD 0.5/m^3 for large-scale plants, while market prices for desalinated water are usually between USD 1/m^3 and USD 2/m^3 [6]. The parameters most influencing the desalination cost are the salinity level of the feed and product water, energy costs and economies of scale [24]. Desalinating brackish water is generally less costly compared to seawater due to lower salinity levels of the feed water which requires lower applied pressure and allows for higher recoveries of permeate [29]. When it comes to using renewable energies the cost of desalination largely depends on the cost of the respective renewable energy technology. As a general rule, if compared to the cost of conventional desalination plants which either make use of fossil fuels for thermal energy production or are driven by network electricity, the cost of desalination through renewable energy sources is still greater [2]. Nevertheless, technology improvement in this field has seen the costs decreasing over the last years and it is expected to continue at this pace. In isolated areas where energy transmission and distribution is typically more expensive than distributed generation, renewable desalination has already become cost-competitive [6]. For renewable-based seawater desalination plants with a capacity from a few cubic meters to 1000 m^3, the cost are between USD 1.2/m^3 and USD 15/m^3 due to lower economies of scale [30].

At this point it is important to mention that the economic calculations undertaken in most papers regarding desalination plants diverge quite significantly resulting in a rather poor validity when compared to one another. The costs per m^3 of produced fresh water are based on different installation capacities and methods, energy sources, components, taxes and permits, brine disposal and water sources. They are highly site-specific which is why generalisations should be

avoided. The economic performance of a particular desalination plant or technology compared to others is thus a complex task and should be interpreted with caution.

2.3 Reverse osmosis process

In order to dive deeper into the reverse osmosis technology, it is important to first understand how the process of osmosis works. Osmosis is a naturally occurring phenomenon and widely employed in the cells of all living species. The process involves the natural migration of a low-saline solution, the solvent, towards a strong saline solution, the solute, until the concentration is at equilibrium. If a semi-permeable membrane, that allows water but not salt to pass through it, is placed in a tank with salty water on one side and fresh water on the other side, the fresh water will flow through the membrane to the salt water side lowering its salinity and at the same time reducing the quantity of fresh water. In desalination however, the aim is to increase the quantity of fresh water which is why a pressure has to be exerted on the salt water side in order to prevent the fresh water flow through the membrane. The principle of osmosis and reverse osmosis is illustrated in Figure 5.

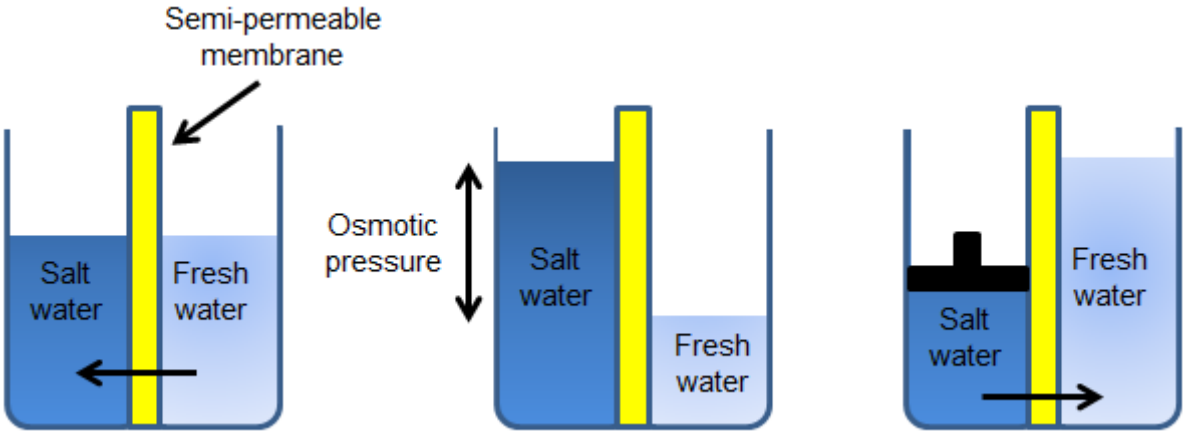

Figure 5. a) direct osmosis b) osmotic equilibrium c) reverse osmosis [31].

The minimum pressure which needs to be applied to a solution in order to avoid the inward flow of fresh water is called the osmotic pressure which differs depending on the feed water source. For instance, the osmotic pressure of typical seawater (35 000 ppm) is about 26 bar which must be overcome by the HPP in order to reverse the flow. Based on this number, a theoretical minimum specific energy consumption of 0.7 kWh/m^3 of produced permeate can be calculated. In practice, the applied pressures are substantially higher compared to the osmotic pressure, amounting to about 40-70 bar [25].

The RO array consists of one or more pressure vessels connected in parallel and/or series. Each of the pressure vessel contains from one to eight individual membrane elements placed in series in their housing. The RO elements are operated in cross-flow mode: the feed flow travels parallel to the surface of the membrane and only a low quantity of the feed flow passes through the

membrane (between 1% and 13% per element) producing fresh water [32]. Hence, a large proportion of the feed water exits the membrane element as concentrate and enters the next element as feed. A pressure vessel with three membrane elements as well as the feed, permeate and concentrate port is depicted in Figure 6a.

The most common type of membrane technology used for the RO process is spiral-wound and it is also the technology used in the FWM system used in this study. In the spiral-wound arrangement, the membranes are built like flat sheets which are assembled to form a sandwich with a feed spacer layer in the middle. On top of the sandwich a permeate spacer layer is added where the product water migrates into and which is glued on each of the three exposed sides while the fourth is connected to a fresh water collection tube. The feed water is forced into the feed channel spacer and the fresh water can pass from all sides through the membrane into the permeate spacer layer. In order to save space and cost, this sheet of layers is rolled onto the core tube to form a membrane element [25]. Hence, the permeate flows in a spiral direction and collects in the core tube. This principle is shown in Figure 6b.

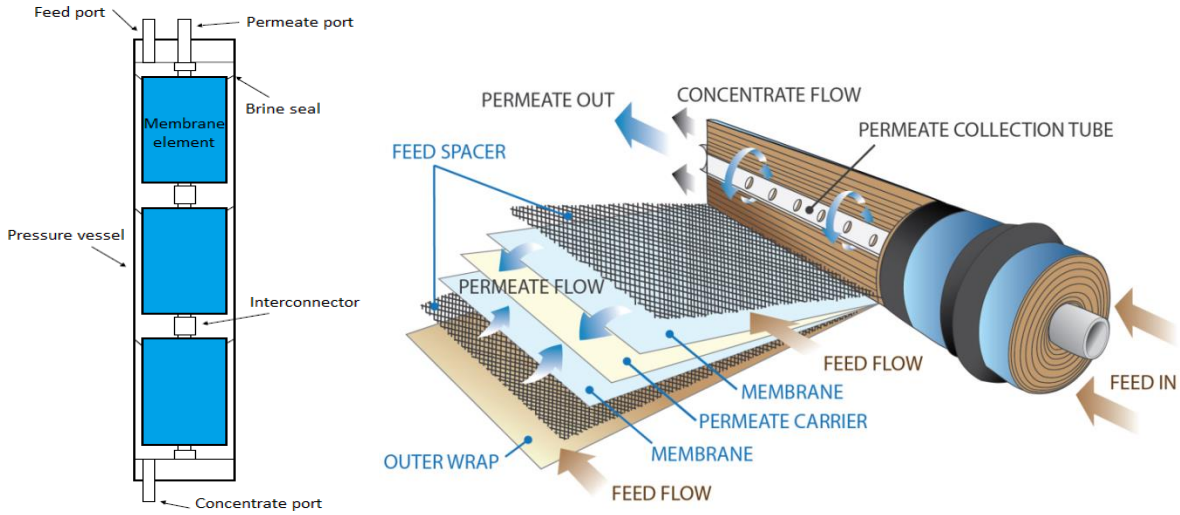

Figure 6. a) RO pressure vessel [33] **b) RO spiral-wound membrane element** [34]**.**

The percentage of permeate to feed is termed recovery ratio. It is very much dependent on the type of feed water used for the water purification process. In the past years, the recovery ratio for typical seawater desalination has constantly increased due to improved salt rejection: from 25% in 1980s to 35% in 1990. To date, recoveries of 45% are not unusual and if second-stage is applied, it can reach 60% meaning the remaining 40% are returned to the sea in the form of concentrate. However, the recovery ratios achieved in areas where the seawater features very high salinity (e.g. Red Sea) are substantially lower [4]. Furthermore, the theoretical minimum energy needed for water purification, as discussed earlier, rises with the recovery ratio due to the fact that the more product water is extracted the higher the salinity of the remaining concentrate resulting in increased osmotic pressure which the pump has to work against in order to gain

further fresh water. This phenomenon applies not only to the RO process but to all desalination techniques [25].

A typical reverse osmosis plant consists of four major components and processes: pre-treatment, pressurization, membrane separation and post-treatment. In Figure 7 the schematic of a simple RO desalination system is presented.

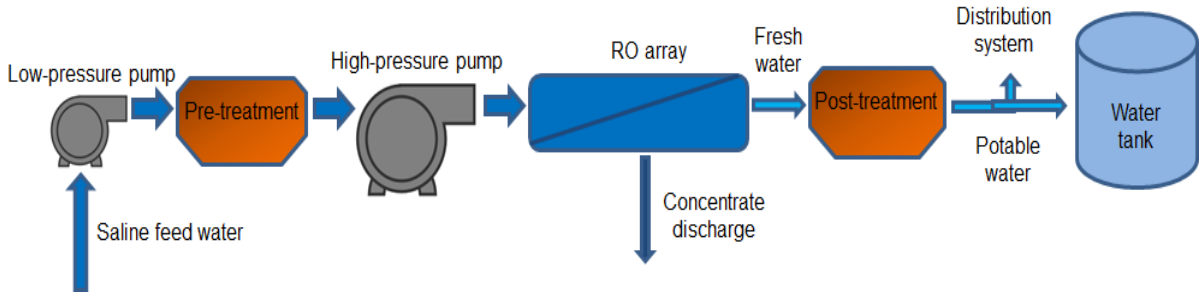

Figure 7. Working principle of a RO desalination plant [31].

Before the feed water can enter the HPP, suspended solids ought to be eliminated, chlorine and anti-scalants are added and the pH needs to be adjusted in order to make the water suitable for the membranes. Else, scaling, corrosion, biological growth or fouling is more likely to occur resulting in blockage of the membrane pores and thus a decrease of permeate flow, pressure drop and salt rejection. This leads to negative effects on the capacity and quality of water production and to a rising in energy consumption. Higher frequencies of membrane cleaning and replacement is the consequence [31].

Scaling which involves accumulation of salts on the membrane surface is more of a problem with brackish feed water due to the high recovery factors and usually occurs in the last membrane element where the concentration of the feed water is the highest [32]. With seawater, the main limiting factor is biological fouling which is caused by the bacteria [25]. Next, the HPP forces the feed water with high pressures through the RO array. The applied pressures strongly depend on the recovery ratio and the quality of the feed water. The semi-permeable membranes permit fresh water to flow through while preventing the migration of practically all dissolved salts. Hence, two streams are produced: a fresh water product stream as well as a highly concentrated brine rejects stream. The concentrate is often discharged right into the sea or used in energy recovery devices while the fresh water usually necessitates pH elevation, disinfection and degasification before being led to the distribution system or a water tank for storage purposes [31].

A RO system is usually designed to operate continuously, however, in reality this is not always the case, especially for off-grid units where the energy supply is often discontinuous. In these situations, membrane flushing at low pressures, i.e. 3 bar, is strongly recommended after shutting down [32]. Else, the impurities that are concentrated on one side of the membrane remain in the pressure vessel which can lead to microbiological activity and fouling [35]. The flushing involves

feeding product water that has been produced earlier through the membranes in order to remove most of the salt until concentrate conductivity matches feed water conductivity [32]. When product water is not available, this flushing process is performed with feed water which means that the recovery factor is simply reduced to a number close to zero [25].

2.4 An innovative concept: FreshWaterMill system

The *FreshWaterMill* is a new concept that mainly employs wind energy for the production of fresh water through the process of reverse osmosis. However, in contrast to conventional methods which utilise an electrical circuit for driving the HPP, the FWM makes use of a hydraulic transmission system. Using a hydraulic transmission rather than a more typical electro-mechanical one to deliver power to a RO unit can potentially eliminate a number of conversion losses such as in the gearbox, generator and electric motor driving the HPP. In conventional large-scale wind turbines the wind energy is first converted to rotational energy via a low-speed shaft. A gearbox connects the low-speed shaft to the high-speed shaft and increases the rotational speeds from about 30-60 rotations per minute (rpm) to about 1000-1800 rpm; this is the rotational speed required by most generators to produce electricity. In the last step, an electrically-driven HPP delivers the required power to force the saline water through the RO plant for the production of clean water.

The FWM concept uses the two-bladed Lagerwey 18/80 wind turbine with a nominal rating of 80 kW and a rated wind speed of 12.5 m/s. Further specifications of the wind turbine model are provided in Table 2.

Table 2. Technical specifications of the two-bladed Lagerwey 18/80 wind turbine [36].

Nominal power:	80 kW
Hub height:	30m/40m
Rotor diameter:	18m
Cut-in wind speed:	3 m/s
Nominal wind speed:	12.5 m/s
Cut-out wind speed:	25 m/s
Speed variable:	60-120 rpm
Nominal torque:	8050 Nm
Rotor speed control	Passive pitching

The innovation regarding the FWM is that the electric circuit with the gearbox and the generator in the top of the nacelle is removed from within the Lagerwey 18/80 turbine and replaced with a pump and a hydraulic circuit. There are two reasons explaining this choice. Firstly, the Lagerwey 18/80 turbine is a model that was introduced into the market in the 90s and hence numerous

turbines of this type have reached the end of their lifetime in the past years. As a result, they are now resold second-hand at very low prices of around € 15 000 [37]. However, the most expensive parts such as the gearbox and the generator in the nacelle need to be replaced and a general refurbishment needs to be carried out. Consequently, using a hydraulic rather than an electromechanical transmission system for the production of fresh water lowers these costs for the overhaul substantially since it only necessitates a pump and a hydraulic circuit which acts as a gearbox. Secondly, according to *SolteQ Energy B.V.*, by employing a hydraulic transmission system for the production of water, the wind turbine can reach up to about 100 kW as the losses in the gearbox and the generator, normally used for the operation of an RO plant, can be eliminated. As a consequence, an efficiency increase of close to 30% can be achieved. The respective wind power curves of the Lagerwey 18/80 with an electric and a hydraulic transmission system are shown in Figure 8. It should however be noted at this point, that the wind power curve involving the hydraulic transmission refers to expected values. The testing of the system is in progress at this moment at the WaterCampus in Leeuwarden.

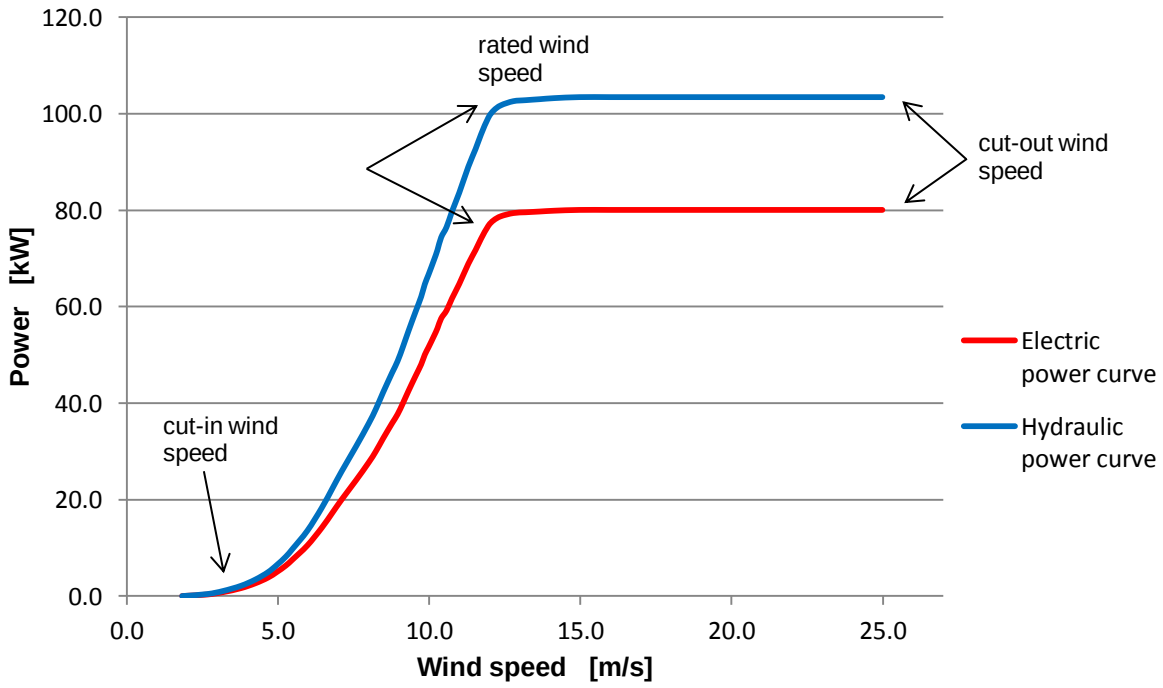

Figure 8. Comparison power curves of the Lagerwey 18/80 with an electric and a hydraulic transmission system according to SolteQ [36]**.**

As it can be clearly observed in Figure 8, with the employment of a hydraulic transmission system it is expected that there will be an efficiency gain not only at the rated wind speed of 12.5 m/s but also at lower than rated wind speeds. As a consequence, the RO system would experience longer operation times, less interruptions and a higher fresh water production.

The concept of the FWM system and its operating principle is illustrated in Figure 9.

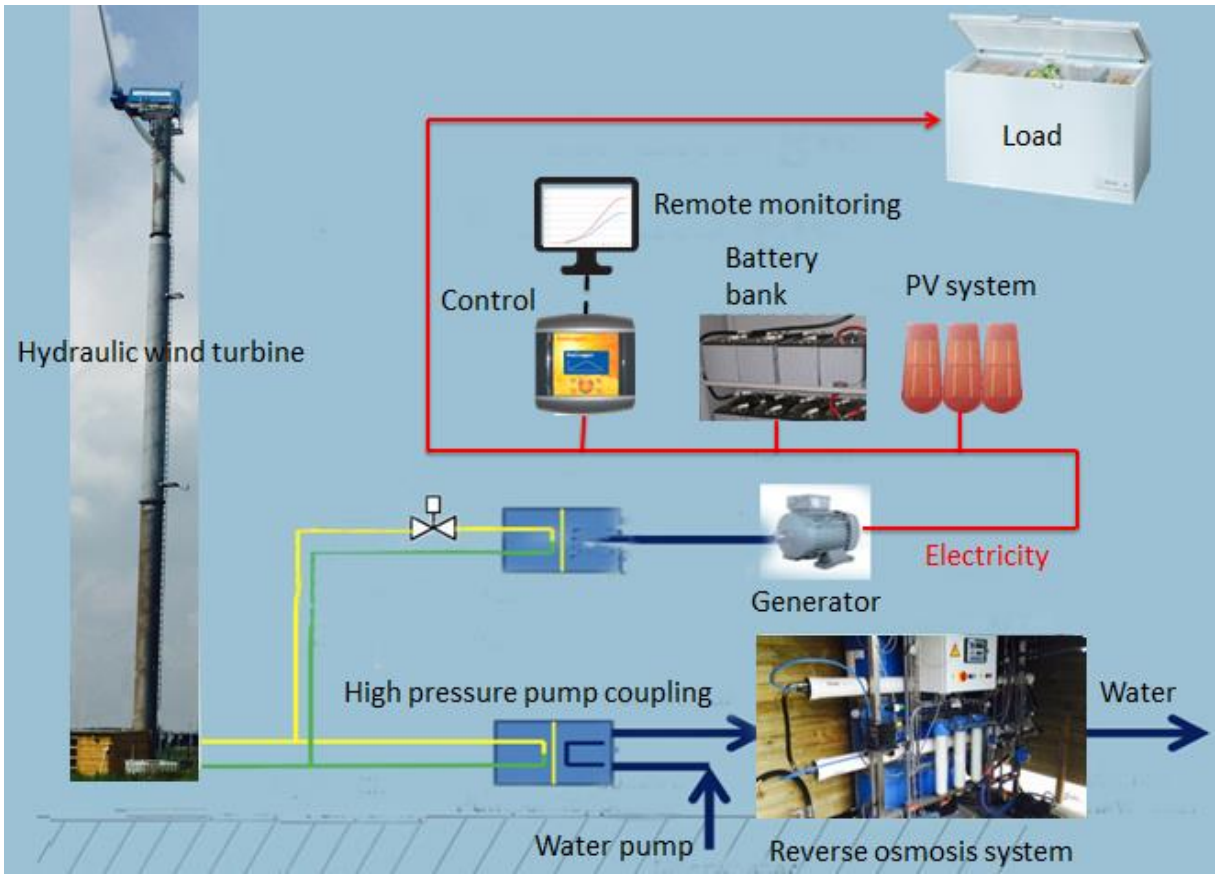

Figure 9. Working principle of the hydraulic FWM system.

The FWM turbine is equipped with a rotor, which is directly connected to a hydraulic pump placed in the nacelle. This pump turns wind energy into pressure energy which is transferred to a hydraulic motor at the bottom of the turbine via a closed hydraulic circuit. The motor is placed on the same shaft as the HPP. The hydraulic motor and HPP are equipped with an input as well as an output side. Hence, the energy from the first hydraulic oil circuit is transferred to the low-pressure saline water entering the HPP in a second separate water circuit. The seawater pumped from sea level to the desalination cartridges is consequently forced into the RO vessels at a pressure of about 50 bar where it exits as desalinated water. Additionally, a hydraulic generator is placed in parallel to the RO plant in order to produce electricity when wind speeds are high and the water desalination system is working at full capacity. The generator is seconded by a PV array and a battery system for storing electricity. The electricity is used by the integrated FWM system to power pumps, sensors, data acquisition and control instruments and for satisfying the electricity demand by the community. Furthermore, a water tank is used to store the produced desalinated water surplus, which is not directly consumed.

At this point, it is also important to mention that hydraulic wind turbines are often less prone to failure and easier to repair as the direct hydraulic coupling solution demands for less electro-mechanical equipment when compared to a classical wind turbine. Moreover, maintenance activities can be performed on a ground-level as the FWM system allows for large and heavy

parts such as the generator to be placed on the ground of the turbine. These are important factors to consider, especially for less developed regions, where specialised technicians are rarely available.

The system under study was developed by *SolteQ Energy B.V.* with the support of the *Delft University of Technology* and with the cooperation of three other companies: *Lenntech B.V.* (responsible for the RO system); *Hydroton B.V.* (responsible for the hydraulic system) and *Hoekstra Suwald Technology* (responsible for the wind turbine).

3

Literature review

In this chapter a literature research is conducted with respect to the state-of-the-art optimisation techniques used for the design and sizing of stand-alone microgrids and RO plants. The first section provides an overview of optimisation methods focussing on those that have mainly been applied in the context of stand-alone electricity generation and water production systems based on renewable energy sources. The following section introduces the most common economic and technical assessment measures and indices of stand-alone power and water systems in addition to reviewing the various optimum sizing approaches and optimisation criteria of RO and power systems respectively, mainly based on PV, wind energy and storage devices. Finally, based on the shortcomings of the past works, the positioning of this thesis with respect to literature is outlined and the way forward is explained.

3.1 Optimisation methods

The process of optimisation can generally be described as finding inputs of a function that minimises or maximises its value which can be subject to constraints. In the past years, a wide range of optimisation methods which differ substantially in their nature have been developed. There are numerous ways to classify these optimisation techniques, for instance based on the type of objective function, number of variables or method of operation. Here, optimisation techniques are divided into three categories: calculus-based techniques, enumerative techniques and guided random search technique. The first two techniques belong to the class of traditional search methods while the third is part of intelligent search methods [38]. Figure 10 presents the classification taxonomy of search techniques used in this thesis.

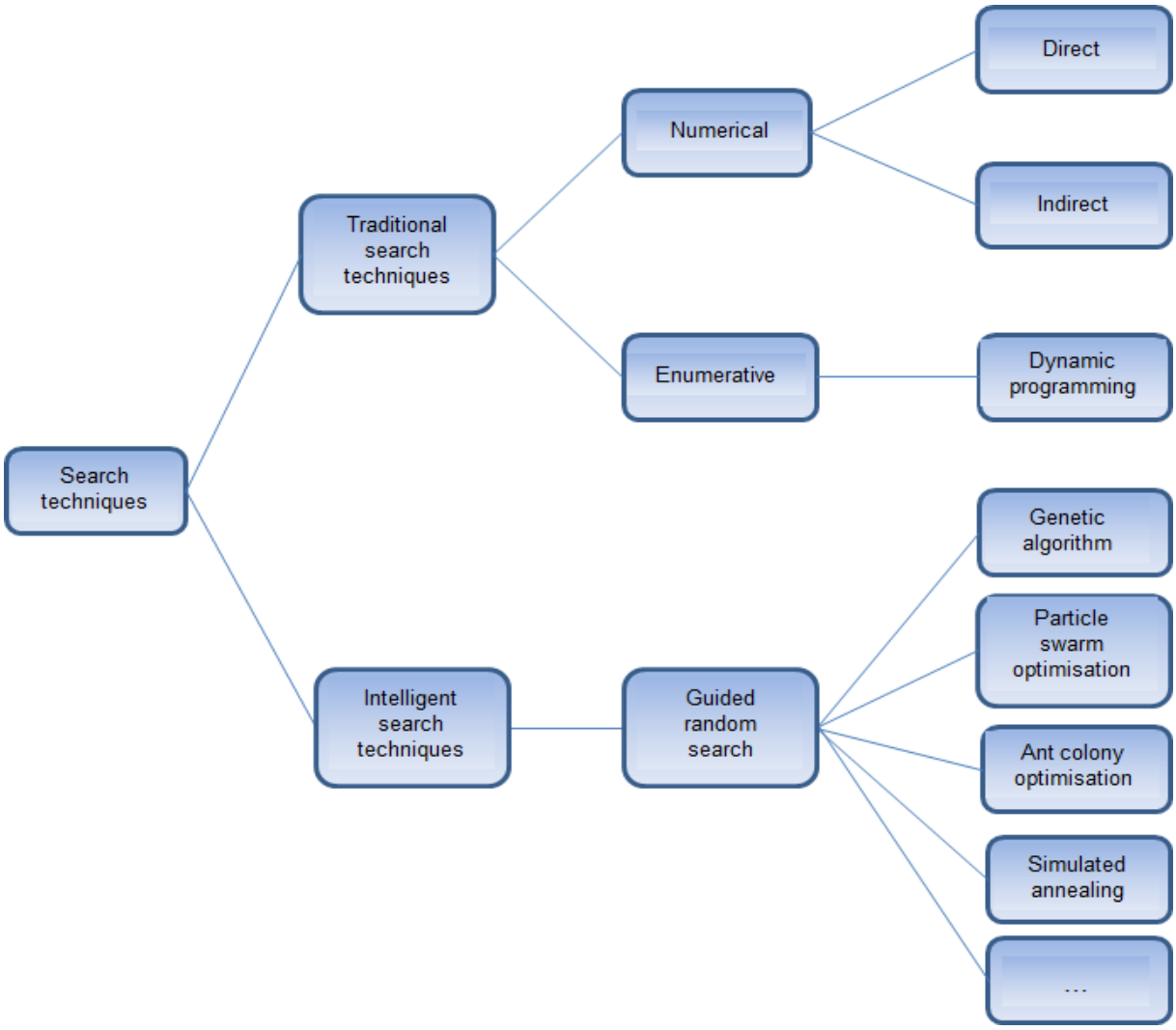

Figure 10. Classification of optimisation techniques [38].

In the following, traditional search methods are shortly outlined while the focus is set on guided random optimisation algorithms as in the past decade these have been widely and mostly used in the optimisation process of stand-alone energy systems.

Calculus-based methods, also termed numerical methods, use a deterministic approach to find a solution which is determined by a set of necessary and sufficient conditions that must be fulfilled. These techniques seek optima either by searching in their environment for points with slopes of zero (indirect methods) or by moving along a function always heading in the direction of the steepest slope (direct method) for which (deterministic) hill-climbing is the most popular technique. The generation of successive results are only based on the information of the previous results. In the event that the optimisation problem is non-convex, i.e. multiple optima exist, these techniques are restricted by local extrema, a shortcoming that can potentially be solved by parallel hill climbing using multiple start points or repeated local search. Finding the global optimum for a multi-modal objective function is nevertheless not guaranteed, especially in noisy search spaces. Also, these optimisation algorithms can solely be used if derivatives of the

objective function representing the problem space exist, i.e. the search space is continuous. Hence, for a certain type of optimisation problems, numerical methods can be highly efficient, however, they cannot be applied to many real-life problems [39].

Enumerative optimisation techniques are characterised by simplicity as they find the optimal solution in a finite and discretised search space by evaluating the objective function value at every point in this space. In this category, the most common technique is dynamic programming. The major drawback of this search method is that although being effective it is highly inefficient due to the calculation of every single point which makes it cumbersome and time-consuming. Hence, when problems are complex and large in space, enumerative optimisation techniques are not suitable [38].

In contrast to traditional optimisation methods which are limited to a specific type of problems, may remain trapped in local optima and cannot deal with parallel computing environment, intelligent search techniques are highly suitable for global search of a wide range of complex problems [38]. Guided random search techniques include genetic algorithm, particle swarm optimisation (PSO), colony optimisation, tabu search (TS) and simulated annealing (SA), among others [40]. These methods do not require the objective function to be continuous or differentiable. Although they have commonalities with enumerative optimisation, they are more efficient as they use the knowledge gained from previous results in combination with randomised features in order to head towards the areas of the problem space where optimal or close-to-optimal points lie without calculating each point in space. Hence, a randomiser helps to make some decisions in the algorithm so that transitions are probabilistic rather than deterministic [38]. This results in the performance being different in an unpredictable fashion between the runs. Based on this behaviour, guided random search techniques cannot be defined as strictly random like Monte Carlo methods, rather their randomness is controlled. These techniques include single-point search such as simulated annealing in which one point at a time is evaluated as well as multiple-point search used in evolutionary algorithms like genetic algorithm in which more points are searched in parallel thus speeding up the calculations and increasing the chance of locating the global optimum [40]. Evolutionary algorithms are inspired by natural evolution. They are linked to artificial intelligence search techniques which have the capability to remember past findings, learn and adapt their performance and act intelligently trying to simulate human behaviour [41]. Artificial intelligence techniques include branches like guided random search techniques, neural networks, fuzzy logic and hybrid algorithms which are a combination of the branches [14]. These techniques are suitable for problems with large search spaces that can be multi-modal (having multiple peaks), noisy and discontinuous. Finding the global optimal solution is not always guaranteed, however, these algorithms provide at least near-optimal solutions which in many real-life problems is already satisfactory [38].

Finally, it should be noted that to date optimisation mostly deals with solving single-objective problems. In real-life however, numerous applications require optimising simultaneously multiple objectives which are conflicting. This is usually done by 'scalarisation', by employing the ε-constraint method or by using Pareto-based optimisation methods. The construction of a single meta-objective function by taking a weighted sum of the individual objectives, which reflect their importance to the user, has its shortcomings as the values of the weights need to be adjusted correctly to the purpose. Also, this technique only returns a single solution, hence ignoring potentially important information of alternatives for the decision-making process. The ε-constraint method is a technique where one objective is chosen to be optimised while the remaining objectives are considered as constraints bound by given target levels which are varied. Pareto-based optimisation is able to return a multitude of non-dominated solutions displaying the relationship between the different objectives on a so-called Pareto front as shown in Figure 11.

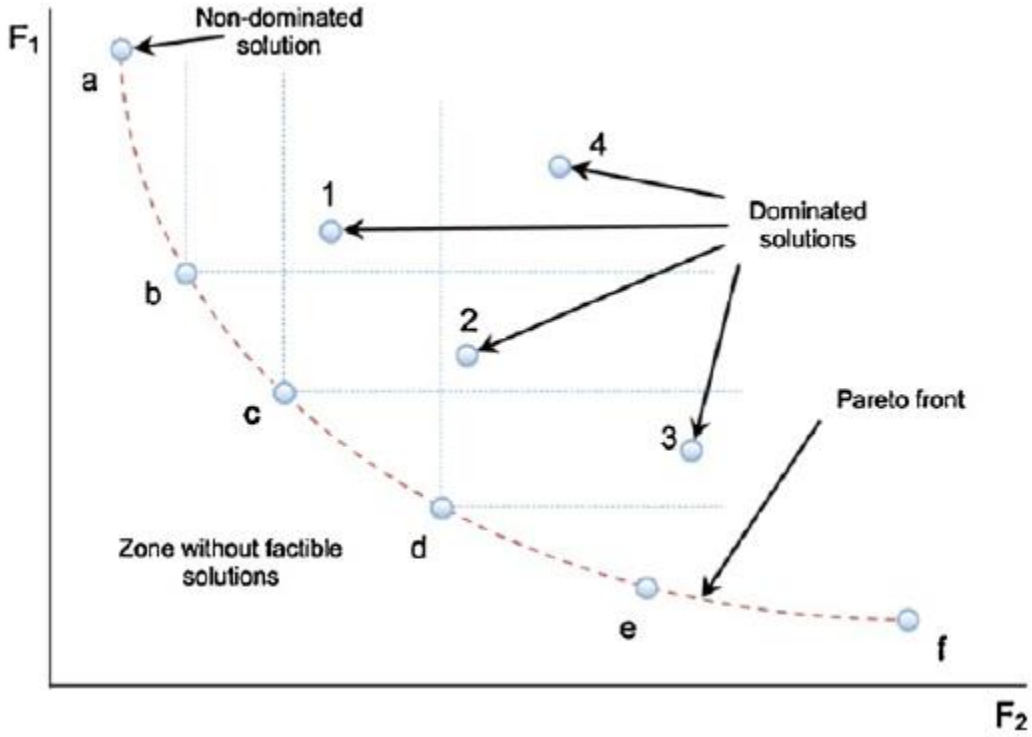

Figure 11. Typical Pareto front of a multi-objective optimisation problem [42]**.**

F1 and F1 indicate two conflicting objectives on which basis the optimisation is performed. Points 'a' to 'f' are non-dominated or Pareto-optimal solutions whereas points 1 to 4 represent dominated solutions. A solution is called Pareto-optimal if no improvement with respect to any objective can be achieved without deteriorating at least one objective [43]. This method is explained more thoroughly in chapter 5.

3.2 Optimal design and sizing approaches of RES-based power and water systems

Due to the complex nature of renewable energy source employment in autonomous power and water systems, optimal sizing of each component becomes a difficult and essential task, especially with respect to economic and technical reasons. Hence, the focus is set on optimal sizing studies addressing the economic performance as well as technical performance in terms of system reliability as the design criteria. Firstly, these performance criteria are introduced and explained. Consequently, the most common sizing approaches for renewable energy power systems are addressed while the last section focuses on design approaches of sustainable water systems.

3.2.1 Economic and technical assessment criteria

In literature, the economic performance of a microgrid is mainly assessed in the form of annualised cost of system (ACS) expressed in €/year, levelised cost of energy (LCE), expressed in €/kWh or net present cost (NPC) expressed in €. The ACS is the sum of the yearly capital, maintenance and replacement cost of all components whereas the LCE is the ratio of the ACS and the total yearly energy production. The same approach of the LCE can be applied to fresh water production systems. The NPC represents life-cycle cost of the system including all outlays and incomes that take place in the plant lifetime with future cash flows discounted back to the present. Revenues gained from electricity and fresh water sales are not included in this calculation [16].

Since irradiation and wind speed and hence power production are fluctuating in time and since 100% renewable energy microgrids do not possess any controllable energy sources such as a diesel generator, power reliability analysis is usually considered as an essential step in any such system design process. A reliable microgrid means that the system has sufficient power to cover the demand during a given time frame. The reliability of a power system is usually measured in terms of probabilistic reliability indices for which different approaches exist [44]. The most common and widely used methods are the loss of power supply reliability (LPSP) and the loss of load probability (LLP) concepts. The LLP, expressed in terms of days/year, hours/day or percentage of time, can be defined as the overall probability that the system load exceeds the available generating capacity leading to a shortage of power. This metric provides specific information regarding the number of times the microgrid experiences a shortage of power. Very often, the LLP is calculated only for peak load levels. The LPSP on the other hand, is the sum of the amount of electricity that the power system is not able to supply during a given period and it is expressed in kWh/year or as the ratio kWh/kWh of total electricity demand in a specific timeframe (percentage of time). The LPSP provides specific information regarding the total yearly magnitude of electricity deficit experienced by the power system. Both concepts are suitable measures of the microgrid performance for a known load distribution. An LPSP or LLP of zero means that all demand can be met for the given time frame whereas a value of 1 means that the demand is at

no times satisfied [45], [46]. It should however be noted at this point that in literature these concepts are sometimes found to be interchanged. The concepts described above can in the same way be applied to fresh water production systems. Both concepts however, have their own shortcomings: the LLP technique is only a suitable metric when the number of times an outage occurs is of importance whereas the LPSP technique solely provides information about the total yearly magnitude of the load deficit. In addition, both concepts consider all loads with the same priority and do not take the severity of the outage into account meaning that a power supply interruption at peak times has a far greater impact than at off-peak times.

LPSP and LLP are statistical parameters which are computed not solely for good or bad resource years. Usually, these concepts represent average values over a longer period of time. Hence, during a bad resource year, the microgrid for which the reliability analysis is undertaken, will suffer from a higher probability with respect to outages [46]. For the employment of the LLP and LPSP reliability indices when designing an autonomous microgrid, two different methods exist: one performs chronological simulations whereas the other uses probabilistic techniques in order to include the intermittent characteristics of the renewable energy sources and the demand. The first approach is computationally cumbersome and enough data need to be available for a given time period, a shortcoming that the second approach does not have [46].

3.2.2 Sizing methodologies for hybrid microgrids

Numerous papers have been written regarding the optimal design, sizing and control of stand-alone renewable energy based microgrids. The reviews of Chauhan et al. [16], Zhou et al. [15] as well as Baños et al. [43], for instance, provide a detailed overview of methodologies employed for the optimal sizing of renewable energy systems, the optimisation algorithm, objective function(s), variables and constraints employed. In the past, traditional optimisation techniques such as (mixed-integer) linear and quadratic programming, Lagrangian relaxation and Nelder-Mead Simplex algorithm were mostly utilised [43]. In recent years, however, approximate methods like guided random search or artificial intelligence techniques have become promising research areas due to their capability of finding an optimal or quasi-optimal solution with relative computational simplicity even for highly complex, non-linear, noisy and discontinuous problems [16]. The amount of research undertaken in the field of optimal sizing of single and multiple RES based autonomous energy systems has grown exponentially in the last decade. The design of multi-source hybrid electricity plants shows an increase in complexity because of the high number of variables and parameters that have to be considered and the fact that the optimum configuration and the optimum control strategy of the system are interdependent. If a proper design is however employed, hybrid power generation systems have proven to be more cost-effective and reliable compared to single-source RES systems [43]. Due to these reasons and the fact that the FWM system employs more than one energy technology, the following literature review is limited to the optimisation of multi-source hybrid microgrids for off-grid applications.

Most of the optimal sizing problems are related to wind and solar technologies due to their decreasing costs and their complementary characteristics [46]. Diaf et al. [45] used an iterative approach for sizing autonomous hybrid solar-wind power systems by increasing the respective capacities in discrete steps in order to minimise the levelised cost of energy (LCE) for a requested LPSP. The model is applied to three different sites with the same load profile but different RES potential. Since all three locations have a similar solar profile but different wind speed conditions, the study concludes that the wind energy potential quality strongly affects the LCE. In [47] Diaf et al. employed a similar iterative method for searching the optimal size of each component and applied it to five different remote sites. In this paper, the optimal results are compared with PV and wind-only solutions concluding that the hybrid system is the option that yields the lowest LCE for all locations considered in the study. The authors remark that at certain times the energy surplus can reach up to 75% of the energy production and thus the use of a third controllable energy source like a diesel generator could be favourable. Belfkira et al. [48] propose a methodology for optimising stand-alone wind-solar-diesel systems using a deterministic algorithm (DIRECT). The optimisation considers the optimal type and number of units among a list of commercially available system devices ensuring that the total cost of the system is minimised while fully meeting the load demand. Bernal-Agustín et al. [49] studied the behaviour of GA applied to the design of PV-wind-diesel-batteries-hydrogen systems. First, the global solution was found by applying an exhaustive enumerative method. Consequently, the GA technique was used and the influence of the number of generations, population size, crossing and mutation rates on the behaviour of the algorithm was studied in order to find the very parameters to reach a global optimal solution with nearly 100% probability. The CPU time for the enumerative method amounted to 1 day and 9 hours whereas the GA reached an optimal solution in about 1 minute. The authors thus conclude that if the right parameters for the GA are used, the algorithm represents a robust technique for finding the global optimum of a problem with little computational effort. Yang et al. [50] and Xu et al. [51] developed an optimal sizing method based on GA to calculate the optimum stand-alone system configuration that can achieve the customers required LPSP with a minimum annualised cost and total capital cost of the system, respectively. The authors have brought into picture two optimisation variables that are rarely used, namely PV array slope angle and wind turbine installation height. Koutroulis et al. [52] presented a methodology to optimally size stand-alone PV-wind systems in terms of total system cost using GA. In their study, different types and sizes of system devices are considered which are fed into a databank for the yearly simulation. The optimisation is carried out with the use of the LPSP technique which rejects all possibilities that do not fully cover the load requirements. The authors also compare the hybrid system configuration to single-energy source systems and show that hybrid plants feature lower costs for the specific case study. Bilal et al. [49] presented an evolutionary algorithm for the efficient design and control of a hybrid power generation system including PV, wind, diesel, batteries and hydrogen storage. The results, which were verified by using an enumerative method, again proved that the evolutionary algorithm was capable to reach

a good solution with low computational effort. Navaeefard et al. [53] applied PSO in order to optimise three different hybrid systems including PV, wind and a storage system in the form of battery or hydrogen tank or a combination of both. The optimisation was undertaken by minimising the net present value (NPV) considering a reliability constraint. The results show that the combinatorial storage option is the most cost-effective one for its high load tracking behaviour. Kaviani et al. [54] employed the PSO technique in order to optimise a hybrid wind-PV system with the use of a fuel cell in terms of ACS and under the condition that the load is fully met at all times. Outage probabilities of the wind turbine, the PV array as well as the converter are taken into account for reliability assessment. The authors conclude that the PSO algorithm developed in the framework of the research is flexible to be implemented to any application and can reach a near-optimal solution with low computational time. Rabhi et al. [55] developed an energy management algorithm based on fuzzy logic to ensure optimal operation of a wind-solar-battery system. Tsuanyo et al. [56] investigated into the optimisation of batteryless off-grid hybrid PV-diesel systems by making use of the optimisation model HOMER which is based on an enumerative method. For a case-study, the scientists compared a 100% diesel system to a PV system with identical diesel generators and diesel generators with different sizes in terms of minimum LCE. Both PV alternatives resulted in about 10% lower LCE compared to a conventional stand-alone diesel generator system. However, the reduction in LCE comes hand in hand with a significant increase in investment cost which is critical for the development of RES technologies in emerging countries. Razak et al. [57] also used the software tool HOMER in order to minimise the excess energy that is often produced and thus dumped in hybrid systems without grid connection. The energy sources employed are pico hydro turbines, wind turbines, PV and diesel generators. The results emphasised the importance of considering the amount of excess energy the system produces for cost reduction.

Recently, an increasing number of researches have been undertaken which involved the optimisation of more objectives at the same time which are conflicting with one another. Bilal et al. conducted several studies using the Pareto-based multi-objective GA optimisation method [58]–[60]. In one of their papers, hybrid solar-wind systems with battery storage are optimised by simultaneously minimising the annualised cost of system (ACS) as well as the LPSP. In this study, Bilal et al. investigate on the influence of three load profiles with the same daily energy consumption but different peak load distribution on the optimal hybrid system configuration. The results show that the cost of the optimal configuration strongly depends on the load profiles. The variables chosen for his research are the number of PV panels, batteries, wind turbines, inverters and regulators [60]. In [58] Bilal et al. focus on the influence different LPSP values have on the system cost indicating that a small decrease in LPSP results in substantially higher costs. In [59] Bilal et al. develop a method to optimally size hybrid power generation systems comprising PV, wind, diesel and battery devices. Here, Bilal employs again multi-objective GA minimising the LCE as well as the CO_2 emissions. Bernal-Agustin et al. [61] applied a multi-objective Pareto-based GA to the design of isolated hybrid RES-diesel systems minimising the total cost

throughout the useful life of the installation as well as the CO_2 emissions. Two different load profiles were taken into consideration obtaining a set of possible solutions from which the designer can choose. Later, this method was applied by the same authors and extended to an optimisation of hybrid PV-wind-diesel-hydrogen-battery power systems with three objectives: total cost, CO_2 emissions and unmet load. In this paper, the system configuration was optimised by employing the triple-objective evolutionary algorithm named SPEA whereas the best control strategy is chosen through a single-objective GA. Relationships and implications are discussed with the aid of 3D and 2D Pareto fronts. The authors argue that as the problem of design is very complex, the classical optimisation techniques are not able to solve the optimisation in a reasonable CPU time, hence the Pareto-based multi-objective GA method used in this study proves to be highly efficient and robust [62]. Similarly, Abbes et al. [63] employed a controlled elitist GA based on a triple multi-objective optimisation which minimised life cycle cost, LPSP and an ecological objective for the design of a hybrid PV-wind-battery system in order to find the best compromise between them. The decision variables include the swept area of the wind turbine, PV array area as well as battery capacity. Sharafi et al. [64] employed a similar approach to Abbes et al. using a simulation based triple-objective PSO algorithm and the ε-constraint method. In this paper, Sharafi et al. compared the proposed approach results with previous methods and concluded that an improvement in the total cost is obtained while achieving the same fuel emission and reliability.

In summary, various methodologies have been employed by the researchers for the optimal sizing of hybrid RES-based microgrids. In the past, iterative approaches in which the respective capacities of the power sources were increased in discrete steps as well as traditional optimisation techniques were mostly used. Recently, intelligent search methods such as heuristics have however become the predominant ones due to their time-efficiency and their capability of finding (quasi-)optimal solutions even for highly complex, discontinuous, multi-modal and noisy problems. The literature study has shown that in this context, PSO and evolutionary algorithms such as GA represent the most commonly employed optimisation techniques when designing renewable energy microgrids for off-grid applications. Multi-objective optimisation, mainly using GA, has now become a promising research are as these have the ability to simultaneously optimise various objectives which are conflicting with one another. Pareto-based algorithms and the ε-constraint method, which both display multiple solutions, are found to be more suitable than scalarisation. With the scalarisation approach the various objective functions are merged into a single one ignoring potentially important information of alternatives for the decision making process. Also, in the majority of cases, the system costs are minimised while important design parameters such as reliability or CO_2-emissions are often implemented in the form of constraints for which the value has to be decided beforehand by the designer. It should moreover be noted that the most common reliability metrics in these studies, namely the LLP and the LPSP, do not take the severity of outages into account assuming the same importance for all loads.

3.2.3 Optimal design and operation of RO units

The deployment of RES for water production through desalination does not face the same barriers as in the case of electricity generation since electrical storage systems to compensate for the stochastic behaviour of RES are far more expensive compared to water storage systems. RO units consume the energy directly for water production and consequently the water can be stored cheaply and in large quantities for long periods. In most of the studies the design of RO plants integrated with RES technologies is performed in such way that the RO plant solely operates at its nominal power. If insufficient energy is available for the desalination process, the RO plant is turned off and the fresh water in the tank, if available, is used to cover the demand [8]. As explained in section 2.3, interruptions of RO plants should however be kept to a minimum as for every switch-off fresh water is required for cleaning the membranes.

Mohamed et al. [65] presented a simplified method for designing RO units coupled with an energy system composed of PV panels, wind turbines and batteries. In the first step, the RO unit is designed so as to cover the maximum daily water demand, dictating the corresponding maximum power requirements. The battery bank's capacity and the water tank volume are determined beforehand. Both equipment are set equal to providing a two-day system autonomy in terms of electricity and fresh water, respectively. The number of PV modules is calculated such that the yearly energy requirements are met. The program then minimises the total system cost by gradually eliminating PV modules, calculating the resulting energy production and replacing them by one or more wind turbines. The combination achieving the least cost of water production is chosen as the final hybrid system configuration. The results also showed that storing fresh water is more economical than making use of great battery capacity sizes. Nevertheless, the battery bank should be kept at an appropriate size for constant RO operation. Manolakos et al. [66] developed and applied a software tool for designing hybrid renewable energy systems consisting of PV modules and wind turbines for the production of electricity and water. The system operation is assisted with batteries and a micro hydraulic plant for energy storage. In order to size the individual components a random number of PV panels, a size for the wind turbine, pump and water turbine is chosen. Hence, a simulation of the system operation is performed and based on the obtained results the power ratings of the solar and wind generator as well as the micro hydro plant are adjusted accordingly. The RO plant as well as the battery bank sizing is taken care of beforehand. Regarding the battery, several days of energy autonomy of the system is considered in case of low irradiation and wind speed. Also, the volume of the desalinated water tank is computed such that it can cover the fresh water demand of the location for a certain amount of days. In this study, the desalination plant is designed to work at variable flows depending on the available power. However, no detailed explanation is provided as to the workings and impact of this assumption. After several program runs and alterations to the equipment's nominal ratings, the optimised system can be calculated.

In contrast to the design methods employed above, in recent years, intelligent search techniques have gained more attention regarding the optimisation and sizing of desalination units coupled with RES. M'Barek et al. [67] employed an optimisation method based on GA which aims at minimising the total water cost while at the same time the desalinated water demand of a community is completely covered. The decision variables are the number and type of RO membrane, PV modules, wind turbines, battery chargers as well as converters, the height of the turbines and the volume of the water storage tank. In this paper, a two-step approach is used. First different RO plants are designed based on water demand, feed water characteristics and desalinated water specifications. Hence, the required energy for running the RO devices can be determined. In the second step, the renewable energy system supplying the energy for the RO plant is designed and the individual components are optimally sized. The configurations are validated by performing yearly simulations in order to examine whether they can meet the water requirements. The RO plant is designed in such way that it operates only at full capacity and only if the required energy is available; else it is switched off and flushing is performed. Bourouni et al. [68] optimised the coupling between the RO process and the power system by considering single and multi-source RES systems. The optimisation methodology is similar to the one employed by M'Barek et al., however, the objective is to minimise the total net present cost of the system. With respect to the RO design for the hybrid system and the single-source systems (PV or wind) including batteries a RO operating time of 24h is assumed. On the other hand, when the RES systems driving the RO unit do not employ batteries, then the operating time is reduced, a fact that needs to be considered in the design of the RO unit as it requires greater capacity in order to produce the same amount of fresh water in a smaller time frame. Compared to the results achieved with ROSA and HOMER software, the outcomes of the model employed in this study were found to be very similar.

In the majority of the optimisation approaches used in literature, the size of the RO plant is first computed according to the fresh water requirements of the location in question and the optimal RES power system supplying the RO plant is thus designed in a further step such that the corresponding energy requirements of the RO unit are satisfied. Figure 12 illustrates the various steps undertaken when faced with the task of designing a desalination plant driven by renewable energies.

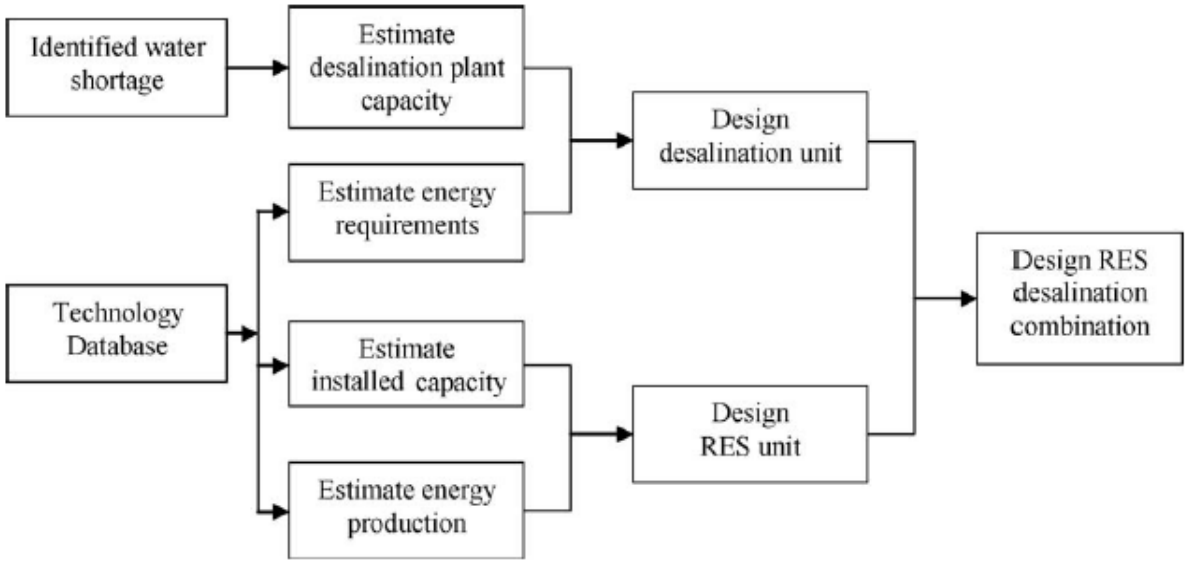

Figure 12. Design methodology of RES based desalination plant [24].

In contrast to the design approaches explained above, few studies can be named which have performed the sizing of the RO unit as well as the RES system in a single step. Koutroulis et al. [5] proposed a GA method for the cost-optimal design of RO systems power-supplied by PV panels, wind turbines and batteries. The simulation-based optimal sizing of the RO unit as well as the hybrid system powering the RO plant is executed in a single run. The decision variables are the number and type of RO desalination units, PV modules, wind turbines, battery chargers, inverters and batteries, the PV module tilt angle (there is the option of having two different ones for summer and winter), the installation height of the turbines and the volume of the water storage tank. A database contains various types of system devices and their respective costs which are fed into the optimisation program. The method has been applied to design a desalination system for a small community as well as a residential household in order to prove its effectiveness in various desalination system size scales. The results were compared to system configurations employing either only wind turbines or PV modules. In both cases, the hybrid systems achieved substantially lower system costs. Clarke et al. [10] performed a multi-objective optimisation minimising NPC and CO_2 emissions of hybrid RES based microgrids while both the electrical as well as potable water load is fully met. Moreover, the LLP method is implemented as a constraint allowing for a pre-set percentage of yearly electrical load not to be met. The autonomous power system includes PV panels, hydrogen storage for smoothening out long-term fluctuations and batteries for short-term storage. Also, a water storage tank is integrated into the system which is responsible for supplying fresh water in addition to being used for the electrolysis. In this paper, the PSO technique is employed which optimises simultaneously the system size as well as the power management strategy. The decision variables are the number of PV panels, fuel cells, RO units, electrolysers, metal hydride canisters, batteries and the water storage capacity. The RO unit is only operated at full capacity and when enough power is available and the water storage tank exceeds a pre-defined limit. The simulations are undertaken for dynamic water demand

using 15 min resolved data and static water demand next to a variable electrical load. Compared to the results obtained for a similar system designed with the software HOMER, the PSO algorithm achieves a lower NPC. Moreover, the author remarks that when a time-varying water profile is used, both the NPC and CO_2 emissions increase.

Few papers have explored the possibility of integrating renewable energy technologies with variable flow RO plants. Operation at variable flow allows the intermittency of RES to be accommodated. It presents an interesting and cost-efficient approach especially when no storage technologies are in place. Variable flow means that the desalination units in question do not only work at nominal power of the high-pressure pump, instead an operating window is defined and the permeate production is adjusted based on the available energy. This concept is further explained in section 4.2. Miranda et al. [27] designed a stand-alone wind-powered RO system without the use of batteries in order to reduce capital and operating costs. Dependent on the output power of the wind turbine, a control strategy is determined that dictates a fixed operating point within the limits of previously established operation window of the designed RO unit. The system was modelled in Matlab so as to predict performance. In this study, Miranda et al. also present other two possibilities to power an RO unit integrated in a stand-alone power system without storage devices or back-up technologies such as diesel generators: on/off switching of the RO units and de-rating the wind turbine. In the first case, multiple RO units with equal or distinct capacity are connected to a wind turbine which are turned on and off so as to match the demand to the total power generated instantaneously by the turbine. The second approach consists of taking advantage of the horizontal end of a pitch controlled wind turbine power curve by changing the settings of the pitching mechanism so that the power generated flattens out at lower wind speeds. Hence, the nominal rating of the turbine is substantially higher than the RO unit capacity. In both cases, an attempt is made to supply the individual RO modules with approximately constant power.

Gilau et al. [69] analyse the cost-effectiveness of a stand-alone seawater RO system aimed at the implementation in developing countries and powered by either PV energy or wind turbines and batteries. The first step of the design involved the simulation of hourly power production from the RES microgrid by using HOMER software. Based on these results, hourly water production was computed employing ROSA, a software developed specifically for the design of RO systems. The model for the RO system is extended in creating an operational window so that it could operate under intermittent power supply. The results demonstrated that wind-powered systems achieve the lowest NPC for the location in question. Also, for RO units powered by PV the use of batteries has a greater effect in producing an increased amount of water.

In summary, the optimisation of RES-based desalination systems for off-grid applications is in almost all cases performed in a two-step approach: first, the desalination plant is sized based on the maximum daily water demand; in a second step the RES power system is optimised in such

way that it provides enough energy throughout the day in order to operate the RO plant. A comprehensive approach where both systems are optimised in a single run is rarely employed. Also, in the past, the optimal design of the power system was mostly done by gradually changing the nominal ratings of the renewable energy sources and calculating the resulting energy production until reaching a satisfactory solution. In this approach, the battery bank's capacity and the water tank are often set equal to providing a two-day system autonomy, hence they were not part of the optimisation process. In recent years however, intelligent search techniques as well as multi-objective optimisation have gained more attention regarding the sizing of desalination units coupled with RES. Furthermore, it should be noted that stand-alone power systems aim at supplying a community with either clean water or electricity; the possibility of satisfying both demands within one system adds a further degree of complexity and it is exclusively discussed in Manolakos et al. and Clarke et al [10], [66]. The literature review has additionally demonstrated that in most cases the operation strategy only allows the running of the desalination unit at full capacity; if it cannot be achieved due to insufficient power supply the plant is switched off. Operation at variable flow allows for the unpredictability and intermittency of solar and wind energy to be accommodated and thus increases operation time and reliability and minimises RO interruptions. Some papers have addressed this issue by introducing an operating window for the RO plant. Nevertheless, the existing literature in this regard remains meagre. Lastly, it is worth mentioning that the water load of a given site is mainly assumed to be static throughout the day, an assumption that often results in lower overall costs.

3.3 Positioning of the thesis with respect to literature

The high initial cost is the main limiting factor for the adoption of renewable-based power systems for off-grid applications, especially for less developed countries. Hence, as outlined in the literature review, the design of these systems is usually done by searching the system configuration and size that renders the lowest total cost. In order to further decrease the capital cost, a trade-off with the system reliability in the form of LLP or LPSP can be made so as to reach the best compromise for both.

The literature review in the previous sections discussed the most important design considerations when sizing cost-optimal RE based microgrids for the production of fresh water and electricity in off-grid areas. At the end of each section, a short summary of its respective shortcomings was provided. In order to clearly highlight how this thesis sets itself apart from relevant literature, Table 3 summarises the main literature gaps and outlines the approach taken in this thesis in order to tackle the limitations.

Table 3. Literature gaps and proposed thesis approach.

Literature gaps	Thesis approach
Single-objective optimisation methods or scalarisation: → One single best solution → No relationship given → Reliability indices are mostly implemented as a constraint	Pareto-based multi-objective optimisation methods: → Set of alternative optimal solutions for the decision-making process → Shows relationship between system costs and reliability index
All loads and hence outages are considered with the same priority	Severity of outages is taken into account based on base, peak and off-peak times
Stand-alone microgrids mainly supply a community with either fresh water or electricity	Co-production of fresh water and electricity within the same system
RO plants only operate at their nominal flow and pressure (and hence power)	Use of an operating window for the RO plant in order to accommodate RE fluctuations, increase operation time and reliability and keep the interruption of the RO plant to a minimum
Static daily water demand	Time-varying water demand
Two-step design approach for RES-based RO systems: 1.) Size of RO plant is based on the maximum daily water demand of the given location. 2.) Size of RE microgrid is based on previously computed size of RO plant.	Single-step approach: Sizing procedure of RO plant and RE microgrid is performed simultaneously and hence their interdependence, the operation at variable flow and the dynamic water demand are considered.

This thesis builds upon the literature review, the respective gaps and the proposed approaches described above. On this basis, the stand-alone FWM system, which integrates a hydraulic circuit with an electrical one, is modelled and a suitable system operation strategy is developed. Next, the optimisation problem is defined with the three objectives of minimising the overall costs next to maximising its power supply and water supply reliability. The sizing method consists of determining the optimal size of the different FWM system components depending on the system reliability for a specific location (case study). This thesis does not aim at a detailed analysis on smart power control; it rather focuses on results on a system level by looking into the technical and economic potential of the FWM system.

The optimal sizing procedure is performed with the Pareto-based multi-objective genetic algorithm solver ‘gamultiobj’ which is available in Matlab. Due to the design complexity of hybrid renewable energy systems, classical optimization techniques have failed to be either effective or

efficient which is why, in recent years, approximate methods such as guided random search and artificial intelligence techniques have dominated the research landscape in this regard as they are computationally less burdensome and highly applicable to complex and multi-modal problems with a large search space. The literature review has shown that GA and PSO are the most widely used and promising search techniques with respect to the design of hybrid RES systems. If the right parameters are used, GA are not restricted by local optima and they represents a robust technique for finding the global optimum of a problem with little computational effort, especially in multi-objective cases. Being a population-based method, GA is well suited to solve multi-objective optimisation because it can find a large amount of Pareto-optimal solutions in a single simulation run. Pareto-based techniques are found to be more inclusive than scalarisation as the latter approach only returns a single solution, hence ignoring potentially important information of alternatives for the decision-making process. Also, when performing a multi-objective optimisation with scalarisation, weights have to be assigned to the respective objectives meaning that preliminary assumptions on which objective is of higher importance have to be taken. With the Pareto-based method this decision can be taken at the end of the optimisation process when more information is available. For this reason the built-in optimisation solver ‘gamultiobj’ within the Global Optimisation Toolbox part of Matlab is chosen to be used without any adaptions. It is a research and industry-proven and widely used solver for multi-objective optimisation procedures. Additionally, NSGA-II which is the genetic algorithm variant use in the ‘gamultiobj’ Matlab solver has proven to provide good performance in solving triple-objective optimization problems.

4

Modelling

This chapter aims at setting up a model of the hybrid FWM system which is the basis of the simulation and optimal sizing procedure. As a first step, the configuration of the extended FWM system is illustrated and the principle of operation is explained. Next, the mathematical formulation of the RO unit and the FWM system is tackled, the interaction between the different components is displayed and the operation strategy for the model is explained. As every model is only as good as its best assumptions, the last section gives an overview of the most important assumptions regarding the formulated FWM system.

4.1 Configuration of the further developed FWM system

In section 2.4 the concept of the innovative FWM system with its hydraulic transmission system has been introduced and discussed. The main part consists of a wind turbine which drives the RO plant as well as the hydraulic generator turned on once the RO unit has reached its nominal power. Furthermore, it is equipped with PV panels and batteries which second the electricity production and storage. While the integrated system seems to be robust in terms of electricity generation due to the multiple sources and storage option, the production of fresh water cannot be assured at all times unless constant and high wind speeds are present, a climatic condition which is not found in many places of the world. In case of insufficient wind power for water production, the fresh water tank can assist for short-term fluctuations, but it is not suitable as a long-term storage option due to size limits. In order to tackle this shortcoming of the current FWM system design, an electric motor is put on the same shaft with the hydraulic motor and the HPP. This motor can be fed with electricity from the batteries and the PV system and either individually drive or assist the hydraulic motor in powering the HPP. Hence, a more integrated system is developed in order to increase operation time of the RO plant making the system more flexible. The extended version of the FWM system is schematically illustrated in Figure 13.

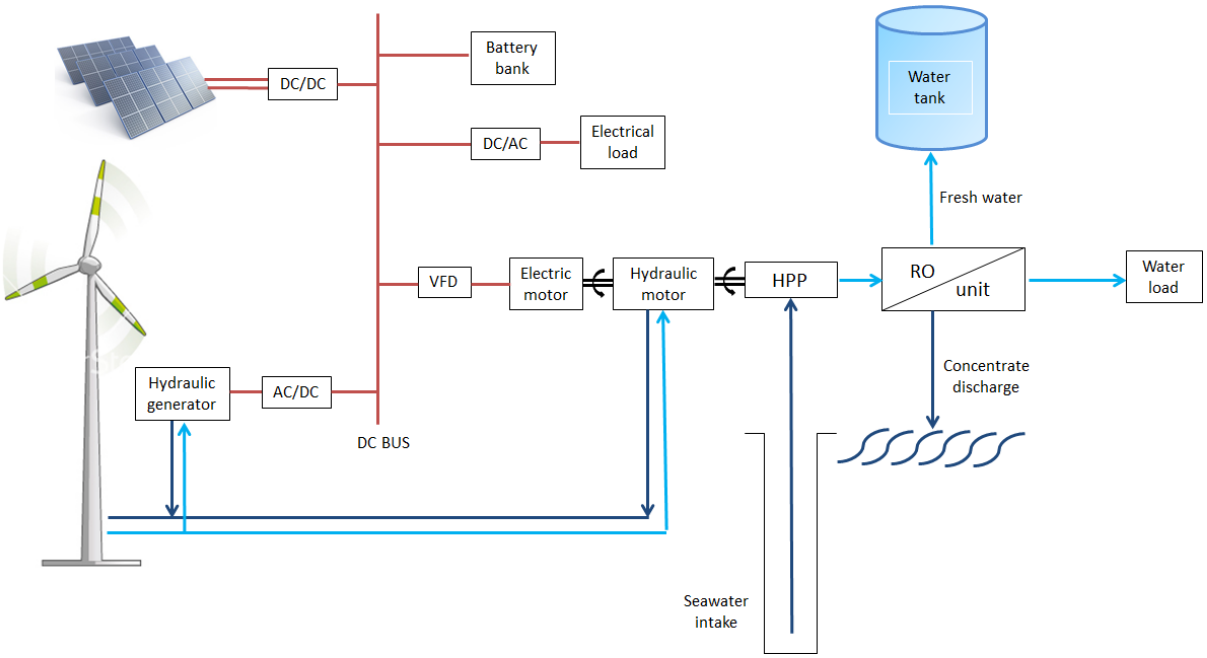

Figure 13. System configuration of the further improved FWM system.

The wind turbine, PV array and the battery bank are connected to a common DC bus. The energy produced by the wind mill and the PV system is transferred to the different energy sinks through an intelligent management system. On one hand, the battery bank, which is of lead-acid type, is charged by the wind turbine via the hydraulic generator and the PV array when excess energy is available. For this purpose, battery chargers are used which are connected to the common DC bus. On the other hand, the battery bank is used to satisfy the electricity demand and to supply the RO desalination units through the electric motor in case of low wind speed conditions and/or insufficient solar radiation. The PV power source is configured in multiple power generation blocks according to the PV panels and battery chargers nominal power ratings and the redundancy requirements. DC/AC converters are employed to interface the DC bus to the AC requirements of the electricity demand. Based on the FWM system described above, the

As explained in section 2.4, the wind mill under study is the two-bladed Lagerwey 18/80 with a nominal rating of 80 kW. However, the gearbox, high-speed shaft and electric generator are removed from the insides of the turbine and replaced with a hydraulic transmission system. According to *SolteQ Energy B.V.,* the usage of a hydraulic drive makes the FWM turbine up to 30% more efficient in terms of water production. One of the reasons for choosing a two-bladed wind mill is the fact that due to their reduced weight, they turn faster (around double the speed) than conventional three-bladed wind turbines. This comes in handy for driving the hydraulic pump placed in the nacelle which is directly connected to the wind turbine rotor.

4.2 RO unit design under variable power flow

Fundamental RO design equations and parameters

In order to achieve a better understanding regarding the choices made when designing RO units, it is considered essential to first describe the major equations involved in this process and to examine the interdependence of the main variables. The set of terms and equations used to define the parameters governing transport across a membrane are taken from [32], [70] and [71]. First and foremost, the equation for the mass balance ought to be introduced which displays the fact that the flow rate and the concentration of the feed are divided between the permeate and the concentrate:

$$Q_f * c_f = Q_p * c_p + Q_c * c_c \,. \tag{1}$$

Q and c denote the flow rate and the salt concentration, respectively, whereas the indexes are used for describing the feed, permeate and concentrate. All three flows are usually expressed in m^3/h, m^3/day, L/h or L/day depending on their magnitude whereas the salt concentration is commonly expressed in g/m^3 or ppm. The rate of product flow Q_p through a semi-permeable membrane is defined as:

$$Q_p = A * S * (\Delta P - \Delta\pi) = A * S * (TMP - \Delta\pi) \tag{2}$$

where A represents a unique proportionality constant for each membrane material type termed membrane permeability coefficient or A-value, S is the membrane surface area in m^2, ΔP is the hydraulic pressure differential across the membrane also termed transmembrane pressure (TMP) and $\Delta\pi$ refers to the osmotic pressure differential across the membrane already touched upon in section 2.3. These pressures can be expressed in bar or Pa. The TMP of the membrane system is an overall indication of the operational pressure requirement. Equation (2) clearly shows that for the feed water to flow through the membrane, the TMP has to be greater than the osmotic pressure of the solution in order to provide a positive driving force. The necessary pressure created by the high-pressure pump to move the desired permeate flow through the system is influenced by permeability of the membranes, feed water quality, temperature, recovery rate and module configuration, among others. The TMP is defined by Equation (3) as:

$$TMP = \left(\frac{P_f + P_c}{2}\right) - P_p \tag{3}$$

with P_f, P_c and P_p being the feed pressure, concentrate pressure and product pressure, respectively. As in every membrane element a small pressure drop takes place due to friction with the walls of the membranes or tubes, the overall TMP is calculated by taken an average between the feed and the concentrate pressure exiting the RO array minus the backpressure or

pressure of the permeate. The net driving force or net driving pressure (NDP) is the measure of the actual driving pressure available to force the water through the membrane. The NDP is defined as the difference between the TMP and the osmotic pressure differential across the membrane as stated by Equation (4):

$$NDP = TMP - \Delta\pi = \left(\frac{P_f + P_c}{2}\right) - P_P - \Delta\pi. \quad (4)$$

Hence, Equation (2) can be rewritten as

$$Q_p = A * S * NDP. \quad (5)$$

The level of salinity of the permeate c_p can be calculated as the ratio between water and salt flow Q_s through the RO membrane:

$$c_p = \frac{Q_s}{Q_p}. \quad (6)$$

Since no membrane rejects all salt, a simplified equation characterizing the rate of salt flow through the membrane is given by:

$$Q_s = B * S * \Delta C \quad (7)$$

where B represents a unique proportionality constant for each membrane type termed salt diffusion coefficient or B-value, S is the same membrane surface introduced earlier and ΔC is the salt concentration differential across the membrane in g/m^3. ΔC acts as the driving force for the mass transfer of salts.

Equations (5) to (7) explain important design considerations in RO systems. The permeate flow through a membrane is proportional to the NDP differential across the membrane whereas the salt flow is proportional to the concentration differential but independent of the operational pressure. This implies that an increase (decrease) in applied pressure leads to a greater (lower) water flow without changing the salt flow which in turn means that the salinity of the permeate is reduced (increased).

The product as well as the salt flow is highly affected by the recovery factor R, expressed in %, or as ratio between permeate flow and feed flow. The percentage of feed that is converted to permeate is defined as:

$$R = \frac{Q_p}{Q_f} * 100\%. \quad (8)$$

A recovery of 30% means that 30% of the feed flow is produced as fresh water while the remaining 70% are turned into concentrate. The permeate recovery of one element is between 1% and 10%, thus in order to gain a higher overall conversion factor more membrane elements must be placed in series leading to a larger total membrane surface [32]. With an increasing conversion factor, the salt concentration differential ΔC across the membrane increases resulting in a greater salt flow rate Q_s according to Equation (7). Furthermore, the osmotic pressure rises when the salt concentration in the feed-brine solution becomes greater thus reducing the NDP which at the same time decreases the product flow as indicated by Equation (4) and (5).

The feed flow is furthermore greatly affected by the water temperature. Hence, it is often corrected to a reference temperature of 25°C to account for fluctuations in water viscosity [71]. The effect of temperature on permeate flow can be evaluated as follows:

$$Q_{p,T} = Q_{p,25} * 1.03^{(T-25)} \quad (9)$$

where $Q_{p,T}$ is the permeate flow at temperature T in °C and $Q_{p,25}$ is the permeate flow at 25°C. Equation (9) clearly shows that higher temperatures lead to higher product flows as the membrane becomes more permeable. An increase in feed temperature of 1°C will cause the product flow to rise approximately 3%, assuming that other parameters are held constant [71]. As a consequence, the feed pressure is adjusted to compensate for water flow changes according to temperature fluctuations. Also, the salt diffusion through the membrane alters with temperature change approximately at the same rate as the permeate flow [71]. Hence, an increase in temperature results in lower operational pressures given that the permeate flow and all other variables are kept constant. However, as the salt flow Q_s through the membrane is not affected by pressure changes the salinity of the permeate rises.

Lastly, a short explanation of the phenomenon of concentration polarisation shall be given since its implications are not to be under-estimated. As water flows through the membrane and salts are rejected by the membrane, a naturally occurring boundary layer develops close to the membrane surface. Here, the salt concentration is greater than the salt concentration in the bulk solution. This phenomenon is termed concentration polarisation. If the feed flows at a high rate, turbulences are caused which reduce the thickness of this salt layer near the membrane surface whereas at low feed flow rates concentration polarisation has a major impact on RO system performance. The same applies to high recovery rates at which the difference between the wall and bulk concentration can be substantial [71]. Concentration polarisation results in a rising osmotic pressure at the membrane surface thus reducing the NDP and with it the permeate flow according to Equation (5). In addition, the salt flow Q_s increases as the salt concentration differential is larger as it can be seen in Equation (7).

The discussion of Equations (1) to (9) are an attempt to provide the reader with a basic understanding of the major variables involved in the RO process. It clearly demonstrated that the design of RO plants is a tedious task which requires much knowledge concerning plant performance when specific variables and thus operating conditions are altered. At this point, it should however be noted that many other equations and parameters such as pH and fouling factor are considered in the design and simulation of RO units within software environments such as ROSA.

RO operation window

RO water desalination units are usually designed to run 24/7 at a constant flow rate. This is however not always feasible, especially in off-grid situations where power supply can be somehow unpredictable when renewable energy sources are employed. As discussed in section 3.2.3, some research papers have recently been published presenting solutions in order to tackle this issue. One of the most promising options is the introduction of a wide operating window meaning that fresh water is produced at variable flow rates and pressures depending on the available power. Hence, instead of a fixed duty point, the RO plant can be operated at a duty range. This concept has first been introduced in the work of Feron in which the author establishes an operational window for which a membrane can safely be run [72]. It is defined as the area limited by the extremes of the following operational parameters:

- maximum feed pressure (due to limited mechanical resistance of the membrane),
- maximum brine flow rate (due to membrane deterioration),
- minimum brine flow rate (due to precipitation which leads to membrane fouling),
- maximum product concentration (occurs when applied pressure is too low) [72].

Figure 14 illustrates an exemplary operational window bounded by feed pressure, brine flow and concentration limits. All hydraulic conditions within this area are valid duty points of the plant.

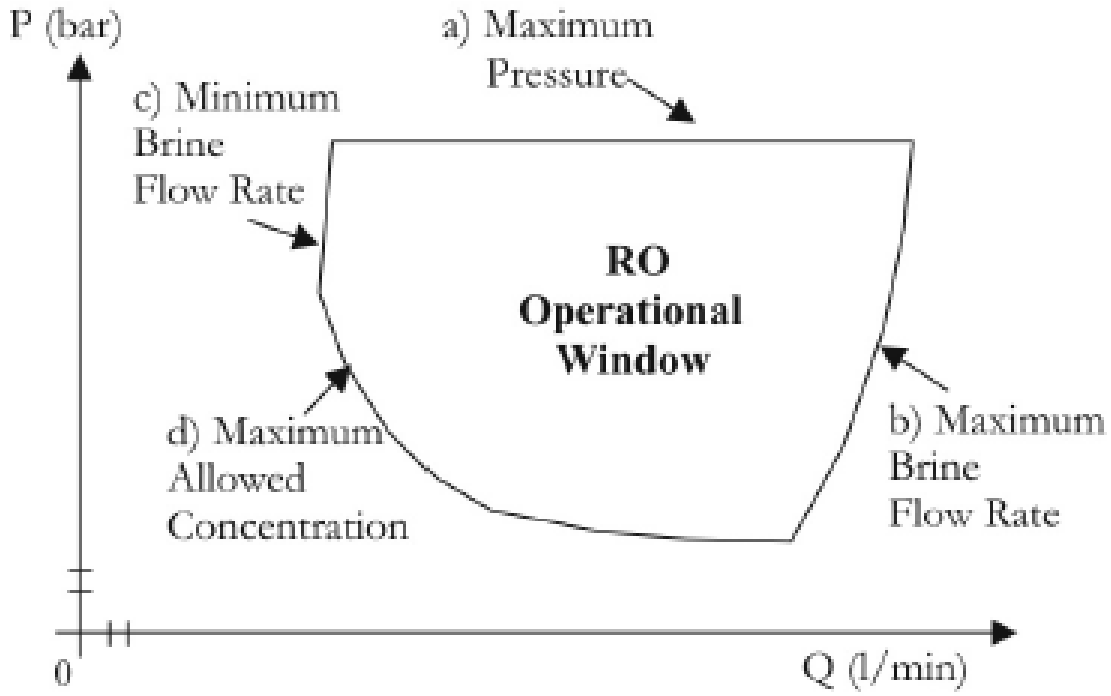

Figure 14. RO membrane operational window [27].

Figure 14 shows that the maximum feed pressure is represented by a horizontal line meaning that it is a set number for a specific membrane type irrespective of the magnitude of the feed or brine flow. The recommended pressure limit for SWRO desalination is usually in the order of 60-70 bar depending on the manufacturer [32]. With regards to the maximum concentrate flow rate, their respective curves reflect the fact that at high feed flows greater pressures need to be applied in order to increase the recovery factor and with it the permeate flow. As a result, the relative brine flow rate decreases avoiding the crossing of the upper limit. The opposite applies to the lower limit of the brine flow rate. This phenomenon becomes apparent by examining Equations (1), (2) and (8). Lastly, the curve of the maximum product concentration can be explained by looking at Equations (5) to (8). Decreasing brine flows mean decreasing feed flows which lead to higher recovery factors, assuming that the product flow rate is kept constant. A higher conversion leads to greater differences in salt concentration across the membrane, thus increasing the salt flow rate and product concentration, according to Equation (6) and (7). In addition, concentration polarisation occurs at the membrane surface. Due to these reasons, the osmotic pressure rises resulting in a lower NDP. Hence, to stay within a pre-defined permeate concentration value, the permeate flow needs to be increased which can be achieved by enhancing the feed pressure. This phenomenon is especially evident when the RO system is run at low feed flows at which concentration polarisation has a greater impact on system performance.

Design of RO unit

For the design of RO systems several software tools can be used in order to simulate the plant's performance. The most common software tools freely available for download are ROSA by *DOW Chemical*, IMSDesign by *Hydranautics*, Winflows by *GE Water* and KMS ROPRO by *KOCH Membrane Systems*. In the framework of this thesis, ROSA 9.1, the latest version, has been chosen as a suitable simulation environment since it has proven notably user-friendly. It includes component models for all the membrane elements available from the manufacturer *DOW Chemical*. The software allows the user to define variables such as feed water composition, pre-treatment method, water temperature, pH, pump efficiency, membrane type, number of membrane elements and pressure vessels, feed or permeate flow rate, recovery factor or feed pressure. Furthermore, trains and arrays of the membrane units can be constructed with multiple stages or passes. The user can run simulations with the proposed system in order to predict overall performance and estimate pump energy consumption and power requirements.

In ROSA, the tedious calculations for a specific RO design are performed for each individual membrane element based on trial-and-error calculations and feedback loops. All the operating conditions of the first element must be known, including the feed pressure. Then the flow, pressure, etc. of the concentrate, which is the feed to the second element, can be calculated. After obtaining the results for all the elements, the original feed pressure may be too high or low, so the trial and error process starts with a new pressure [32]. The optimisation of the FWM system would become very cumbersome if these calculations were to be incorporated in the Matlab model. Also, it is not the aim of the thesis to provide exact calculations and optimised RO unit designs which would be highly time-consuming, but rather give an indication of the FWM microgrid configuration and its overall system cost behaviour for a given location depending on its water and electricity supply reliability. Hence, the objective is to find a way to approximate the calculations for a RO plant which can be used within the FWM optimisation simulation.

The approach employed in this thesis is to design, with the help of ROSA, a single pressure vessel for seawater desalination with acceptable energy consumption values. Consequently, the unit's performance is simulated multiple times under different water flows and pressures in order to create an operational window so that the unit can operate under intermittent power supply. The recovery ratio remains fixed during these simulations. The lower and upper limits of feed flows and the required pressures as well as concentration limits are shown by ROSA as the program gives warnings when limits are crossed. The maximum and minimum power requirements with regards to the operational window of the designed pressure vessel can thus be calculated. It should however be noted that the design employed in this thesis does not consider the limits of the maximum and minimum brine flow rate set by Feron. With this approach an even wider operation window is achieved leading to an increased permeate production in addition to less interruptions of the RO unit. As discussed above, crossing these very limits leads to membrane

deterioration and fouling which will be offset in the model by decreasing the lifetime of the membranes in the cost calculations. Thus, the operation limits respected in the design of the RO unit do only refer to the maximum feed pressure as well as the maximum product concentration to a limited extent.

The specific energy consumption varies within this operation window meaning that, for instance, a change in pumping power of 20% is not equal to a 20% change for the production of fresh water. Several points within the limits were calculated and consequently interpolated in order to display the relationship in the form of a function which reflects the relative changes of pumping power versus water production. When increasing the number of pressure vessels at the same rate as the feed water flow, it was found that the function remains the same. The simulation and optimisation procedure of the FWM system will make use of this fact by choosing the number of pressure vessels as one of the decision variables. This means that based on the input power to the RO plant and its power requirement which is dependent on the number of RO vessels, a fixed operating point is imposed if it lies within the operation window.

The following example serves to illustrate and explain more thoroughly the approach taken. For this purpose, a standard seawater composition of 35 000 ppm with a temperature of 25°C is used as feed water and it was chosen to employ 5 membrane elements of the SW30-4040 type per pressure vessel with an active surface area of 7.3 m^3 each. Furthermore, the recovery factor is set at 35%. As a result, for this specific RO design, the minimum and maximum allowed feed flow rates and pressure levels amount to 0.36 m^3/h and 36.7 bar as well as 3.33 m^3/h and 61 bar, respectively. Based on the feed water input into a single RO unit, the specific operating range of the above introduced RO unit design is displayed in Figure 15. If the number of RO units is increased, the feed water input doubles, whereas the respective pressure remains the same.

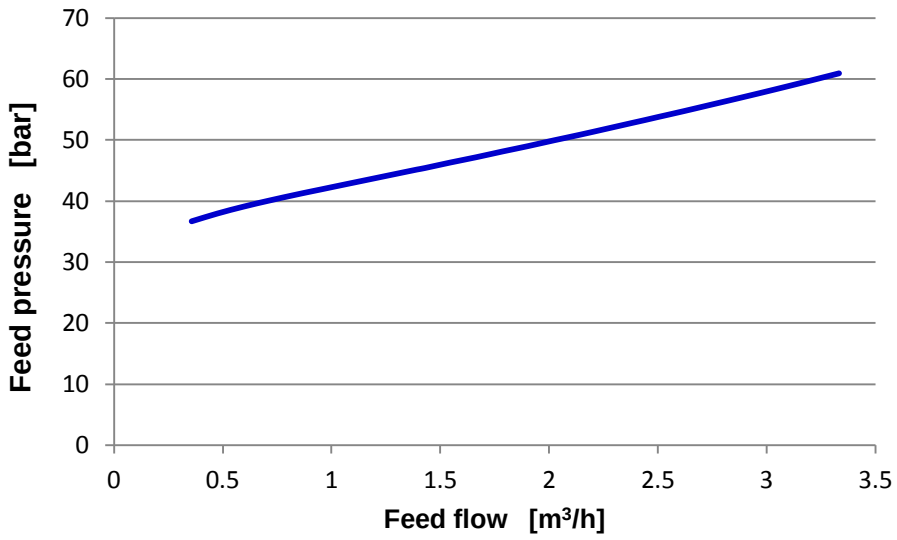

Figure 15. Operating range for a single RO unit designed in ROSA.

Based on the operating range shown in Figure 15, the minimum and maximum power requirements which determine the limits of the operational window is calculated to be 0.46 kW and 7.1 kW, respectively, assuming a constant pump efficiency of 80% over the whole operating range. Figure 16 displays the relative change in permeate production, salinity level and SEC as a function of the relative RO unit power requirement of a single pressure vessel. The same relationship applies when more pressure vessels are employed within the RO plant.

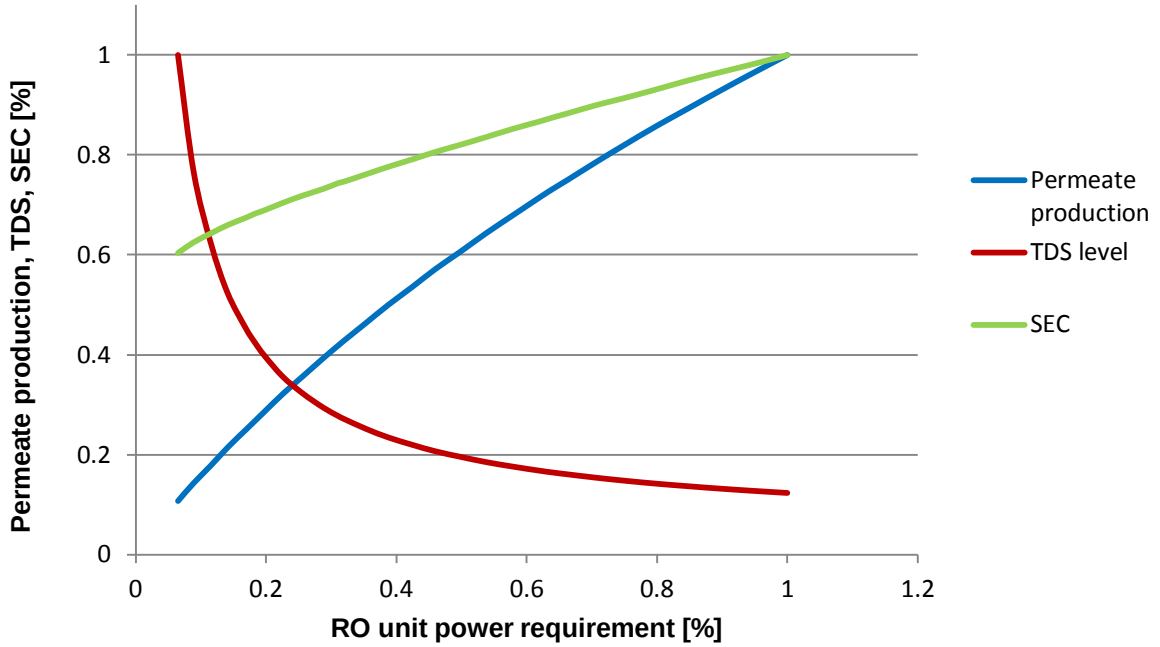

Figure 16. Relative permeate production, TDS level and SEC vs. available power for the specified RO system design.

Figure 16 clearly shows that the relationship between power consumption and permeate production is not linear. The function rather reflects the fact that at lower feed flows/pressures less energy is used in order to produce one m^3 of fresh water. Although the specific energy consumption is smaller compared to higher feed/permeate flows, the permeate quality in the example above deteriorates from 150 ppm to 1211 ppm when comparing the upper and lower feed flow limit. The reason for this is that at higher feed flows increased pressures are applied leading to a purer product water [73]. It can also be seen that at low pumping powers (low feed flows) the salinity level of the product water increases exponentially, however, when added to a fresh water storage tank this small amount of high salinity water does not really impact the quality of the fresh water.

The width of the operating window is considerably influenced by the design and geographical location of the system. The same applies to the relationship between relative pumping power requirements and permeate production as well as salinity level, however to a smaller extend. Different designs have been simulated with the help of ROSA by changing the feed water temperature, recovery factor, number and type of membranes. It has been found that the

relationships shown in Figure 16 disclose a very similar behaviour for all designs proving that the approach taken in the FWM system model for the calculation of fresh water production can be applied to different RO designs.

4.3 Mathematical formulation and system integration

The sizing of the FWM system is influenced by the performance of the different components and the interaction among them. Hence, in order to evaluate and predict the system's performance, the individual power sources need to be modelled first. The operation of the FWM system is simulated for an entire year with an hourly time step during which the power generated by the wind turbine and the PV system, the power consumption of the equipment, the flow rate and pressure of the HPP and the water as well as electricity load are assumed to be constant. As an hourly time step is employed, the power generated and consumed is equal to the respective energy and water capacity. It should be noted that for simplicity reasons the operation of the RO system is described based on power flows. The power flows are however a function of pressure and feed flow rate which in turn are dependent on the torque and the shaft speed of the motor. For positive displacement pumps and motors which are the ones employed in the FWM system, motor shaft speed and flow rate are directly proportional.

A PV system usually consists of different units with a pre-defined number of PV modules connected in series and parallel, respectively. Each of these PV units includes a solar charge controller (DC/DC converter) which regulates the voltage and current coming from the solar panels going to the battery bank. It basically keeps the batteries form overcharging. The number of PV modules connected in series N_{pv}^{s} and parallel N_{pv}^{p} is dependent on the solar charge controller's maximum input voltage V_{ch}^{max}, expressed in V, and maximum input current I_{ch}^{max}, expressed in A, the open-circuit voltage V_{oc}^{STC} and short circuit current I_{sc}^{STC} of the employed PV module under standard test conditions (STC). STC indicated the performance of PV modules under specified conditions, namely a cell temperature of 25°C and an irradiance of 1000 W/m^2 with an air mass of 1.5. N_{pv}^{s} and $N_{pv}^{p}$are calculated according to Equations (10) and (11):

$$N_{pv}^{s} = \frac{V_{ch}^{max}}{1.2 * V_{oc}^{STC}} \quad (10)$$

$$N_{pv}^{p} = \frac{I_{ch}^{max}}{1.25 * I_{sc}^{STC}}. \quad (11)$$

The I_{sc} and V_{oc} under STC are in most cases the highest voltage and current values a PV module can reach. However, a PV module's voltage and current output are variable values that are primarily affected by temperature. Under extreme weather conditions, i.e. very low or high temperatures, the V_{oc}^{STC} and I_{sc}^{STC} can be exceeded. Hence, according to Equations (10) and (11), they are multiplied by a safety factor of 1.2 and 1.25, respectively, as the limits of V_{ch}^{max} and I_{ch}^{max} should never be surpassed [74]. In the event that the number of modules connected in series or

parallel does not result in an integer, the program uses the floor function which rounds it to the nearest integer less than or equal to the value.

The total number of solar charge controllers N_{ch} which is equal to the number of PV power units, depends on the number of modules connected in series N_{pv}^{s} and the number of modules connected in parallel N_{pv}^{p} within one PV power unit as well as the total number of PV modules N_{pv} and is calculated as follows:

$$N_{ch} = \frac{N_{pv}}{N_{pv}^{s} * N_{pv}^{p}}. \quad (12)$$

In the event that the number of charge controllers does not result in an integer, the program uses the ceil function which rounds them to the nearest integer greater than or equal to the value.

The nominal power of the PV system P_{pv}^{nom} is calculated according to Equation (13):

$$P_{pv}^{nom} = N_{pv} * P_{module}^{nom} \quad (13)$$

where P_{module}^{nom} represents the nominal power of one single PV module.

In order to calculate the hourly output power $Pm_{unit}(t)$ (W) of each PV power unit at hour t ($1 \leq t \leq 8760$) the technical parameters of the respective PV module under STC and the hourly temperature of the surrounding $T_a(t)$ (°C) as well as the hourly global solar radiation $G(t,\beta)$ (W/m^2) incident on the PV module installed at tilt angle β (°) are used:

$$T_c(t) = T_a(t) + \frac{NOCT - 20°C}{800} * G(t,\beta) \quad (14)$$

$$V_{oc}(t) = V_{oc}^{STC} + K_V * (T_c(t) - 25°C) \quad (15)$$

$$I_{sc}(t,\beta) = [I_{sc}^{STC} + K_I * (T_c(t) - 25°C)] * \frac{G(t,\beta)}{1000} \quad (16)$$

$$Pm_{unit}(t,\beta) = N_{pv}^{s} * N_{pv}^{p} * V_{oc}(t) * I_{sc}(t,\beta) * FF \quad (17)$$

where $T_c(t)$ represents the hourly cell temperature, $NOCT$ is the Nominal Operating Cell Temperature provided by the manufacturer, both expressed in °C, $V_{oc}(t)$ the hourly open-circuit voltage with K_V being the open-circuit voltage temperature coefficient (a negative value as inversely related to the temperature), expressed in V/°C, $I_{sc}(t,\beta)$, the hourly short circuit current with K_I being the short circuit current temperature coefficient in A/°C and FF represents the fill factor, expressed in %, of the respective PV module [5].

The actual hourly PV power output $Ppv_{unit}(t,\beta)$ from the solar charge controller of each PV unit is dependent on its efficiency according to Equation (18):

$$Ppv_{unit}(t,\beta) = Pm_{unit}(t,\beta) * \eta_{ch} \quad (18)$$

where η_{ch} (%) represents the efficiency of the charge controller which is influenced by the battery charging algorithm. If the solar charge conroller operates according to the Maximum Power Point Tracking (MPPT) mode, its efficiency can be close to 1, else it has a much lower value [75].

Finally, the total PV power produced $Ppv_{tot}(t,\beta)$ by the PV system is calculated according to Equation (19):

$$Ppv_{tot}(t,\beta) = N_{ch} * Ppv_{unit}(t,\beta). \quad (19)$$

The output power of a wind turbine is mainly influenced by the power curve of the chosen wind turbine, the wind speed distribution at the location under study and the height of the tower. The power output of the wind turbine versus the wind speed depends on the size and type of the chosen wind turbine and it is provided by the manufacturer in the form of a power curve. For the FWM model, the values of the wind power curve of the Lagerwey 18/80 are used, however with the expected improved efficiency as shown in Figure 8. The wind power output of the chosen wind turbine $Pwind(t,h)$ at hour t and at a height h is calculated using a look-up table which is introduced into the model in order to simulate the wind turbine performance. When the wind speed is less than the specified cut-in wind speed v_{cut-in} or greater than the cut-out wind speed of the turbine $v_{cut-out}$ the power production of the wind turbine is equal to 0.

As the wind speed measurements of a given site are often taken at altitudes different than the hub height of the turbine, it is important to translate the measured data from lower altitudes to the height of the turbine rotor. This is often done by means of the logarithmic wind profile provided in Equation (20):

$$v(t,h) = v_{ref}(t) * \frac{\ln\left(\frac{h}{zo}\right)}{\ln\left(\frac{h_{ref}}{zo}\right)} \quad (20)$$

with h being the hub height of the chosen wind turbine in m, v_{ref}, expressed in m/s, is the measured wind speed at the reference height h_{ref} and zo is defined as the surface roughness (m) representing a characteristic of the type of terrain [76]. The values of the ground roughness zo go from 0.0002 m which is found over the open sea, to a value of 1.6 m which is used in very large cities with tall buildings and skyscrapers [77].

The hydraulic power produced by the wind turbine which is used for electricity production $Pwind_{el}(t,h)$ is transferred through the hydraulic circuit to a hydraulic motor which in turn drives

an electric generator. The AC power output of the generator is input into an AC/DC battery charge controller which inverts and regulates the voltage and current coming from the generator to the nominal DC bus voltage V_{bus}. The effective electrical power $P_{gen}(t,h)$ generated from the wind turbine is computed as follows:

$$P_{gen}(t,h) = Pwind_{el}(t,h) * \eta_{gen}(t) \quad (21)$$

with $\eta_{gen}(t)$ being the total efficiency calculated by multiplying the individual efficiencies of the hydraulic motor, the generator and the charge controller. The efficiency η_{gen} varies in time as it is influenced by the input power $Pwind_{el}$ and the nominal power of the generator P_{gen}^{nom}.

The number of batteries connected in series in each of the parallel connected battery strings which make up the battery bank, N_{bat}^{s}, is related to the nominal DC bus voltage V_{bus} and the nominal voltage of each individual battery V_{bat} according to Equation (22):

$$N_{bat}^{s} = \frac{V_{bus}}{V_{bat}}. \quad (22)$$

The nominal capacity of the battery bank C_{bb}^{nom}, expressed in Ah, is dependent on the total number of batteries N_{bat}, the number of series connected batteries N_{bat}^{s} and the nominal capacity of each individual battery C_{bat}^{nom} according to Equation (23):

$$C_{bb}^{nom} = \frac{N_{bat}}{N_{bat}^{s}} * C_{bat}^{nom}. \quad (23)$$

The maximum allowed battery depth of discharge DOD (%) is the minimum capacity level of the battery bank during discharging C_{bb}^{min}. The degradation and thus lifetime of the batteries are very much influenced by this value. For this reason it should be chosen with care by the user of the simulation program at the beginning of the optimisation process:

$$C_{bb}^{min} = (1 - DOD) * C_{bb}^{nom}. \quad (24)$$

The capacity of the battery bank $C_{bb,soc}(t)$ varies throughout the year depending on the hourly generated electricity from the PV system and the wind turbine and the electricity consumption of the given location according to Equation (25):

$$C_{bb,soc}(t) = C_{bb,soc}(t-1) + \eta_{bat}(t) * \frac{P_{bb,flow}(t)}{V_{bus}} * \Delta t \quad (25)$$

where $C_{bb,soc}(t-1)$ is the battery bank capacity at hour $(t-1)$, $P_{bb,flow}(t)$ is the power flow to the battery, in which case it is a positive value, or from the battery, in which case it is a negative value, and $\eta_{bat}(t)$ represents the round-trip efficiency of the battery bank which is 1 if the battery

is being discharged and 0.8 if the battery is being charged. The state of charge of the battery bank needs to be within its limits according to Equation (26):

$$C_{bb}^{min} \leq C_{bb,soc}(t) \leq C_{bb}^{nom}. \quad (26)$$

As the battery degradation and lifetime is furthermore influenced by the amount of current being drawn from and supplied to it, the maximum allowed battery bank charging and discharging current is set to $C_{bb}^{nom}/5h$ [5].

The electrical load of the given location can be provided by the PV system, the hydraulic wind turbine via the generator as well as the battery bank if the available power coming from the renewable energy sources is insufficient. The total DC power input $P_{load}(t)$ to the DC/AC inverter at hour t is calculated according to Equation (27):

$$P_{load}(t) = \frac{P_{demand}(t)}{\eta_{inv}} \quad (27)$$

where $P_{demand}(t)$ is the AC power output from the inverter supplying the electricity demand and η_{inv} represents the efficiency of the DC/AC inverter.

The hydraulic power produced by the wind turbine which is used for water production $Pwind_w(t,h)$ is transferred through the hydraulic circuit to a hydraulic motor which in turn drives the HPP. The effective hydraulic power $P_{HM}(t,h)$ generated from the wind turbine is calculated according to Equation (28):

$$P_{HM}(t,h) = Pwind_w(t,h) * \eta_{HM}(t) \quad (28)$$

where $\eta_{HM}(t)$ represents the efficiency of the hydraulic motor. It is time-dependent for it varies at every time step t according to the input power $Pwind_w$ and the nominal power of the hydraulic motor P_{HM}^{nom} as well as the HPP which are equal. The rating of the hydraulic motor and HPP are assumed to be equal as the RO unit should be able to be operated at nominal power by the wind turbine without the assistance of the electric drive.

The power supply to the RO system can additionally be assisted by an electric motor which is directly coupled to the hydraulic motor and the HPP. This electric motor is preceded by a DC/AC inverter and further equipped with a variable speed drive (VSD) in order to align the speed of the shaft with the one of the hydraulic motor. The electric motor can be driven by the electricity produced from the PV system as well as the battery bank. The actual power output of the electric motor $P_{EM}(t)$ is computed according to Equation (29):

$$P_{EM}(t) = P_{el}(t) * \eta_{EM}(t) \quad (29)$$

with $P_{el}(t)$ being the electrical power input into the inverter and $\eta_{EM}(t)$ representing the total efficiency which takes into account the efficiency of the electric motor, the VSD as well as the DC/AC inverter. The efficiency $\eta_{EM}(t)$ varies in time because it is dependent on the input power P_{el} and the nominal power of the electric motor P_{EM}^{nom}.

The power input into the HPP $P_{HPP}(t)$ is the sum of the power output from the electrical and the hydraulic motor as described in Equation (30):

$$P_{HPP}(t) = P_{EM}(t) + P_{HM}(t). \quad (30)$$

As explained in section 4.2, the RO system has a maximum and minimum power requirement with regards to the operational window of the designed pressure vessel in order to produce fresh water. The maximum and minimum power requirements of the RO system P_{RO}^{min} and P_{RO}^{max} are related to the number of pressure vessels N_{RO} and the upper and lower power consumption limits $P_{RO,unit}^{max}$ and $P_{RO,unit}^{min}$ of a single RO unit as follows:

$$P_{RO}^{min} = P_{RO,unit}^{min} * N_{RO} \quad (31)$$

$$P_{RO}^{max} = P_{RO,unit}^{max} * N_{RO}. \quad (32)$$

The power output of the HPP $P_{RO}(t)$ at time t needs to be within these limits in order to produce fresh water:

$$P_{RO}^{min} \leq P_{RO}(t) \leq P_{RO}^{max}. \quad (33)$$

If the total input power from the hydraulic as well as electric motor to the HPP is insufficient to perform the desalination process, the RO system is switched off and only turned on again when enough power is available. The power output $P_{RO}(t)$ can be calculated according to Equation (34):

$$P_{RO}(t) = P_{HPP}(t) * \eta_{HPP} = Q_f * P_f * \eta_{HPP} \quad (34)$$

where η_{HPP} represents the efficiency of the HPP. The feed flow $Q_f(t)$, expressed in m^3/s and the feed pressure $P_f(t)$, expressed in Pa, which depend on the hourly input $P_{RO}(t)$ are computed according to a look-up table loaded into the model.

The quantity of potable water production by the desalination system depends, among others, on the power input into the HPP and thus the input feed pressure and feed flow which vary in time, the number of RO units or pressure vessels and the size, type and number of membranes used in a pressure vessel. Once the design of a single pressure vessel has been chosen, its hourly fresh water production volume $W_{RO,unit}(t)$, expressed in m^3, is determined through a look-up table inserted into the model. This look-up table is based on the relative permeate production against available power curve for a specific RO unit design calculated in a previous step. An example of such a curve is given in section 4.2, Figure 16. The corresponding feed pressures at different feed flow rates were obtained using the simulation program ROSA with the same elements and at the same conditions. If another RO system design is chosen and/or the salt water parameters change, a new series of feed pressures and feed flows has to be computed and hence a new look-up table needs to be loaded into the optimisation model. The total desalinated water produced $W_{RO}(t)$ at hour t which corresponds to the power input $P_{RO}(t)$ can be calculated as follows:

$$W_{RO}(t) = N_{RO} * W_{RO,unit}(t). \quad (35)$$

In the event that the water demand $W_{demand}(t)$ is smaller than the fresh water production at hour t, the difference of desalinated water can be stored in a water tank for later use. Hence, the water level in the tank $W_{WL}(t)$ varies throughout the year, but must stay within the limits set by the system designer at the beginning of the optimisation process:

$$W_{WL}^{min} \leq W_{WL}(t) \leq W_{WL}^{max}. \quad (36)$$

Lastly, a short note on the efficiencies of the respective components part of the FWM system should be added at this point. As the renewable energy sources are fluctuating and there is not always sufficient power available from the battery bank, most components such as the motors and the generator, operate at part-load at certain times meaning that for most devices the efficiencies would be lower than the one at nominal power. Instead of a fixed duty point, there will be a duty range for most of the devices which in many cases can be very wide. Hence, it is pivotal to consider part-load efficiencies of the FWM equipment, i.e. efficiencies which are dependent of the respective hourly power input and thus time-varying, within the simulation model. The efficiency of the solar charge controller can safely be assumed to be constant throughout the simulation period due to its working principle [75]. Also, the efficiency of the HPP is assumed to be constant because positive displacement pumps (as the one employed in the FWM system) are characterised by the fact that the pressure is almost independent of pump speed and thus flow rate as they are directly proportional. Hence, a PD pump can be run at almost any point on its curve without with only minor differences in efficiency [78]. The efficiencies of the hydraulic motors (gear-pumps), the generator and the electric motor are however assumed

to be load-dependent and thus time-dependent. Since the size of the respective components is only determined after the optimisation process, generic efficiency curves of each device are employed within the simulation model. These efficiency curves are attached in the Appendix and introduced as look-up tables into the model.

4.4 System operation strategy

The results of the simulation and optimisation process are greatly dependent on the system operation strategy employed for the FWM model. The operation control is the heart of the FWM system that provides the information and communication among various components. It regulates the output of the renewable energy sources and determines when the battery is used in addition to defining when energy needs to be dumped. It also protects the battery bank from overcharging and makes sure to operate the batteries in a prescribed manner. The system operation strategy defines how to distribute the energy from the different energy sources to the respective energy sinks. Since the FWM system aims at meeting the electricity as well as water demand of a given location, two different loads have to be satisfied at the same time. Hence, the system includes two types of power demand: the power load for satisfying the electricity demand and the power load for the RO system which meets the fresh water demand of the location. The electricity load is an instantaneous one whereas the water load can potentially represent a deferrable load in case that the water tank contains sufficient water for the very time step.

For the FWM system three different control strategies are employed which either prioritise the electricity demand or the water demand first, in case insufficient energy is available for meeting both loads. Which of the control strategies is chosen at hour t depends on both the water level in the storage tank and the SOC of the battery bank. These two weighting factors, i.e. w_{wt} and w_{SoC} which can take a value between zero and one, form part of the decision variable vector and hence vary for each yearly simulation. Their value also determines the extent to which the electricity load is prioritised over the water load or vice versa.

In the following, the energy and water flows among the FWM system subunits are described for the three control strategies:

- $W_{SOC}(t-1) \leq w_{wt} * W_{WL}^{max}$
    - Fresh water production is prioritised over electricity demand coverage.
    - The RO unit operates at its nominal power if sufficient energy is available and the respective component capacities allow for it.
    - The energy sources of the FWM system are used in the following order for operating the RO unit: wind energy, electricity generated from PV system, electricity from battery bank.
    - If sufficient energy is still available, it is used for covering the electricity demand at hour t, else the battery bank is charged.

- $W_{SOC}(t-1) > w_{wt} * W_{WL}^{max}$ AND $C_{bb,soc}(t-1) \leq w_{SOC} * C_{bb}^{nom}$
    - Meeting the electricity demand is prioritised over fresh water production.
    - The RO unit only operates if the generator has reached its maximum capacity and there is any remaining wind energy left in order to run the HPP at nominal or lower than nominal flows.
    - Electricity generated by the PV system or stored in the battery bank is not used for fresh water production. The priority is rather set in charging the battery bank.
    - Electricity generated by the PV system is only used for fresh water production in case the current going to the battery bank exceeds the maximum allowed current or the maximum battery SOC is reached.

- $W_{SOC}(t-1) > w_{wt} * W_{WL}^{max}$ AND $C_{bb,soc}(t-1) > w_{SOC} * C_{bb}^{nom}$
    - Meeting the electricity demand is prioritised over fresh water production.
    - In order to meet the electricity demand, the energy sources of the FWM system are used in the following order: PV energy, battery bank, wind energy.
    - Fresh water is only produced if there is any surplus wind or PV energy.
    - The battery bank is not used for fresh water production.

The water demand $W_{demand}(t)$ is at all times covered from the water storage tank independent of the control strategy used and whether the desalination plant is in operation or not. In case that the water tank is empty and hence not sufficient water can be drawn from it, the water demand is regarded as uncovered at hour t.

Lastly, it should be noted that the nominal capacity of each component, namely the hydraulic and electric motor, the HPP and the generator, which has been determined by the optimisation program before performing the yearly simulation, cannot be exceeded. Additionally, if the battery has reached its maximum SOC or the maximum charging or discharging current is exceeded, the excess energy must be dumped.

The FWM system modelling and energy management strategy described above is used to simulate the system operation on a yearly basis. It is incorporated into the optimization process in order to analyse the performance of the various solutions proposed by the optimization algorithm.

4.5 Model assumptions

The model of the FWM system which has been developed for the optimal sizing procedure is based on a number of assumptions. First and foremost, as explained in section 2.4, the power

curve of the Lagerwey 18/80 wind turbine is assumed to experience an efficiency increase not only at its rated wind speed but also at lower than rated wind speeds by employing the hydraulic transmission system. This assumption is however based on expected values; the testing of the system is in progress at this moment at the WaterCampus in Leeuwarden. Also, in case the Lagerwey 18/80 is oversized for the fresh water and electricity requirements at a certain location, two options for dissipating the surplus energy exist. The nacelle can be moved out of the wind by means of its active yawing system once the nominal ratings of the hydraulic motors are reached. Additionally, there is a separate hydraulic circuit in place where the oil gets heated up and a cooling system dissipated the heat [36], [79].

In order to transport the seawater to the RO unit for desalination, a seawater pump needs to be in place. The power required for this undertaking is not taken into account in the optimal sizing calculations. It should however be noted that the power requirements are far smaller when compared to the HPP which is why its consideration is not expected to have an impact on the results. Also, as explained in section 2.3, once the RO system is turned off due to insufficient power or a full water tank, the membranes should be flushed with fresh water from the storage tank in order to avoid fouling. For the membrane size (4'') employed in the RO design in this thesis, one pressure vessel should be flushed with about 10 l/min for 30 minutes amounting to about 0.3 m^3 per cleaning procedure [32]. The flushing process has however not been included in the modelling of the FWM system. Preliminary results have shown that for the specific location of the case study, the RO unit is shut down around once a day. Compared to the daily fresh water requirements, the amount of water needed for flushing is thus negligible. With respect to the temperature and salinity level of the seawater, it is assumed that these variables stay constant throughout the year. As explained in section 4.2, higher water temperatures make the membranes more permeable leading to an increased product flow but also salt flow. The market of the FWM is aimed at locations in warm regions such as close to the equator where temperatures do not vary much. Consequently, assuming constant temperatures seem to be a fair assumption.

With respect to the model of the PV system, the global irradiance is used as input and no difference is made between direct and diffuse radiation. Generally speaking, the larger the percentage of diffuse radiation, the less the total insolation. However, since the market of the FWM system is aimed at countries with tropical climates where the tilt angle of the PV module would inherently be close to 0°, most of the diffuse light would be caught. Also, in tropical places the ratio of direct to diffuse radiation is much greater [80]. Lastly, the FF of the photovoltaic panels is assumed to be constant and not dependent on temperature and other environmental factors.

The efficiency and capacity of a lead-acid battery is dependent on multiple factors such as the battery SOC, the charge/discharge rate (C-rating) and the temperature. The capacity of the

battery mainly depends on the charging/discharging current, but also on the temperature and the general history of the battery. The rated capacity is usually measured by its performance over 20 hours of constant current discharge at a temperature of 20°C (0.05C rate). When the charge/discharge current is less than the 20 hour rate, the capacity increases and vice versa. Additionally, raising ambient temperature increases the capacity, however, at the same time, decreases lifetime. The efficiency of the battery is mainly a function of the battery SOC and again, the rate of charge or discharge with higher currents exhibiting lower efficiencies [81]. The SOC of the battery while being charged does not increase linearly over time, even under a constant charging rate. With the battery at 50% or less of its rated capacity, the charge efficiency may be over 90%, however dropping to about 60% when the battery is above 80% charged. Overall, an efficiency level of 85% is often assumed [82]. Although a lead-acid cell battery shows a highly non-linear behaviour with respect to the above mentioned variables, the model in the framework of this thesis is assumed to be linear. The drastic decrease in capacity with high charging currents is accounted for in the battery model of the FWM system by limiting the charging/discharging current to a 0.2C rate. Additionally, the round-trip efficiency is assumed to be 80% and a self-discharge rate is not taken into account as lead-acid batteries are known for having one of the lowest self-discharge rates. It is also assumed that the capacity of the battery remains constant during its lifetime.

For the FWM system components like the hydraulic and electric motor, the generator and the HPP, generic efficiency curves are employed. However, depending on the capacity ratings calculated by the simulation and optimisation procedure, the component efficiencies with higher nominal power are generally higher and vice versa. Also, the start-up times of the different FWM components (wind turbine, motors, HPP etc.) are considered negligible in this model due to hourly simulations. Hence, it is assumed that the power output can increase from zero to nominal power within each time step. The same applies to the PV panels which are assumed to react immediately to the solar radiation. There is no time delay of the PV panels.

Due to the inherent nature of solar and wind energy in fluctuating energy production, high-frequency switching of devices can be the result. The model assumes that this frequent on and off switching of components has no impact on the subsystems. Moreover, failures of the different FWM system components and maintenance activities are not included in the yearly simulation. Lastly, due to smaller distances required for power transportation when using an autonomous microgrid in rural areas, transportation losses are not taken into account as they are less significant.

5

Optimisation

This chapter provides the optimisation framework of the thesis. First, the optimisation problem is set up and the various decision variables, their bounds and the objective functions are determined. Next, the functioning of the GA optimisation method is explained with a focus on the NSGA II technique which is used in the 'gamultiobj' optimisation solver in Matlab. This is followed by an overview and an explanation regarding the implementation of the proposed optimal sizing procedure of the FWM system. Finally, the different GA operators and options are envisaged and specified for the case study.

5.1 Problem formulation

This section is divided into two parts: the first part introduces and explains the decision variables, bounds and constraints of the optimisation problem. The second part describes the three conflictive objective functions which are employed in the triple-objective optimisation procedure within the Matlab solver. The first objective function aims at minimising the costs of the FWM system, whereas the second and third objective functions maximise the FWM system reliability, a fundamental issue in the design of stand-alone microgrids which completely depend on oscillating renewable energy sources.

5.1.1 Decision variables and constraints

The optimisation problem of the FWM system includes eight independent variables which have already been introduced and discussed in the modelling and system operation strategy sections in section 4.3 and 4.4:

N_{pv} – Number of PV modules [-],

N_{bat} – Number of batteries [-],

N_{RO} – Number of RO units [-],

W_{tank} – Fresh water tank volume [m^3],

P_{EM}^{nom} – Nominal power of electric motor including inverter and VSD [kW],

P_{gen}^{nom} – Nominal power of generator including hydraulic motor and converter [kW];

w_{wt} – Water tank weighting factor with respect to the chosen system operation strategy [-];

w_{SOC} – Battery bank weighting factor with respect to the chosen system operation strategy [-].

The decision variables N_{pv}, N_{bat} and N_{RO} represent integers, whereas the remaining decision variables are continuous. Since the multi-objective GA function 'gamultiobj' within the Matlab environment does not allow the usage of integers, the variables N_{pv}, N_{bat} and N_{RO} are rounded to the nearest integer for the optimisation calculations. Furthermore, the following optimisation problem bounds and constraints apply:

$$N_{pv}, N_{bat}, N_{RO}, W_{tank}, P_{EM}^{nom}, P_{gen}^{nom} \geq 0 \quad (37)$$

$$N_{RO} \geq 1 \quad (38)$$

$$W_{tank} \leq W_{tank}^{max} \quad (39)$$

$$C_{bb,soc}(8760) \geq C_{bb,soc}(1) \quad (40)$$

$$0 \leq w_{wt}, w_{SOC} \leq 1 \quad (41)$$

where W_{tank}^{max} (in m^3) represent a case-specific upper bound for the fresh water tank due to space restrictions at the location in question.

The number of PV battery chargers is not part of the decision variables vector since, as expressed in Equation (12), it depends on the number of PV modules. The same applies to the HPP and hydraulic motor capacity ratings as they are dependent on the number of RO units and the generator, respectively. Also, the size of the inverter is determined based on the highest yearly electricity load that has been met by the FWM system. Naturally, these dependent variables do affect the total system cost, thus the associated cost of these components are taken into account in the cost calculation.

Lastly, it should be noted that the yearly simulation of the FWM system operation does also involve a number of system operation constraints with respect to the dependent variables, as outlined in section 4.3:

- The energy flow (energy produced by or entered to each component) in every time step t should be less than or equal to the capacity of the respective component.
- The energy flow into the RO unit should be greater or equal to the lower limit applied to it which cannot be underrun as else no fresh water is produced.
- The battery bank can only supply energy or be charged until its lower and upper SOC limits in order to avoid a fast degradation.
- The amount of electricity coming from or going into the battery bank has to meet the maximum and minimum current limit at all times
- The water tank can only supply or be filled with fresh water until its lower and upper limits.

5.1.2 Objective functions

Low cost and high power system reliability are conflictive objectives when designing a stand-alone microgrid. The optimization procedure in the framework of this thesis aims to find the cost-optimal FWM configuration depending on its corresponding system reliability value in terms of loss of water and electricity supply. In the following, the three counter-acting objectives which form an integral part of the FWM system optimisation model are introduced and discussed.

Economical assessment criteria

The cost objective function used for the economical assessment of the FWM is the net present cost (NPC). The NPC includes the capital or initial investment costs in addition to the discounted present values of all future costs during the lifetime of the system. In detail, the following costs are taken into account:

- costs for purchasing the second-hand Lagerwey 18/80 wind turbine, refurbishment of the wind turbine including the instalment of the hydraulic transmission system, the PV modules, the solar battery chargers, the batteries, the inverters and rectifiers, the RO units including pre-filter system and membranes, the hydraulic motors, the high-pressure pump, the water tank, the generator and the electric motor including the VSD;
- costs for the replacement of certain components due to their limited lifetime which is inferior than the total system lifetime of 15 years and
- costs for the operation and maintenance of the various components during the system lifetime.

The cost objective function, namely the net present cost is calculated according to Equation (42):

$$\boldsymbol{OF(1)}: \quad Min_x \quad \sum_i NPC_i(x) = \sum_i P_i * C_i(1 + m_i * (a_{tot} - a_i) + a_i) \tag{42}$$

$$\text{with} \quad x = (N_{pv}, N_{bat}, N_{RO}, W_{tank}, P_{EM}^{nom}, P_{gen}^{nom}, w_1, w_2) \tag{43}$$

where i refers to the respective system component, x is the optimisation variables vector, C_i indicates the capital costs of the i-th component expressed in $€/kW$, $€/kWh$ or $€/m^3$ depending on the FWM system component, m_i refers to the maintenance costs in % of the corresponding capital costs, a_{tot} and a_i represent annuity expressions in order to discount the replacement as well as operation and maintenance costs of component x to the present [83]. These are calculated according to Equations (44) – (46):

$$a_i = \sum_{k=1}^{Y_i} (1+r)^{-L_i * k} \tag{44}$$

$$Y_i = floor\left[\frac{K-1}{L_i}\right] \tag{45}$$

$$a_{tot} = \sum_{k=1}^{K-1} (1+r)^{-k} \tag{46}$$

where a_{tot} indicates the annuity factor for the total lifetime of the FWM system K and a_i denotes a component-specific annuity which discounts the replacement costs of the respective component in year k to the present. Y_i and L_i indicate the number of component replacements and the component lifetime, respectively, throughout the total lifetime of the FWM system and r refers to the discount rate.

It should be noted that for the calculation of the NPC, dependent variables such as the number of solar battery chargers, inverters and the HPP are also taken into account, although they do not form part of the decision variable vector. Moreover, replacement costs solely apply to the batteries, the RO membranes, the inverters and the solar battery chargers whereas the remaining system devices have a lifetime equal or greater to the total lifetime of the FWM and thus their respective number of replacement is equal to zero. The capital, maintenance and replacement costs of each of the above mentioned component are listed in section 6.2.3.

Technical assessment criteria

Since irradiation and wind speed and hence power production are fluctuating in time and since the FWM system does not possess any controllable energy sources such as a diesel generator, it is pivotal to take the reliability of the power system into account. As discussed in chapter 3, the most common measures to assess the power system reliability of a stand-alone microgrid are the LLP and LPSP concept. The LLP, expressed in percentage of time, can be defined as the overall probability that the system load exceeds the available generating capacity leading to a shortage of power. The LPSP on the other hand, is the long-term average fraction of the loss that is not supplied by the power system and it is expressed in kWh/year or as the ratio kWh/kWh (percentage of time). A LPSP or LLP of zero means that the load will always be satisfied while a LLP of one means that the load will never be satisfied [14]. Both concepts however, have their

own shortcomings: the LLP technique is only a suitable metric when the number of times an outage occurs is of importance whereas the LPSP technique solely provides information about the total yearly magnitude of the load deficit. In addition, both concepts consider all loads with the same priority and do not take the severity of the outage into account meaning that a power supply interruption at peak times has a far greater impact than at off-peak times and should consequently be penalised more heavily. Hence, a more suitable system reliability index should be used in order to address this shortcoming.

In the framework of this thesis, the reliability assessment calculations of the FWM system make use of the literature definition of loss of power supply probability, LPSP, and loss of water supply probability, LWSP. These are statistical parameters which can be calculated in two different ways: one performs chronological simulations whereas the other uses probabilistic techniques in order to include the intermittent characteristics of the renewable energy sources and the demand. The first approach is computationally cumbersome and enough data need to be available for a given time period, a limitation that the second approach does not have [46]. However, taking into account the energy and water accumulation effect of the battery and the water tank, respectively, to present the FWM system operation more accurately, the chronological approach is employed in this research. In addition, in order to take account for the severity of the power and water outage, a weighting factor, sf_{el} and sf_w respectively, is included in the calculations according to Equations (47) and (48):

$$\boldsymbol{OF(2)}: \quad Min_x \quad LPSP_{sev} = \frac{\sum_{t=1}^{T} ED(t) * sf_{el}(t)}{\sum_{t=1}^{T} P_{demand}(t) * \Delta t} \tag{47}$$

$$\boldsymbol{OF(3)}: \quad Min_x \quad LWSP_{sev} = \frac{\sum_{t=1}^{T} WD(t) * sf_{w}(t)}{\sum_{t=1}^{T} W_{demand}(t) * \Delta t} \tag{48}$$

where $LPSP_{sev}$ and $LWSP_{sev}$ refer to the loss of power supply probability and loss of water supply probability, respectively, taking into account the severity of the outages, T is the total number of time steps in hours (here, $T = 8760$), ED is the energy deficit and P_{demand} the electricity load at hour t when a power outage occurs. In this case the available energy generated by the PV system and the wind turbine as well as the energy being stored in the battery at time t is not sufficient in order to cover the load. WD represents the water deficit and P_{demand} the water load at hour t when the water outage occurs in the event that the fresh water produced at time step t in addition to the water stored in the water tank is insufficient for covering the water load. In this case, the numerator is the sum of all energy or water deficits in one year whereas the denominator is the total yearly sum of the electricity and water demand, respectively. The severity factors sf_{el} and sf_w at time step t are calculated as follows:

$$sf_{el}(t) = \frac{P_{demand}(t)}{P_{demand}^{avg}} \tag{49}$$

$$sf_w(t) = \frac{W_{demand}(t)}{W_{demand}^{avg}} \quad (50)$$

with P_{demand}^{avg} and W_{demand}^{avg} being the average yearly electricity and water demand of the location in question. Hence, it is clear that the dependence of the respective severity factors is twofold: on the one hand, the magnitude of the load at time step t is considered which is assumed to reflect the base/peak/off-peak situation at hour t; on the other hand, the average yearly demand is taken into account. Base load happens when the load at hour t is equal to the average yearly load in which case the severity factor is equal to 1. Consequently, it can be followed that the bigger the difference between P_{demand} and P_{demand}^{avg} or W_{demand} and W_{demand}^{avg}, the higher/lower the severity of the outage at hour t.

5.2 Genetic algorithm

Genetic algorithm

The genetic algorithm method, which is based on Darwin's theory of evolution, makes use of natural selection and genetics in order to reach an optimised solution. The GA algorithm is a population-based search method meaning that multiple potential solutions are assessed simultaneously. Each potential solution, also called chromosome, contains a specific value for each optimisation variable, also called gene. Hence, every chromosome contains the same amount of genes as the optimisation problem has decision variables. The variation of the genes' values causes its movement which is used in the search process [41].

The process is initialised by introducing a random population of chromosomes within the design space. The performance of each individual chromosome part of the population is evaluated based on (a) fitness or objective function(s). While there are many different types of selection, the most common type is roulette wheel selection, in which each chromosome is given a certain probability of being selected that is directly proportionate to its fitness [84]. After the selection (reproduction) process, the population is enriched with better individuals. However, reproduction makes clones of good strings but does not create new ones. Hence, before the selected chromosomes can move on to the next generation, the so-called genetic operators, namely mutation, cross-over (and elitism), are applied in order to vary them. Crossover is the process of combining two chromosomes (parents) to produce a new chromosome (children) with a certain crossover probability. The mutation operator mainly aims at avoiding establishing a uniform population unable to evolve and staying within a local optimum. This operator is used to modify the genes of a chromosome selected with a certain mutation probability. Elitism involves copying a small proportion of the fittest candidates, unchanged, into the next generation. This can sometimes have a dramatic impact on performance by ensuring that the GA does not waste time re-discovering previously discarded partial solutions [84]. The new pool of children chromosomes is consequently evaluated based on the objective function. These children chromosomes then act

as parent chromosomes and the process continues until the stopping criterion is met. The stopping criterion may be based on number of iterations or convergence of control variable values stored in chromosomes.

Non-dominated Sorting Genetic Algorithm

The Non-dominated Sorting Genetic Algorithm (NSGA) is one of the most popular multi-objective optimization algorithm which is often used for optimisation problems with more than one competing objectives. Two different NSGA algorithms have been developed where the first one, NSGA, is an example of a non-elitist algorithm whereas NSGA II uses elitism as a GA operator. Within NSGA, the population is sorted into a hierarchy of sub-populations based on the principle of Pareto dominance. A chromosome ‘p’ dominates the chromosome ‘q’ if ‘p’ is strictly better than ‘q’ in at least one objective and ‘p’ is not worse than ‘q’ in all objectives. Two chromosomes 'p' and 'q' are considered to have equal ranks if neither dominates the other [85]. Based on this principle, a non-dominated rank is assigned to each chromosome using the relative fitness after which chromosomes with the same ranking score are grouped into the so-called Pareto-front. Hence, multiple Pareto-fronts are produced according to their non-dominated rank. Figure 17 illustrates the multiple Pareto-fronts produced within a generation with f_1 and f_2 being two objective functions.

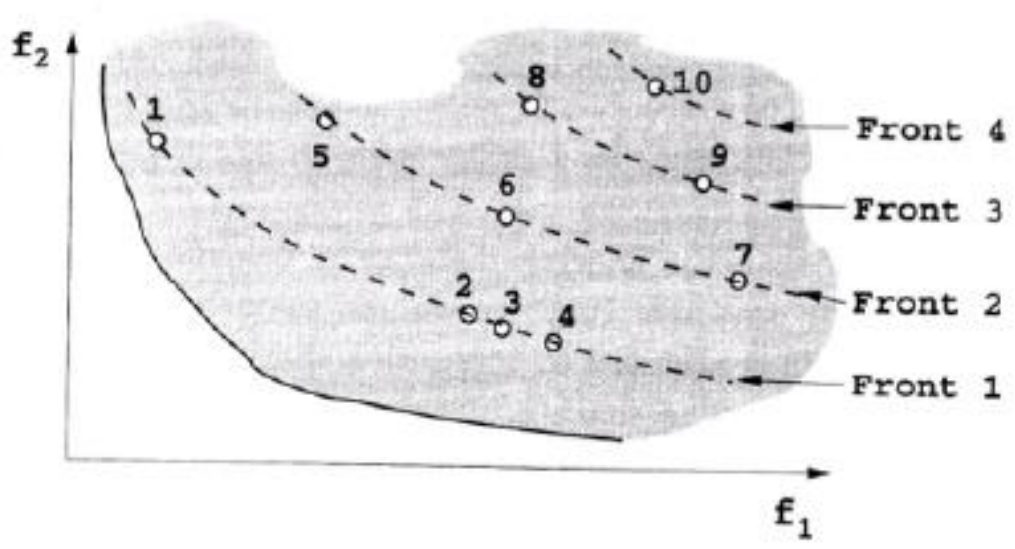

Figure 17. Multiple Pareto fronts containing non-dominated solutions [86]**.**

Once the sorting is complete, the crowding distance value is assigned to each chromosome for each Pareto front. This value is a measure of how far a chromosome is situated from his neighbours having the same rank. The chromosomes within a population are selected based on rank and crowding distance.

In the framework of this thesis, the Global Optimisation Toolbox within the Matlab environment is used for the design optimisation of the FWM system. As the optimization problem involves more than one objective, the multi-objective GA function 'gamultiobj' is employed which uses a controlled elitist genetic algorithm, a variant of the NSGA II algorithm explained above. In contrast to the NSGA II algorithm, which is purely elitist and thus always favours chromosomes with a better fitness value, the controlled elitist GA within Matlab also favours chromosomes that can increase the diversity of the population even if they display a lower rank [85]. This is achieved with the two options 'ParetoFraction' and 'DistanceFcn' which are used to control the elitism. The Pareto fraction option limits the number of chromosomes on the Pareto front whereas the distance function favours chromosomes that are relatively far away on the Pareto front. This is very important in order to avoid early convergence to a local minimum and to maintain diversity of population for convergence to an optimal Pareto front.

5.3 Optimal sizing methodology and implementation

The simulation and optimal sizing methodology employed in this thesis is illustrated in Figure 18.

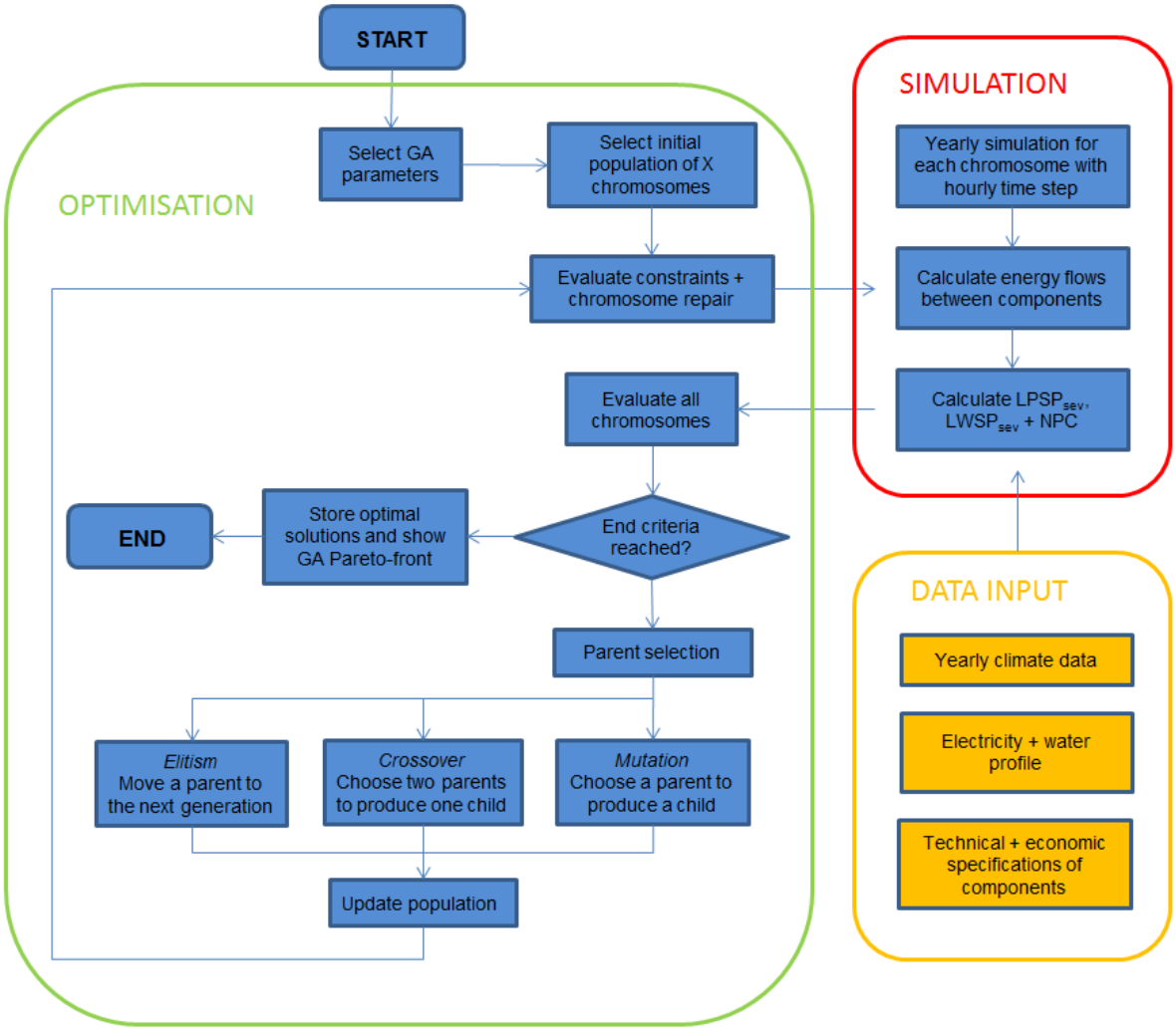

Figure 18. Flowchart of optimal sizing methodology by means of multi-objective GA [64].

Three different blocks which interact with one another form part of the proposed method: the GA optimisation algorithm, the yearly simulation of the FWM system configurations computed by the GA algorithm and the data input into the model.

First, an initial population of a pre-defined number of solutions or chromosomes are chosen randomly within the indicated design space by the GA algorithm. The constraints and bounds of the optimisation problem are evaluated for each individual solution and a reparation mechanism is applied in case they do not comply. In a second step, a yearly simulation of the system operation is performed for each potential solution, comprising a certain number or size of system components, and the hourly power flows are calculated with the input of the yearly climate and load data as well as the technical specifications of every component. The climate data include the hourly solar irradiation, wind speed and temperature, whereas the load data refers to the electricity and water demand of the chosen location. Based on the calculations and the economic specifications of the various components, the objective functions are then computed and their fitness is evaluated by the GA algorithm. Finally, depending on the fitness and the crowding distance of the respective chromosomes, suitable parents are selected on which the various GA operators are applied. Hence, a new population is extracted that will be used for the calculations of the next generation. Each newly chosen chromosome is subject to a constraints and bounds evaluation after which they are sent to the yearly simulation of the system operation. The algorithm stops when one of the end criteria such as maximum number of generations is reached. All of the Pareto-optimal solutions are then displayed on the Pareto-front showing the relationship between system costs and system reliability.

The optimisation procedure of the FWM system consists of two main Matlab scripts. The first script contains the ‘gamultiobj’ function which is provided with input arguments such as the fitness function call, the number of decision variables, their bounds and the optimisation options of the ‘gamultiobj’ solver. The options include population size, maximum amount of generations, crossover fraction, Pareto front population fraction and time limit, among others. On this basis, the optimisation is initialized and an initial population is generated in the form of a vector for each chromosome containing a certain value for each gene or decision variable which is input into the second script. In the second script, these generated values of the decision variables are then rounded to the nearest integer and replaced with the corresponding variables in the model. The second Matlab script, contains the modelling and control logic of the FWM system and the objective functions. The model of the FWM system is built in an equation-based manner and does not call upon the Simulink mode. The way the simulation and optimisation procedure works is that first, the data of the hourly solar irradiation, wind speed, temperature, fresh water and electricity load of the given location are loaded into the script. Based on this data and the initial random values for the decision variables, the yearly operation of the FWM system is simulated for each chromosome. Once the simulations for all chromosomes of the population are finalised, the objective functions (cost function and LLP) can be evaluated and their relative fitness is input into

the first Matlab script. Consequently, the procedure outlined in section 5.2 is followed until the stopping criteria is met after which the first script returns the Pareto front. Also, the respective values of the objective functions and decision variables are provided.

5.4 Genetic algorithm options and operators

Table 4 gives an overview of the main parameters used for the optimisation procedure of the FWM system within the optimisation toolbox in Matlab environment. Additionally, in the last column, an explanation of the various 'gamultiobj' solver options is given and the stopping criteria are specified. In the case of the FWM system optimisation two stopping criteria are in place. The algorithm run is either stopped by a pre-defined number of objective function evaluations (maximum generations) or a maximum number of stall generations which is dependent on the set function tolerance as specified in Table 4. The rather big population size has been chosen in order to have a high number of different solutions and combinations so that a thorough analysis of the relationship between the three objectives can be done.

Table 4. Options for the ‚gamultiobj' solver in Matlab [85].

'gamultiobj' options	Value	Explanation
Pareto fraction	0.6	Determines the fraction of chromosomes to keep on the first Pareto front whereas the solver selects individuals from higher fronts for diversity purposes.
Function tolerance	1e-5	The algorithm stops if the average relative change in the best fitness function value over 'maximum stall generations' is less than or equal to this value.
Maximum generations	200	Sets the maximum number of iterations for the genetic algorithm to perform.
Maximum stall generations	100	The algorithm stops if the average relative change in the best fitness function value over 'maximum stall generations' is less than or equal to 'function tolerance'.
Population size	1000	Specifies the number of chromosomes in each generation. With a large size, the chances to get trapped in a local minimum are reduced. However, the computational time increases.
Crossover fraction	0.8	Specifies the fraction of the next generation that are produced by crossover.

The upper boundaries used for the optimal sizing procedure are chosen based on previous simulations. If the upper bounds were set at 'infinite', the optimisation process would have a very high running time for finding accurate solutions. Hence, multiple simulations were performed by means of the case study and consequently a maximum number/size of the components was found. The upper bounds were then chosen by adding an extensive range to the maximum found values for each component.

6

Case study

The intended purpose of this chapter is to provide the reader with the essential background information regarding the case study and give an overview of the model input data used for performing the simulation and optimal sizing procedure. The proposed approach is applied to the case study for the design and optimal sizing of the FWM system. First, geographic details of the chosen location are discussed. Consequently, the electricity as well as the water profiles of the site are displayed followed by an examination of the meteorological conditions in terms of solar irradiation and wind speed pattern. Lastly, the technical and economical specifications of the individual components of the FWM system are indicated with which the simulation optimisation will be performed.

6.1 Background information

The location which will serve as a case study for the FWM system is a small Caribbean island named Johnny Cay, located about 1.5 km north of the main island of San Andrés as shown in Figure 19. The Colombian island of San Andrés is part of the Archipelago of San Andrés, Providencia and Santa Catalina situated about 700 km north of the coast of Colombia and 200 km east of Nicaragua.

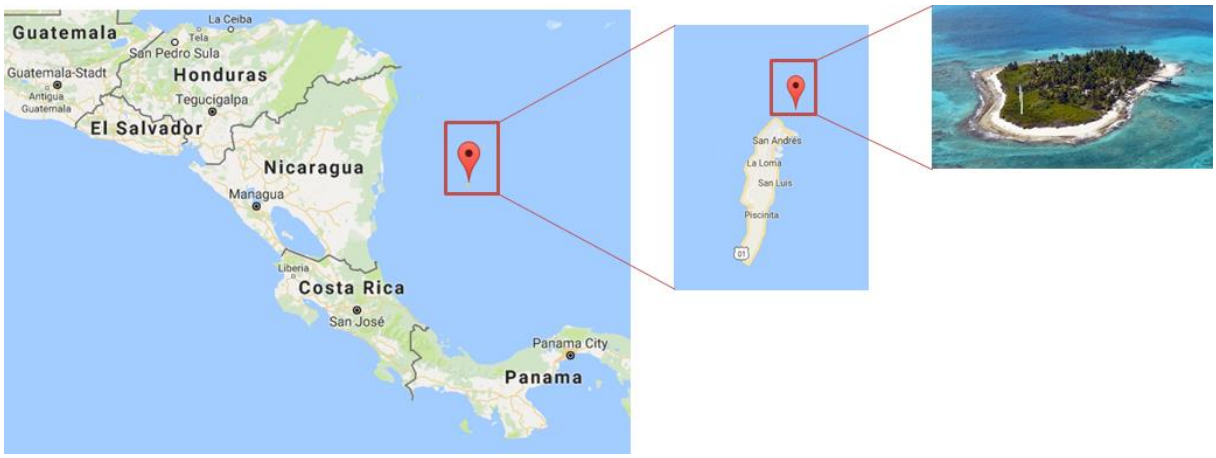

Figure 19. Location of the island of Johnny Cay [87]**.**

Johnny Cay has mainly been chosen because both fresh water and conventional electricity are non-existent on the island and due to the high average wind speeds throughout the year, a basic requirement for the FWM system to be economically feasible. Due to its location in the tropics it is characterised by high temperatures with an annual average of 27.3 °C. The trade winds, which blow from the northeast, determine to some extent the rainy season starting in May, peaking in October and lasting until November. San Andrés and Johnny Cay are however seldom hit by hurricanes and tropical storms even though they are located in the open Caribbean Sea. The small coral island of Johnny Cay is especially frequented by tourists as well as residents coming from San Andrés due to its picturesque beaches. According to the regulation it is not allowed to stay overnight in the island, likewise there is no people living there [88].

6.2 Simulation data

The case study data, namely load profiles and meteorological data, which are used as input for the model is mainly taken from two sources. The water as well as electricity need of the island and the wind measurements are retrieved from a report that has been prepared by the local Colombian energy utility Empresa de Energia del Archipiélago de San Andrés (EEDAS) [89]. The yearly temperature and solar irradiation data on the other hand, is taken from the computer software Meteonorm. It should however be noted that since San Andrés does not have a weather station which measures the global irradiance, Meteonorm extrapolates this data from neighbouring locations.

6.2.1 Load profiles

Johnny Cay is a small tourist island with no inhabitants. It is frequently visited by tourists and locals who spend the day and travel back on boat to the main island of San Andrés in the evening. The Caribbean island counts an average of 1000 tourists per day, a number which however varies according to the seasons. The rainy season starts in May, peaks in October and ends in November. The yearly precipitation reaches on average 1700 mm, 80% of which occur during these months. As a result, less visitors travel to Johnny Cay in this period and

consequently the electricity and water demand are lower. June and July are however an exception to this rule as then many students on their vacations visit the island [89]. Figure 19 displays the yearly fluctuation of visitors to Johnny Cay and its yearly precipitation figures.

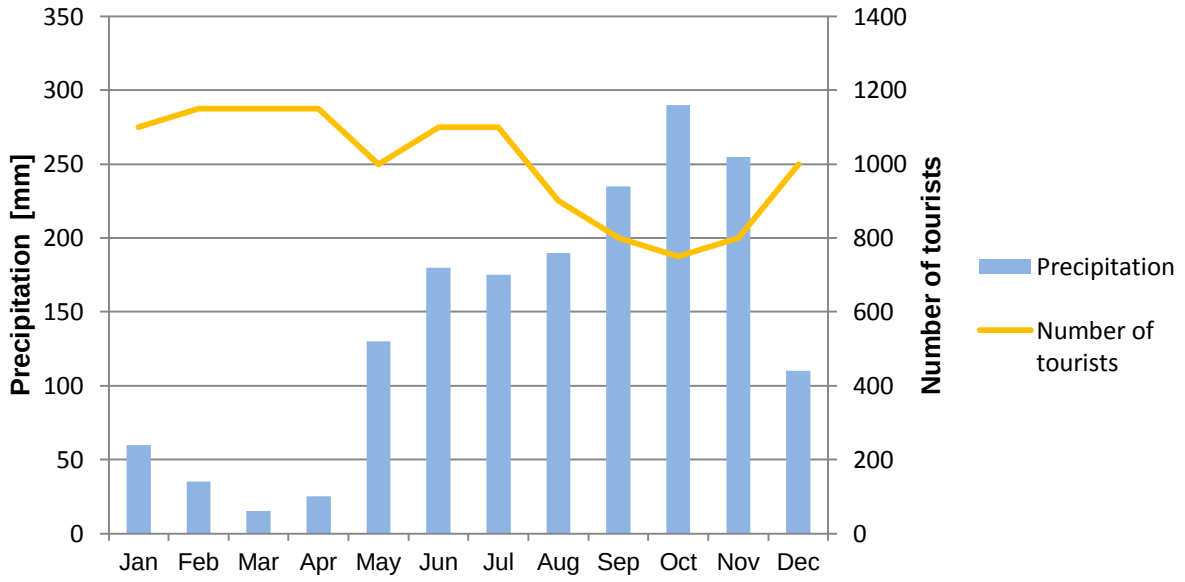

Figure 20. Yearly precipitation and tourist fluctuation on Johnny Cay [89]**.**

Food and drinks on the island are provided by 15 so-called 'cabañas', huts, which are used as bars, restaurants and craft sales. As of now, the island does not dispose of an electrical network or any other source for electricity generation. However, a census was performed in 2008 in collaboration with the vendors and merchants of the huts related to their priority needs once electricity would be available on the island. The census has revealed that most of the electricity would be consumed for lighting and refrigeration as well as some additional equipment for food processing. According to the answers provided by the owners of the huts, the cumulative daily energy demand on an average day would amount to about 148 kWh [89]. The expected distribution of the electricity consumption on Johnny Cay throughout an average day is illustrated in Figure 21.

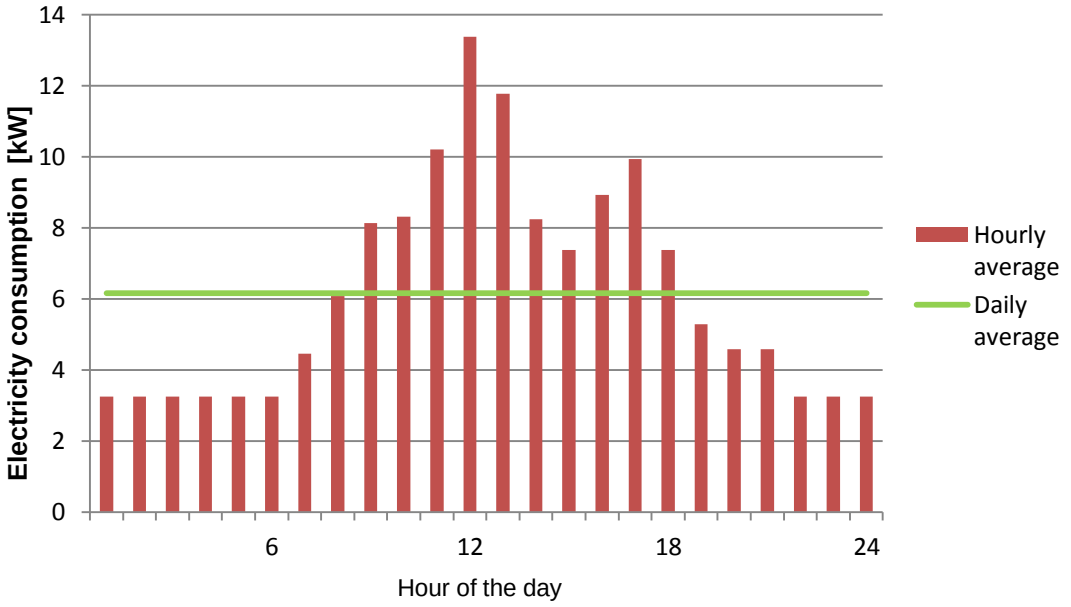

Figure 21. Average daily electricity consumption distribution on Johnny Cay [89]**.**

It can be observed that during night time little power is consumed as no people dwell on the island. The demand starts to go up in the morning hours when the first tourists arrive on Johnny Cay. There are two power peaks throughout the day, one during lunch hours and the other in the afternoon before the visitors head back to the main island of San Andrés. The average power consumption throughout the day amounts to 6.2 kW, whereas the peak amounts to 13.4 kW.

With respect to the fresh water needs of the island, it is used for drinking, food processing, cooling (in the form of ice) and showering. As of now, all potable water and ice are shipped in bottles and bags to Johnny Cay from the main island of San Andrés. This has been much discussion for a long while as it produces big amounts of trash every day. The cumulative daily fresh water needs on an average day would amount to about 14.1 m^3 [89]. The distribution of the water consumption on Johnny Cay throughout an average day is illustrated in Figure 22.

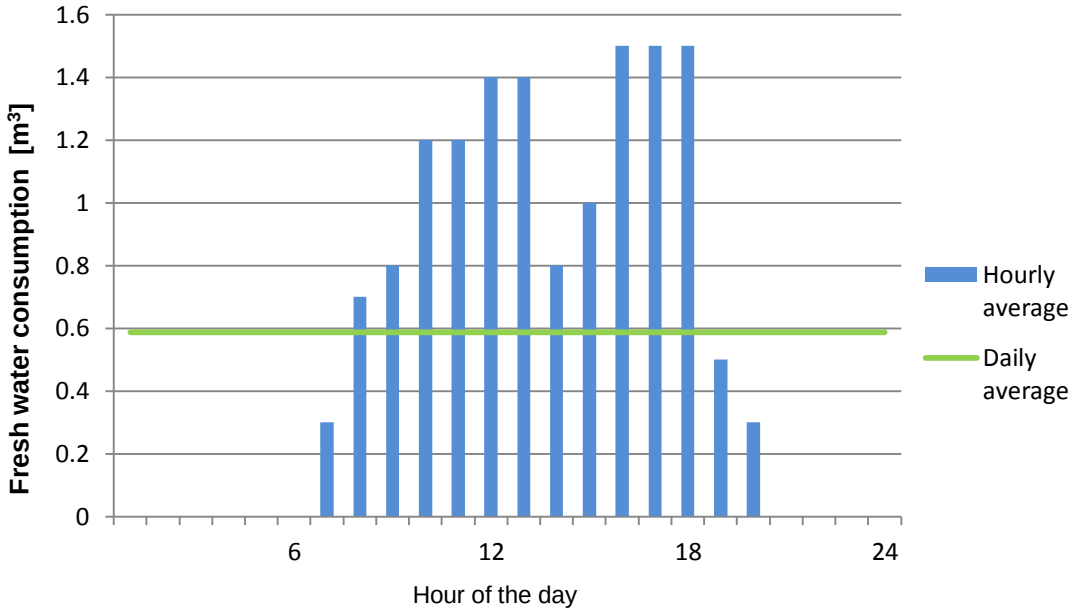

Figure 22. Average daily fresh water consumption distribution on Johnny Cay [89]**.**

The average daily distribution of the fresh water consumption on the island follows a similar trend to that of the electricity consumption. The average fresh water demand throughout one day is close to 600 litres whereas during peak hours at lunch time and just before leaving the island in the evening, the demand can increase up to 1.5 m^3 an hour. During night time, no fresh water is needed on the island.

6.2.2 Wind and solar resources

Wind speed pattern

Since the island of Johnny Cay does not have a weather station, the wind speed data was retrieved from measurements taken at the airport of the island of San Andrés. The eolic potential was evaluated at a height of 10 m above ground level on a site that is marginally higher than the average sea level.

Figure 23 represents the wind rose based on the prevailing wind directions and the average speeds recorded during a 19-year study period at the selected site.

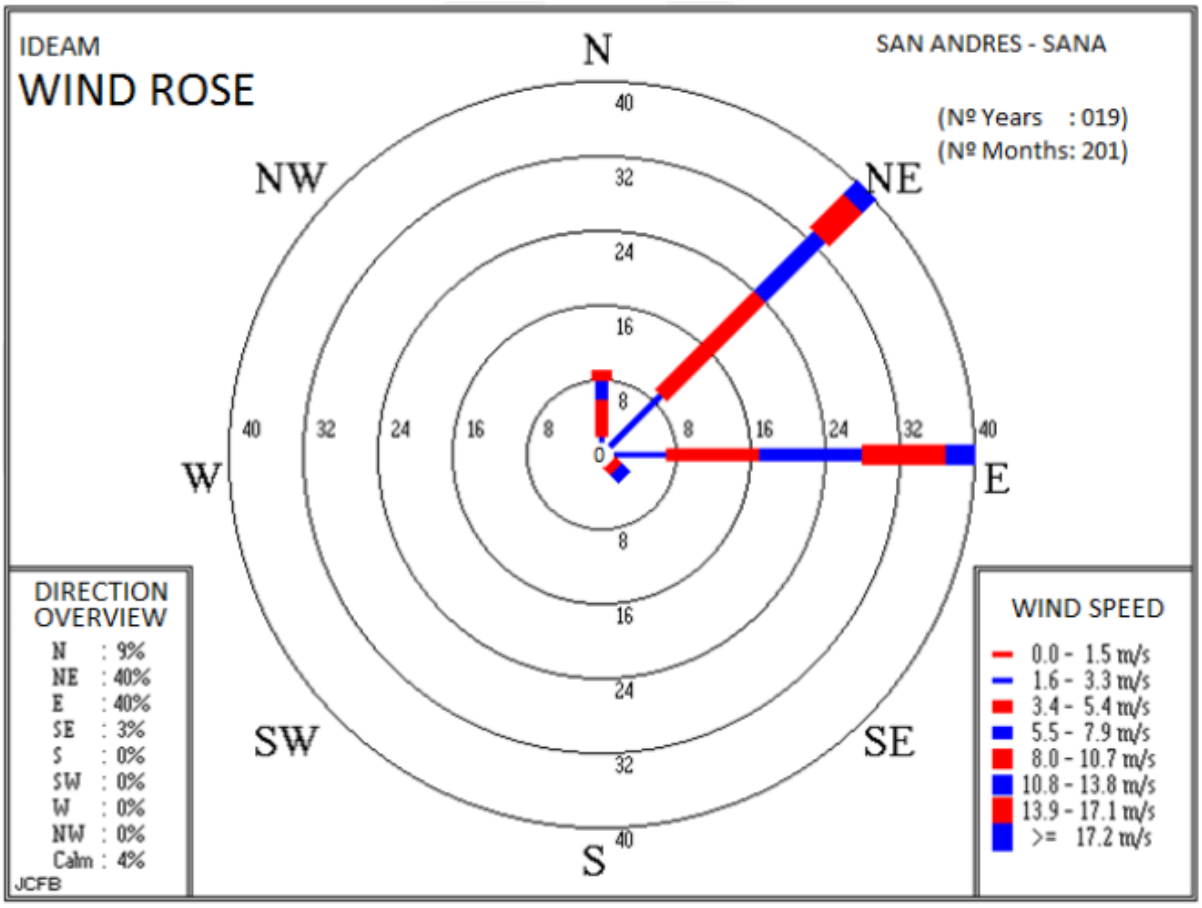

Figure 23. Yearly wind profile of San Andrés island [89]**.**

The wind rose displays the fact that most of the time the wind direction is between the Northeast and East. In addition, Figure 23 shows that wind speeds in San Andrés can predominantly be found in the range of 8-10.7 m/s with an average of 7 m/s [89].

The wind measurements taken at the airport of San Andrés have also revealed that the eolic potential fluctuates considerably throughout the year as illustrated in Figure 24. Average wind speeds peak in January and June, whereas the lowest average values are observed in the months between September and November. These wind speed fluctuations are important to be taken into account for the input data into the model as water as well as electricity production from the wind mill is expected to vary considerably based on the seasonal variability.

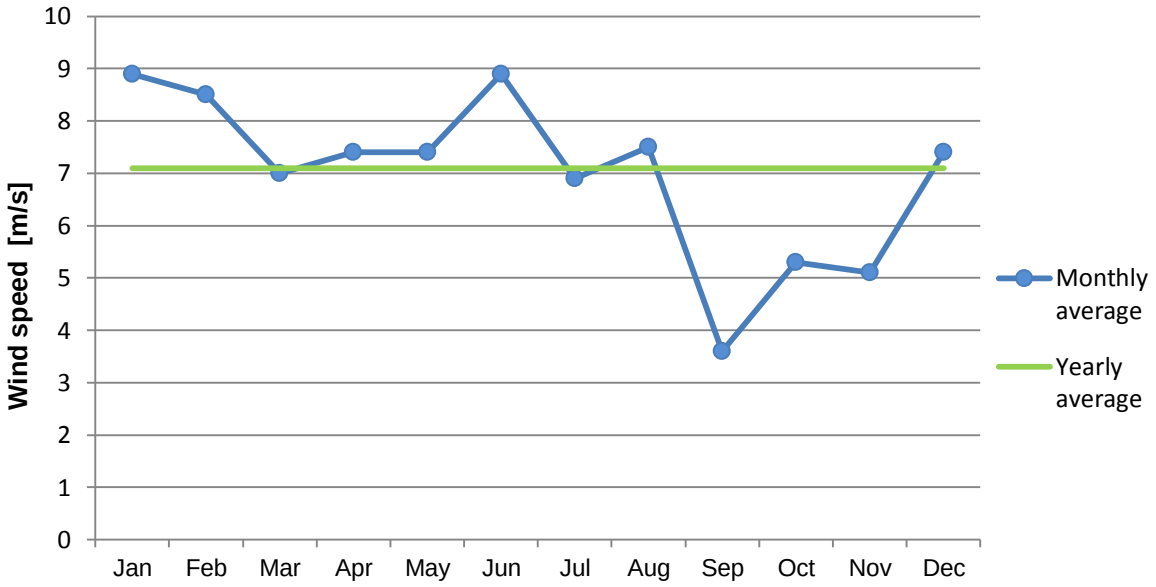

Figure 24. Monthly and yearly average wind speeds in San Andrés island [89]**.**

Lastly, it is important to point out that the average monthly wind speeds depicted in Figure 24 are the ones measured at a reference height of 10 m. The hub height of the Lagerwey 18/80 however, amounts to 30m or 40m depending on the model [36]. Since it is a requirement of the island community to hide the wind turbine behind the palm trees of Johnny Cay, the tower was shortened to 15 m. Using the logarithmic law introduced in Equation (20) one obtains an average wind speed of 7.34 m/s at a height of 15 m; a gain of 5%. The roughness length considered in this calculation is about 0.0024 m as the site in question is characterized by an open terrain with a smooth surface in the very north of the island [89].

Solar irradiation pattern

The monthly average solar irradiation incident on a horizontal surface in San Andrés is depicted in Figure 25. As the island of Johnny Cay is situated close to the equator, PV power production reaches its maximum when the panels are placed horizontally with no tilt angle. The monthly as well as hourly data which serves as input into the optimization model has been retrieved from the software Meteonorm. The global irradiance has been measured in a period of 19 years and thus represents an average over this timeframe.

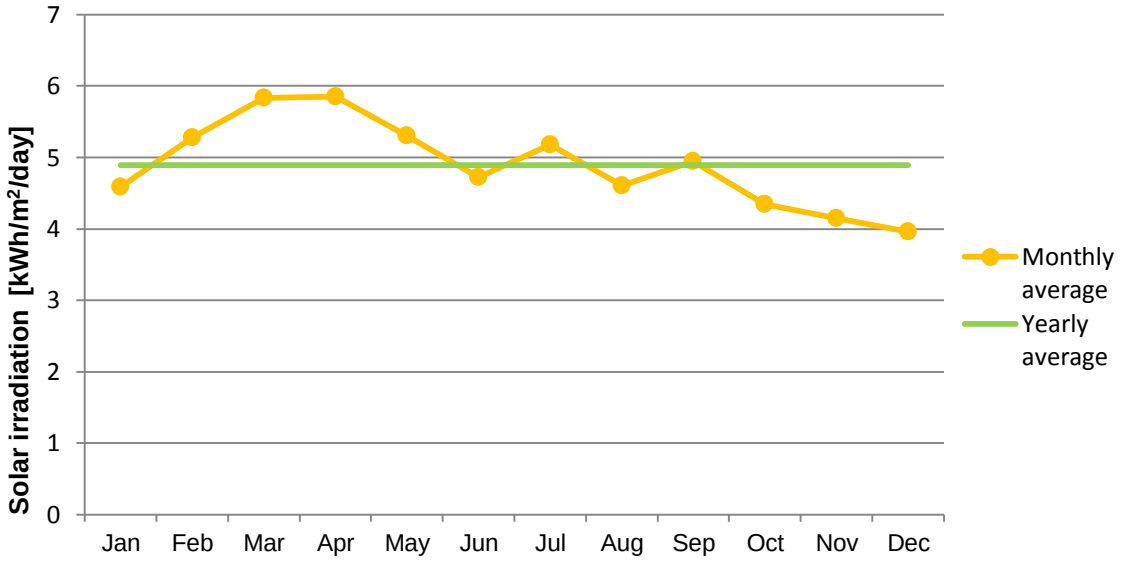

Figure 25. Monthly and yearly average solar irradiation incident on a horizontal surface [90].

Figure 25 clearly shows that the solar resources throughout the year are subject to variability. The fluctuation is however not very striking since the island is located in the Caribbean Sea close to the equator. It can be observed that the daily solar irradiation on horizontal plane peaks in the months of March and April where it nearly reaches 6 kWh/m^2. In the months between October and January on the other hand, it reaches its lowest average daily values of about 4 kWh/m^2 which is due to cloud coverage during the rainy season. The yearly average insolation per day amounts to 4.9 kWh/m^2.

When comparing the yearly solar irradiation and wind speed profiles of San Andrés, it can be observed that the solar and wind resources do complement one another during most of the time. However, one can also notice that during the time period in which the insolation and eolic potential do not complement each other, both resources reach their lowest values, an observation that will probably have a substantial impact on the sizing of the FWM system. During the months that wind speeds reach their peaks as it is the case in January and February, the insolation in San Andrés is around its yearly average values. Consequently, in the months of March to May when the insolation peaks, the average monthly wind speeds decrease. The climate resources follow this trend until September. Subsequently, in the months of September to November monthly wind speeds as well as solar irradiation show their lowest values.

6.2.3 Costs and technical specifications of components

In the following, an overview of the individual costs of each of the components used in the FWM system is given. In order to calculate the NPC of the optimal FWM system configurations the costs are divided into capital, maintenance and replacements costs. All calculations are performed with a discount rate of 7.5 % which is the current discount rate in Colombia [91]. In addition, the required technical specifications of the FWM system components which are input

into the simulation model are shown in separate tables. At the end, the most important assumptions regarding the cost calculations are presented.

Table 5. Capital, O&M and replacement cost of FWM system components [5], [37], [92], [81], [92]–[94].

System component	Capital cost	Maintenance cost (% of capital costs)	Lifetime (years)	°N of replacements
Wind turbine and hydraulic transmission system	75 000 €	0.5	15	-
PV array	1 200 €/kW	2	25	-
Battery charge controllers	110 €/kW	1	10	1
Lead-acid batteries	145 €/kWh	2	5	2
Inverters	125 €/kW	1	10	1
Electric motor (incl. VSD)	200 €/kW	1	15	-
Hydraulic motors	150 €/kW	2	15	-
HPP	500 €/kW	9	15	-
RO system and pre-filtration	2000 €/ RO unit	3	15	-
RO membranes	600 €/RO unit	7	2	7
Water tank	200 €/m^3	1	25	-
Generator	200 €/kW	1	15	-

Table 6. Technical characteristics of the hydraulic Lagerwey 18/80 wind turbine [36].

P_{nom} (kW)	v_{cut-in} (m/s)	$v_{cut-out}$ (m/s)	v_{rated} (m/s)	$height$ (m)
103	3	25	12.5	15

Table 7. Technical characteristics of the PV modules [93].

P_{module}^{nom} (W)	V_{oc}^{STC} (V)	I_{sc}^{STC} (A)	K_I (A/°C)	K_V (V/°C)	$NOCT$ (°C)	FF (-)
230	48.3	6.05	0.0035	- 0.135	46	0.7

Table 8. Technical characteristics of the battery charge controllers [94].

P_{ch}^{nom} (kW)	V_{ch}^{max} (V)	I_{ch}^{max} (A)	η_{ch} (-)
3	145	50	0.95

Table 9. Technical characteristics of the lead-acid batteries [81].

C_{bat}^{nom} (Ah)	V_{bat} (V)	V_{bus} (V)	DOD (-)
260	12	48	0.7

Table 10. Technical characteristics of one RO membrane element [32].

Membrane type	Number of elements (-)	Element surface (m^2)	P_f^{min} (bar)	P_f^{max} (bar)
SW30-4040	5	7.3	36.7	69

Table 11. Technical characteristics of one RO unit/pressure vessel [95].

$P_{RO,unit}^{min}$ (kW)	$P_{RO,unit}^{max}$ (kW)	Recovery factor (-)	Q_f^{min} (m^3/h)	Q_f^{max} (m3/h)	SEC^{nom} (kWh/m^3)
1	7.09	0.35	0.71	3.33	6.1
$W_{RO,unit}^{min}$ (m^3/h)	$W_{RO,unit}^{max}$ (m^3/h)	TDS^{min} (ppm)	TDS^{max} (ppm)	η_{HPP} (-)	
0.25	1.2	149	634	0.8	

The FWM system lifetime is determined by the lifetime of the Lagerwey 18/80 wind turbine. An average lifetime of a wind turbine is usually about 25 years. However, since the Lagerwey 18/80 is purchased on the second-hand market, its lifespan is assumed to be lower, even after a general overhaul. Some of the FWM sub-systems, e.g. the PV array, do show higher lifetimes. The remaining value of these elements is not recovered at the end of the system lifetime which results in a marginally higher NPC. Additionally, all components' efficiencies are assumed to remain constant over their lifetime.

For some devices such as the motors and HPP, average prices per unit are used in the cost calculations. However, depending on the calculated component ratings by the optimisation procedure, the prices could be lower or higher due to economies of scale. Also, initial costs for installation, land purchase, tax pays and supply chain are not considered in the NPC calculations. Furthermore, regarding the O&M costs, these are assumed to be constant throughout the system lifetime. In addition, for simplicity reasons, it is assumed that also during the years in which replacements of system components take place, the respective O&M cost apply.

Lastly, the simulations are performed on an hourly basis for a single year of which the most recent data could be sourced, mainly averaged over a great number of periods. Whereas seasonal resource variation is considered in the simulation, yearly demand and production is assumed to be constant over the system lifetime of 15 years.

7

Results and discussion

This chapter shows the results of the simulation and optimal sizing approach of the FWM system for the Colombian island of Johnny Cay. As a first step, the 3D and 2D Pareto fronts are illustrated in order to visualise the relationship between FWM system costs and system reliability. An analysis with regards to the varying system configuration based on their respective electricity and water supply reliabilities follows. As a second step, a sensitivity analysis is performed for several wind speeds which shows how the sizes of the different FWM components change in these cases. Next, as the current FWM system design does not make use of the electric motor for the production of fresh water, a comparison is made between the two variations in order to see if the addition of an electric drive for powering the HPP is beneficial. To conclude, the Pareto fronts for three different reliability indices are presented and confronted in order to stress the importance of choosing a suitable reliability index. At the end, the main findings and observations with respect to the obtained results are summarised.

7.1 Pareto fronts and FWM system reliability analysis

The triple-objective optimisation procedure aims at minimising the three objective functions: NPC (€), $LPSP_{sev}$ (%) and $LWSP_{sev}$ (%). These objectives are conflicting, hence a compromise needs to be found. In contrast to single-objective optimisation, the result in this case is a set of optimal solutions rather than a single one. This set of optimal solutions is also referred to as Pareto-optimal front. As explained in chapter 5, all of the solutions on the Pareto front are optimal meaning that no improvement can be achieved on any of the three objectives without at the same time deteriorating at least one of the two other objectives.

The 3D Pareto front obtained from the simulation and optimisation procedure for the location of Johnny Cay is shown in Figure 26. It contains 358 optimal solutions which are a combination of

the three objectives. In order to represent the Pareto front in a clear and readable manner, a surface interpolation was performed for all optimal points.

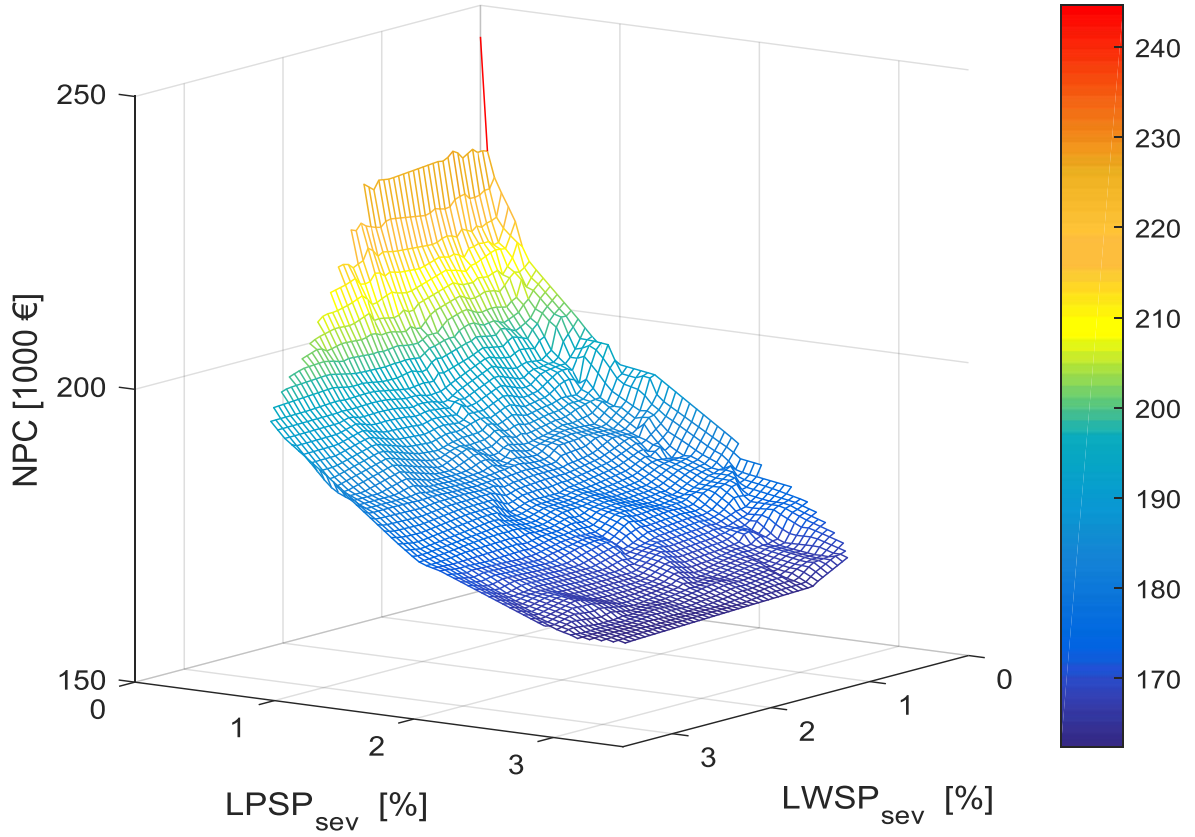

Figure 26. 3D Pareto front of the simulation and optimisation procedure for Johnny Cay.

Figure 26 clearly shows that smaller loss of power and water supply probabilities imply a larger FWM system and consequently higher cost. Moreover, it can immediately be observed that the main correlation regarding the three objectives exists between the cost and the $LPSP_{sev}$. As expected, the highest FWM system costs of about € 245 000 are found at a system reliability of 100% after which they fall off exponentially, mainly in the direction of higher $LPSP_{sev}$ values. This downward trend regarding the cost is also given for the $LWSP_{sev}$, however it is much less visible. Indeed, a rather steep slope with respect to the NPC can be observed for $LWSP_{sev}$ values as low as about 0.5%, irrespective of the corresponding $LPSP_{sev}$. After that the downward trend seems to flatten considerably meaning that the cost no longer differ for higher $LWSP_{sev}$ values. The dependence of the FWM system cost is hence much more prominent with respect to the $LPSP_{sev}$.

In order to be able to analyse the results more thoroughly, a 2D graph of the Pareto front was created which shows the relationship between the cost and the $LPSP_{sev}$ for different fixed $LWSP_{sev}$ values.

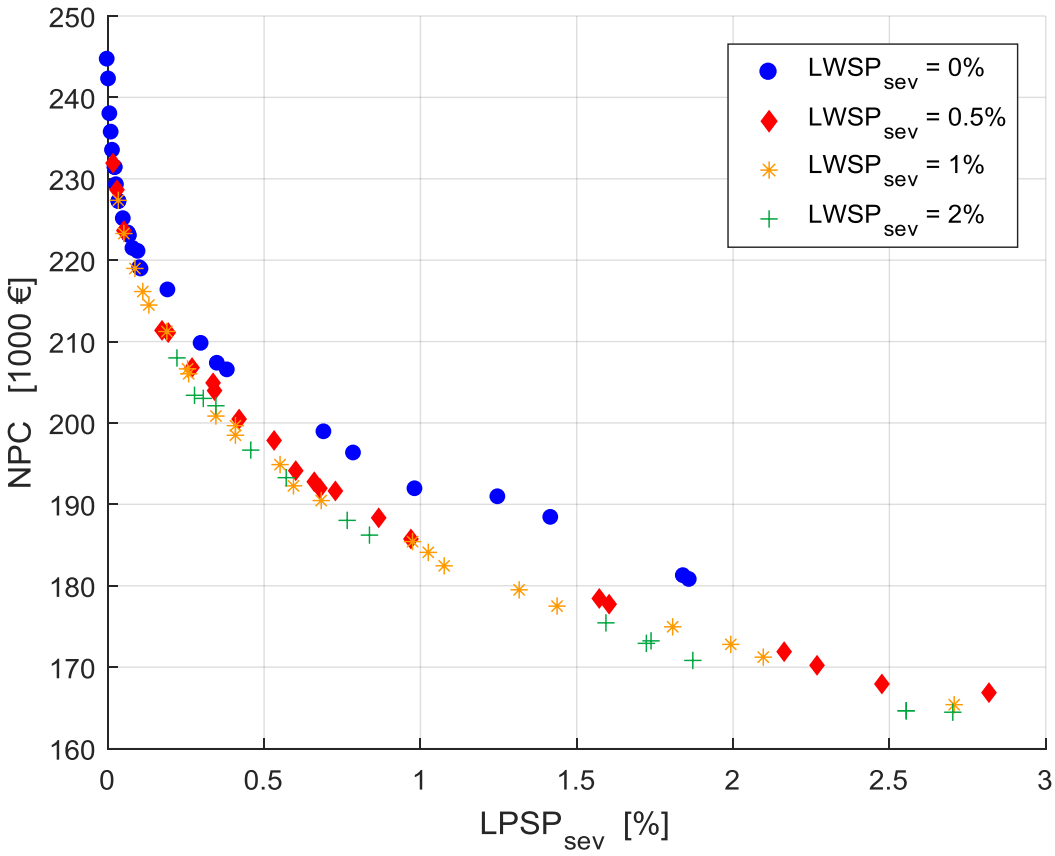

Figure 27. 2D Pareto front of the simulation and optimisation procedure for Johnny Cay with different fixed $LWSP_{sev}$ values.

Figure 27 represents the four Pareto fronts for $LWSP_{sev} = [0, 0.5, 1, 2]$. All four curves behave similarly, showing an exponential trend until an $LPSP_{sev}$ value of around 1% followed by a near-linear trend for higher $LPSP_{sev}$ values. Hence, it can immediately be observed that the greatest cost decrease can be achieved within the first third of the curve. The graph shows again that the FWM system cost dependence is considerably greater with respect to the electricity reliability. The cost for the optimal FWM system configuration without a single outage amounts to about 245 000 €. For 0.5% and 1% energy deficit ratios to the total yearly electricity demand, an average cost reduction of around 18% and 22%, respectively, can be achieved compared to the 100% reliable FWM configuration. For higher $LPSP_{sev}$ values the gains are minor, especially compared to the low generation system reliability that would have to be accepted in this case.

With respect to the system reliability in terms of water supply, Figure 27 shows that the overall cost can be reduced if the stand-alone FWM system requires a $LPSP_{sev}$ close to zero whereas the water supply reliability requirements are not as strict. In the event that the $LPSP_{sev}$ is close to 0% and the $LWSP_{sev}$ amounts to 1%, the FWM system cost can be lowered by about 7%. Compared to the cost reduction for the opposite situation, the gains are however minor. Moreover, regarding the cost reduction potential incurred by smaller $LWSP_{sev}$ values exclusively, for electricity reliability requirements smaller than 100%, around 3% of costs can be saved by accepting a 0.5%

ratio of water supply deficit to the total yearly fresh water demand; every water supply reliability lower than 99.5% no longer results in cost reductions. Again, it is important to mention that the gains are minor when compared to cost declines related to smaller $LPSP_{sev}$ values.

To summarise, the reliability analysis has shown that for the case study of the Caribbean island of Johnny Cay a substantial FWM system cost reduction of about 20% can be achieved with a water supply reliability of close to 100% and an electricity supply reliability greater than 99%. For lower $LWSP_{sev}$ values, the cost reduction potential remains minor compared to the water supply losses that would have to be accepted. Moreover, depending on the stand-alone system reliability requirements of the community, different optimal points can be found with the reliability analysis approach taken above.

Finally, it is important to stress that the average hourly energy and water demand on the island of Johnny Cay is not in the same order of magnitude. As shown in section 6.2.1 the average hourly fresh water demand amounts to 0.6 m^3 which, assuming an average SEC of 5.9 kWh/m^3 for the RO plant, results in about 3.5 kWh. Compared to the average hourly electricity demand of 6.2 kWh, this value is around 44% lower. As a consequence, the greater cost reduction potential with respect to lower $LPSP_{sev}$ values is to some extend based on the reason outlined above.

7.2 Optimal system configurations

In section 7.1 the general relationship between the three objective functions, namely NPC, $LWSP_{sev}$ and $LPSP_{sev}$ was described. In the following, the optimal FWM system configurations for several different water and electricity supply reliabilities are identified and examined and a comparison is made. In Table 12 the number of RO units as well as the size of the PV system, the battery bank, the fresh water tank, the electric motor and the generator are specified based on their respective $LWSP_{sev}$ and $LPSP_{sev}$ values. As the power sources of the FWM system are exclusively renewable and due to their intermittent nature, it is also important to consider the amount of electricity and fresh water dumping for a comprehensive analysis. Hence, the electricity and water dumping with respect to the total production (%) is included in the table. It should be noted that for the case study of Johnny Cay the upper bound of the fresh water tank size is 60 m^3 which results in about 4 days of fresh water storage.

Table 12. Optimal FWM system configurations for different $LPSP_{sev}$ and $LWSP_{sev}$ values.

	$\boldsymbol{LPSP_{sev} = 0\%}$ $\boldsymbol{LWSP_{sev} = 0\%}$	$\boldsymbol{LPSP_{sev} \sim 0\%}$ $\boldsymbol{LWSP_{sev} \sim 1\%}$	$\boldsymbol{LPSP_{sev} \sim 1\%}$ $\boldsymbol{LWSP_{sev} = 0\%}$	$\boldsymbol{LPSP_{sev} \sim 0.5\%}$ $\boldsymbol{LWSP_{sev} \sim 0.5\%}$	$\boldsymbol{LPSP_{sev} \sim 1\%}$ $\boldsymbol{LWSP_{sev} \sim 1\%}$
Costs [€]	244 626	227 352	191 844 190 860	197 851	182 447
PV [kW]	38.9	41.6	32.9 38	33.6	28.3

Battery [kWh]	218.4	162.2	93.6 68.6	112.3	87.4
RO unit [-]	1	1	1	1	1
Water tank [m^3]	47	35	45 42	36	44
Electric motor [kW]	1.5	1.4	1.2 1.3	1.1	0.9
Generator [kW]	8.1	7.7	7.5 7.5	7.8	7.5
Electricity dumping [% of total production]	39	41	31 36	35	29
Water dumping [% of total production]	20	20	19 20	19	18

As to the PV system, Table 12 clearly shows that the value of the $LPSP_{sev}$ determines its size. Indeed, with 100% power system reliability, the PV capacity amounts to about 40 kW, about 25% bigger compared to an $LPSP_{sev}$ of 1%. This relation also implies that fresh water is mainly produced by the wind turbine making little use of the electricity coming from the PV system or the battery. The capacity of the electric motor underlines this fact as well. For all reliability cases listed in Table 12, the electric motor sizes are between 1 and 1.5 kW compared to a nominal power of the HPP of 7 kW.

Regarding the battery bank, the most striking point is that for a 100% FWM system reliability, its capacity is substantially bigger when compared to all other cases. With an $LPSP_{sev}$ and $LWSP_{sev}$ value of 0% the size of the battery bank amounts to about 220 kWh. Given the average hourly electricity consumption of Johnny Cay of 6.2 kW, it implies that the stand-alone FWM system possesses a 1.5-day autonomy. This calculation assumes that the battery is solely used for covering the electricity demand of the island which seems to be a rather fair assumption given the reasons outlined in the former paragraph and considering the system operation strategy outlined in section 4.4. Another point that should be emphasised is the relationship between the battery bank capacity and the $LPSP_{sev}$ values: for an electricity supply reliability of 99% the size of the battery bank decreases by 60-70% compared to a 100% reliable power system. This results in a system autonomy of about half a day which reflects the fact that in such case there is a higher share in electricity demand coverage by the wind turbine. Additionally, it follows that the wind and solar resources generally complement each other well at the location under study and the FWM system is rightly sized. The drastic drop in PV system and battery bank capacities indicates that the FWM system is substantially oversized for most of the time in case it features a 100% system

reliability. It implies that there are short bad resource periods with low renewable energy production and/or high fresh water and electricity consumption in which the increased capacities are needed. This can also be observed by examining the average yearly ratio of electricity dumping: for $LPSP_{sev}$ values of 1% only about 30% of the total electric energy production is being unused compared to 40% in case of a $LPSP_{sev}$ of 0%. A positive correlation is also given between battery bank capacity and $LWSP_{sev}$, however to a much lower extent. Indeed, in case the water supply reliability drops to 99%, less battery capacity is needed due to an increased electricity production by the wind turbine. A last remark shall be made regarding the FWM system configuration for a $LWSP_{sev}$ of 0% and a $LPSP_{sev}$ of 1%. For this case, two different optimal FWM system configurations are listed in the table in order to show that for similar reliability values different configurations are computed by the simulation and optimisation procedure. In this case, it can be observed that the biggest difference is found between the size of the PV system and the battery. The results imply that a 5 kW increase of the PV system is somehow equal to a battery bank capacity increase of 25 kWh which is very much plausible if assuming an hourly average energy production of 3.5 kWh for 8h a day by a PV system size of 5 kW.

The amount of electricity being dumped due to a battery bank SOC of 100% and a greater electricity production at time t compared to the demand is about 30-40% for all reliability cases shown in the table. This seems to be a rather big amount, however, considering that solely uncontrollable energy sources are used in the FWM system, this ratio is in the expected range. Additionally, it can be observed that the amount of electricity dumping is determined by the size of the PV system. This correlation is plausible as the optimal size of the wind generator computed by the optimisation procedure is in all cases about 8 kW which is much smaller compared to the PV system capacity.

For all reliability cases shown in Table 12 there is no clear relation between the size of the water tank and the electricity and water supply reliability values. However, it can be said that the optimal size of the water tank amounts to about three days of fresh water autonomy given the island's average daily fresh water need of 14 m^3. This result is not surprising as storing fresh water in a tank is considerably cheaper than alternatively making use of a battery bank as storage technology. A higher storage capacity results in the system being less prone to failures and hence the computed three-day fresh water compared to the 1.5-day or lower electricity autonomy of the different optimal FWM system configurations does also to some extend explain the higher dependence between NPC and $LPSP_{sev}$.

Lastly, in order to make an assessment regarding the operation of the RO plant, the average TDS (ppm) and SEC (kWh/m^3) as well as the number of RO interruptions for the different optimal FWM configurations are listed in Table 13.

Table 13. RO operation specifications of the optimal FWM system configurations for different $LPSP_{sev}$ and $LWSP_{sev}$ values.

	$LPSP_{sev} = 0\%$ $LWSP_{sev} = 0\%$	$LPSP_{sev} \sim 0\%$ $LWSP_{sev} \sim 1\%$	$LPSP_{sev} \sim 1\%$ $LWSP_{sev} = 0\%$	$LPSP_{sev} \sim 0.5\%$ $LWSP_{sev} \sim 0.5\%$	$LPSP_{sev} \sim 1\%$ $LWSP_{sev} \sim 1\%$
Average TDS [ppm]	169	171	171 172	173	164
Average SEC [kWh/m³]	5.9	5.9	5.9 5.8	5.9	6
°N of RO interruptions [-]	359	398	392 396	396	456

For all different reliability cases it can be observed that both the average SEC as well as the average TDS are in the same order, namely around 5.9 kWh/m^3 and 170 ppm, respectively. The SEC and the TDS of an RO plant are inversely related meaning that permeate of lower quality (higher TDS) necessitates less energy. As disclosed in Table 11 the minimum value of the TDS and the maximum value of the SEC amount to 149 ppm and 6.1 kWh/m^3, respectively in the event that the HPP is running at its nominal flow and pressure. Hence, it can be concluded that the RO operates close to its nominal power most of the time. However, it should also be taken into consideration that at lower feed flows less permeate is being produced and as a consequence the lower quality water with higher TDS values has a decreased impact on the average TDS of the permeate in the storage tank. Also, the RO unit is being shut down about 400 times a year or once a day on average with less frequent shut-downs in case of higher water and electricity supply reliabilities and an increased number of interruptions when the reliabilities are lower.

In conclusion, the optimal FWM system configuration and hence overall cost based on its respective reliability values is mainly determined by the size of the PV system and the battery bank which are the variables that vary the most. All other components are in similar ranges irrespective of the $LWSP_{sev}$ and $LPSP_{sev}$.

7.3 Optimal sizing for different wind speeds

In order to get an insight into the effect of different average wind speeds on the FWM system size, the simulation and optimisation procedure is applied to the same case study for an average wind speed of 4 m/s and 5 m/s, respectively. These two scenarios are compared to the reference scenario which features a yearly average wind speed of 7.1 m/s. Additionally it was decided that for comparison purposes, the wind pattern remained the same for all scenarios.

Since the FWM system components or decision variables are of different units, the results are normalised with respect to the reference scenario in order to show the results by means of a bar chart. This implies that the optimal size of each FWM system component for the reference

scenario is 100%. The exact sizes in their respective units can be viewed in the tables provided in the Appendix. Figure 28, Figure 29 and Figure 30 display the results obtained for the three wind speed scenarios for 3 different cases:

(1) $LPSP_{sev} = LWSP_{sev} = 0\%$

(2) $LPSP_{sev} \sim 0\%$, $LWSP_{sev} \sim 1\%$

(3) $LPSP_{sev} \sim 1\%$, $LWSP_{sev} = 0\%$.

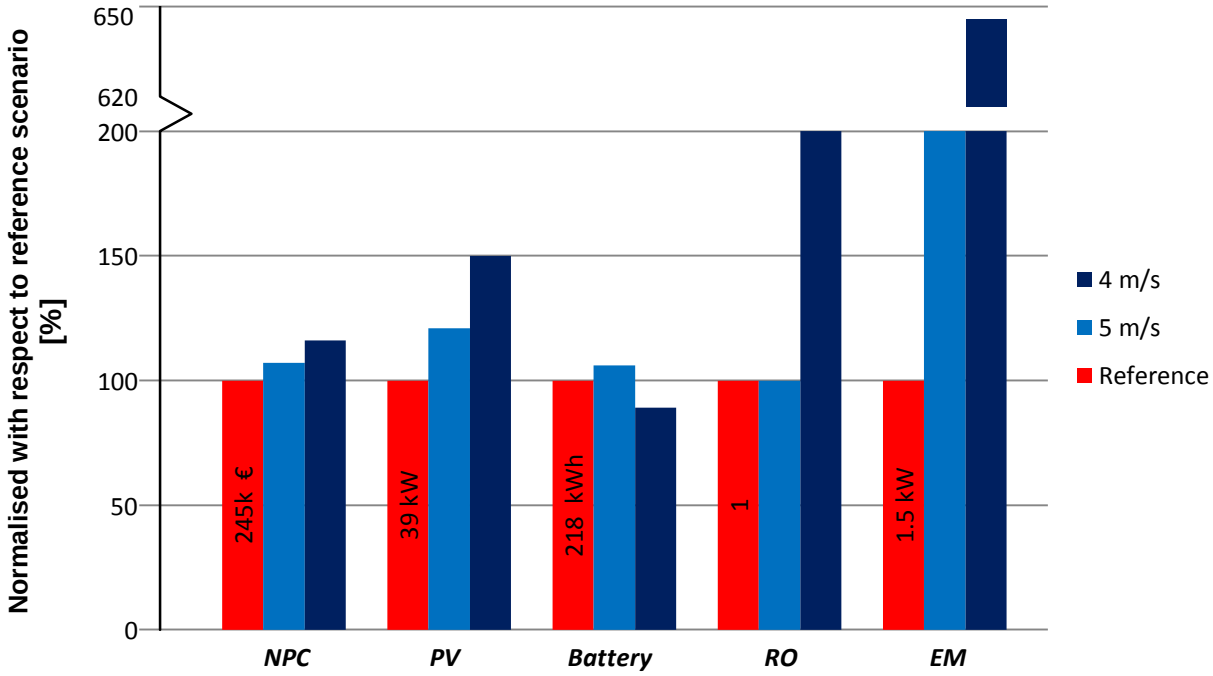

Figure 28. Optimal FWM system configurations for different wind speeds and $LPSP_{sev} = LWSP_{sev} = 0\%$.

Figure 28 shows that for a 100% reliable microgrid, the NPC of the FWM system increases by 7% and 16% for an average wind speed of 5 m/s and 4 m/s, respectively, compared to the reference scenario. The higher costs are mainly a result of the increased PV system capacity compared to the reference scenario. Also, for the 4 m/s wind speed scenario, a second RO unit is needed which substantially adds to the overall system cost. This indicates that for the 4 m/s wind speed scenario, it is more cost-effective to increase the size of the RO system and thus produce a greater amount of fresh water when sufficient energy is available in contrast to increasing the PV system (and storage capacity) in order to generate additional electricity for a more continuous operation of the desalination unit.

The increased capacities of the PV array for the 5 m/s scenario and especially for the 4 m/s scenario indicate that since less energy is produced by the wind turbine, the size of the PV system has to be stepped up. However, by looking at the respective sizes of the electric motor (1.5 kW vs. 10 kW), it is clearly visible that for an average wind speed of 4 m/s the electricity

generated by the PV system is no longer mainly used for electricity demand coverage, but to a great extent also for water production. This is not so much the case for the 5 m/s scenario and even less for the reference scenario.

The battery bank is for all wind speed scenarios of similar size when the FWM system features 100% reliability resulting in a system autonomy of about 1.5 days. As the average wind speed drops, the share of the PV system in the total energy production increases. A PV system can however only produce energy throughout the day which makes the FWM system more dependable on a storage technology in order to be able to cover the electricity load during night. Figure 29 and Figure 30 display the optimal FWM system configurations for a $LPSP_{sev}$ equal to 0% and a $LWSP_{sev}$ equal to 1% and vice versa for the different wind speed scenarios.

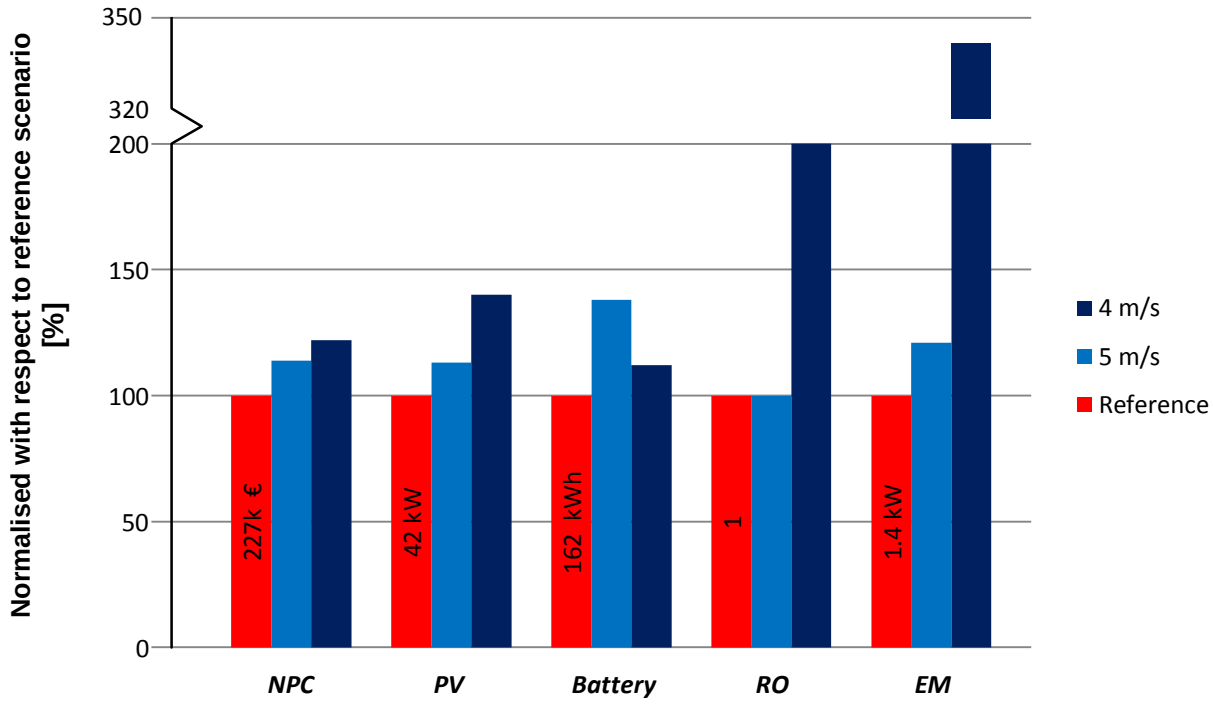

Figure 29. Optimal FWM system configurations for different wind speeds and $LPSP_{sev}$ = 0% and LWSP = 1%.

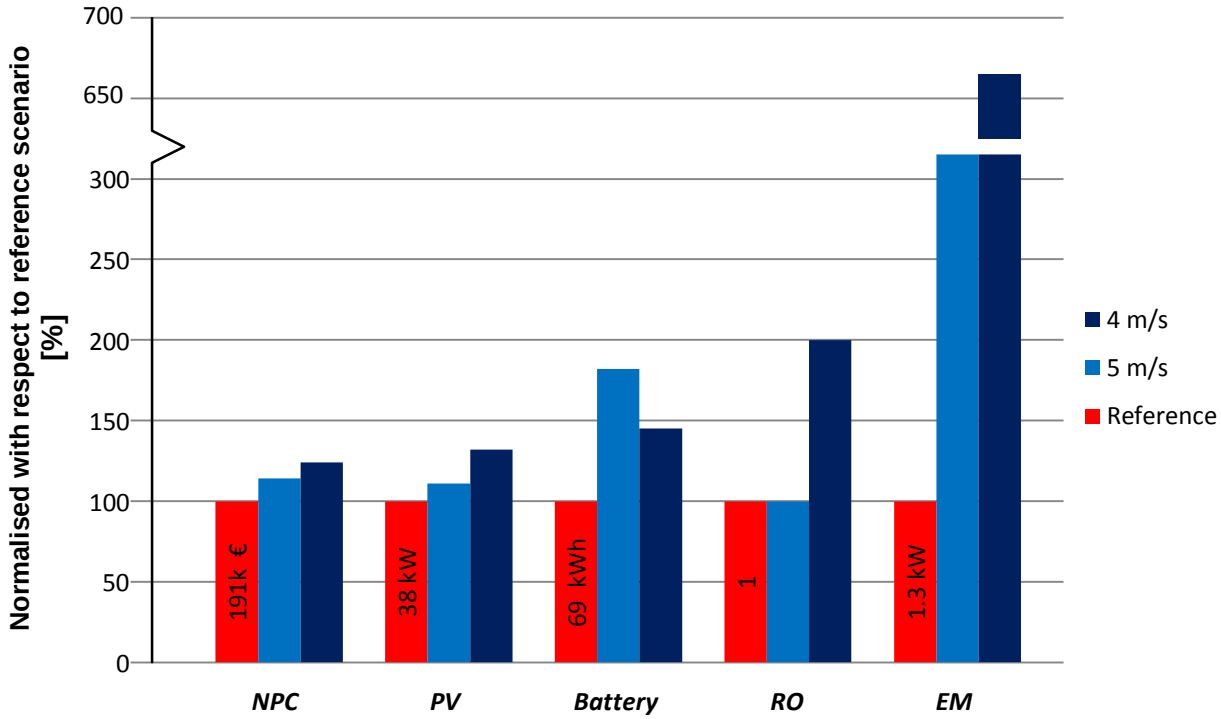

Figure 30. Optimal FWM system configurations for different wind speeds and $LPSP_{sev}$ = 1% and $LWSP_{sev}$ = 0%.

It can be clearly seen that for a lower water and electricity reliability, the spread in the FWM system cost becomes more pronounced with around 14% cost increase for the 5 m/s wind speed and about 23% increase for the 4 m/s wind speed compared to the reference scenario. The bar graphs do not display this information, however, in the tables provided in the Appendix it can be observed that for the 4 m/s and 5 m/s wind speed scenario the FWM configuration is the same in case of a $LWSP_{sev}$ value of 1% and 0% resulting in no change of the respective NPC. On the contrary, a gain in cost when lowering the electricity reliability to 99% is given, however, to a lesser extent than for the reference scenario. This shows that for both wind speed scenarios, the 100% reliable FWM system is well-sized for the given fresh water demand on Johnny Cay in terms of efficient use of the available energy as a steep cost decrease indicates a system that is oversized for most of the time.

The higher costs are in these cases mainly a result of the increased PV system and battery storage capacities compared to the reference scenario. Also, with an average wind speed of 4 m/s, the second RO unit is still needed even for a decreased water supply reliability. As mentioned above, assuming a $LWSP_{sev}$ of 1% and a $LPSP_{sev}$ value of 0%, the battery size hardly changes for an average wind speed of 4 m/s and 5 m/s in contrast to a 26% decrease for the reference scenario. In the reverse case, a battery bank capacity decrease of close to 50% can be observed for 4 m/s and 5 m/s wind speed, whereas in the reference scenario it drops close to about 30% of its original value with 100% reliability. Hence, for 4 m/s and 5 m/s average wind speed, the battery bank still possesses a system autonomy of 18h, whereas for the reference

scenario an autonomy of 7h can be observed in this case. This again indicates that as far as the reference scenario is concerned, the FWM system is for most of the times oversized and the relatively big battery bank capacity seems to be attributed to a small number of bad resource periods. This can also be verified in the tables provided in the Appendix by observing the ratio of dumped electricity to the total electricity produced throughout the year which is substantially higher in the reference scenario.

The sizes of the water tank as well as the generator are not displayed in the figures above as their variation is minimal for all scenarios. It can however be said that for an average wind speed of 4 m/s the volume of the fresh water tank is slightly higher than in the other cases. Also, the generator size placed in parallel to the RO unit has a similar capacity for all wind speed scenarios and reliability cases with a small decrease for the 4 m/s wind speed scenario due to obvious reasons.

A last remark shall be made regarding the average SEC and TDS values as well as the number of RO interruptions for the three different wind speed scenarios. In contrast to the reference scenario, the average quality of the produced fresh water is slightly lower for 4 m/s and 5 m/s wind speed with TDS values around 180 ppm. This is however still a very low values. This naturally implies that the average SEC is lower for both wind speed scenarios meaning that less energy is needed in order to produce one m^3 of water. Also, as expected, the number of RO interruptions shows an upward trend when comparing the reference scenario to 4 m/s and 5 m/s wind speed. For 4 m/s wind speed, it was found that the system experiences over 500 interruptions which is about 1.4 times a day.

7.4 Comparison of current and extended FWM system design

With the current design of the FWM system, the RO unit can only be powered by wind energy. However, as already explained, an extended version is intended to be developed in which electricity from the PV array or the battery bank can assist with the production of fresh water via an electric motor. Indeed, the simulation and optimisation procedure in this thesis was performed with the extended version of the FWM system. It is expected to provide more system reliability in terms of fresh water production and decrease the dependence of the FWM system on the occurrence of high average wind speeds at the installed location. In order to verify this assumption, a comparison is made between the cost-optimal configurations of the current design as well as the extended design of the FWM system. For this, the simulation and optimisation procedure is applied to both versions as the developed model in Matlab can easily be adjusted for this purpose. The same case study of Johnny Cay is used, however, in order to be able to draw a more general conclusion the simulations are run with different average wind speeds (see section 7.3). As a reminder, the extended design of the FWM system with the electric drive (marked in red) that is placed on the same shaft as the hydraulic motor is illustrated in Figure 31. Removing

the red circle results in the current FWM design for which no electricity can be used for operating the RO system.

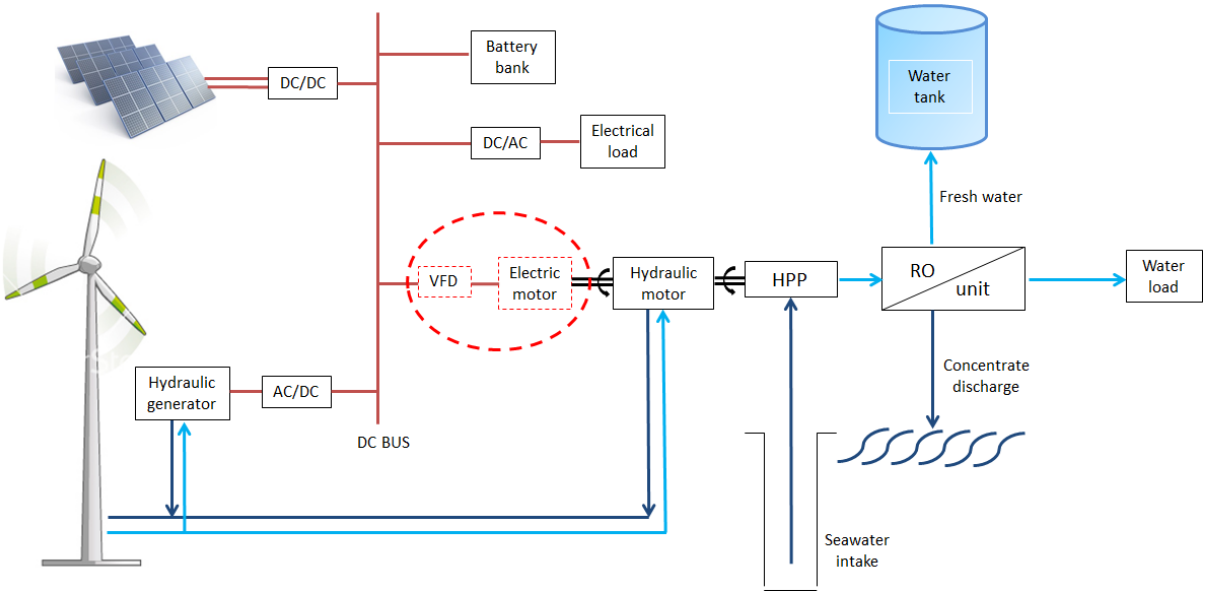

Figure 31. System configuration of the current and further improved FWM system.

The 3D stem graph in Figure 32 disclose the optimal configurations of the current and extended FWM design for 10 combinations of $LPSP_{sev}$ and $LWSP_{sev}$ values for the reference case study with an average yearly wind speed of 7 m/s. Not all optimal solutions can be calculated by the simulation and optimisation procedure due to the limited number of the GA population size. Hence, in order to perform a proper comparison between the motor and no-motor configuration, the respective points in the solution space are chosen which show a similar combination of $LPSP_{sev}$ and $LWSP_{sev}$ values. The blue spherules in the graph refer to the extended FWM system version whereas the red ones belong to the current design with no electric drive for the RO unit.

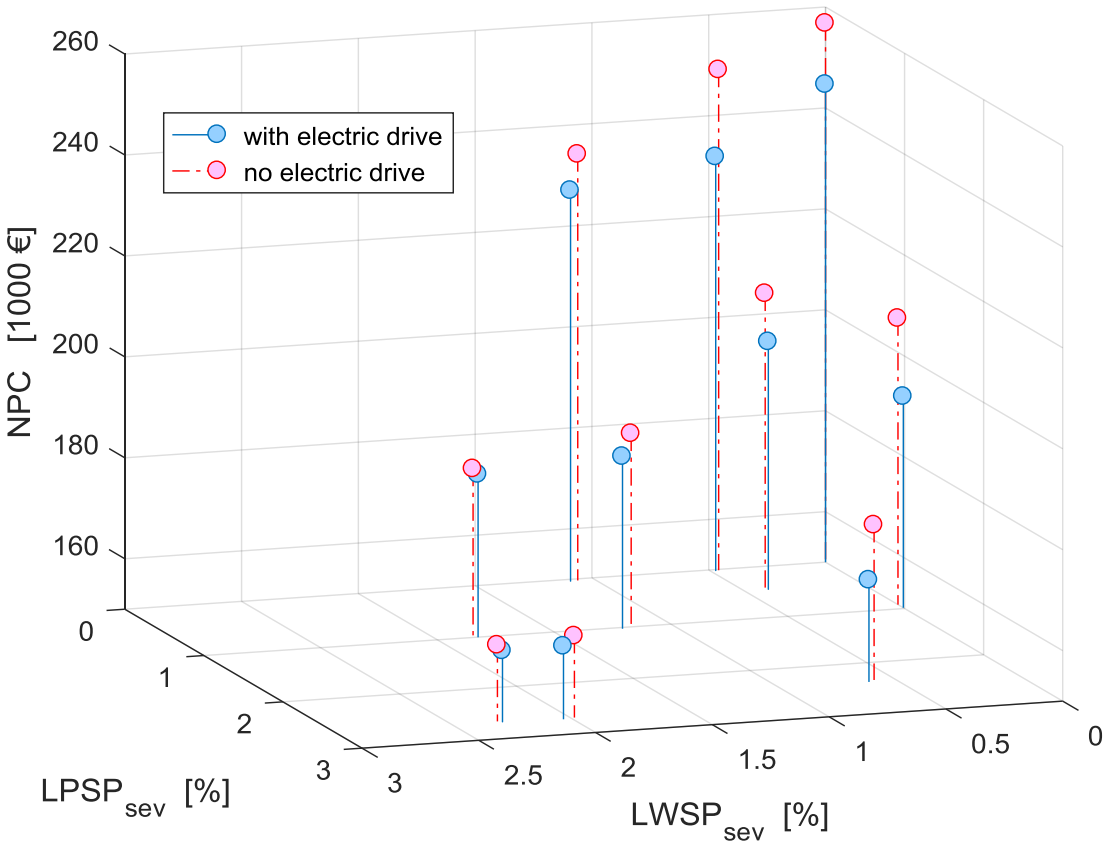

Figure 32. Comparison of optimal configurations for the current and extended FWM design for an average wind speed of 7 m/s.

The figure clearly displays that for all reliability combinations the NPC is lower for the FWM system including an electric drive. This is due to a more intelligent energy use since the RO unit can also operate during low or no wind speed periods resulting in higher overall flexibility. Also, in case the battery storage has reached its maximum SOC, the surplus electricity which is not needed for covering the electricity load can be used for water desalination. In the current FWM system design, it would simply be dumped.

It can also be observed in the graph that the cost spread is completely determined by the value of the $LWSP_{sev}$. Higher $LWSP_{sev}$ values result in a lower spread between the two FWM system versions as in these cases the wind energy seems to be sufficiently available for producing the requested fresh water load on Johnny Cay. Also, the cost spread seems to become negligible once a $LWSP_{sev}$ value of 1% is reached. On the other hand, assuming a constant water supply reliability, the difference in NPC between the two FWM system designs remains almost the same with increasing electricity supply reliabilities. This result was pretty much expected as the addition of an electric drive for the RO unit should not have a significant impact with respect to the energy use for electricity load coverage when average yearly wind speeds are as high as the ones on Johnny Cay. Hence, for the case study of Johnny Cay, it can be concluded that for a requested fresh water supply reliability of higher than 99% the additional motor is very much recommended

in order to considerably save costs. For lower $LWSP_{sev}$ values, the electric drive no longer results in significant cost gains.

Figure 33 depicts the same comparison as above, however for an average yearly wind speed of 5 m/s. Nine different solutions are represented in the 3D stem graph. Again, the optimal points which show a similar combination of $LPSP_{sev}$ and $LWSP_{sev}$ values have been chosen for reasons of comparison.

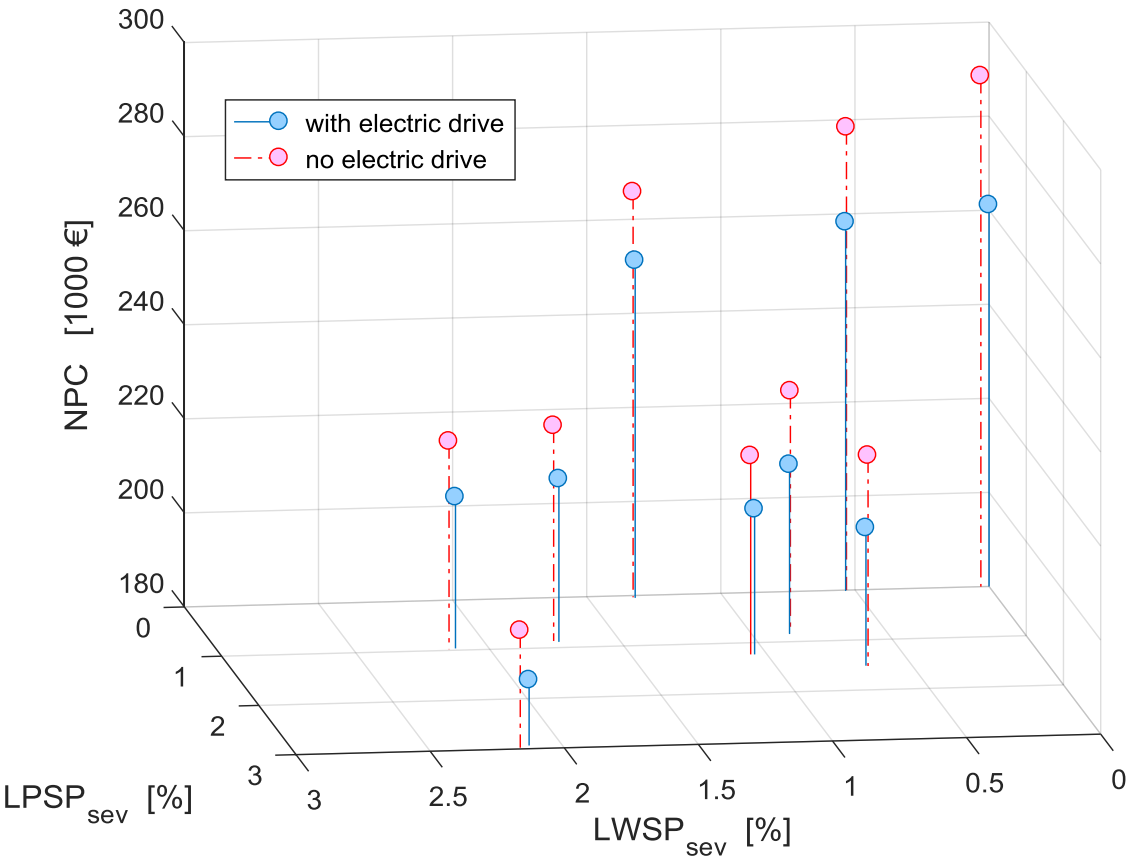

Figure 33. Comparison of optimal configurations for the current and extended FWM design for an average wind speed of 5 m/s.

The 3D stem graph shows the same relationship as in the case of the reference scenario with an average wind speed of 7 m/s. What is however clearly visible when comparing the two graphs is that the spread in NPC is much greater in the case of a wind speed of 5 m/s. As the average wind speed decreases, less wind energy is available for the production of fresh water meaning that if no electric drive is added to the system, the RO unit experiences more frequent interruptions. Consequently, a bigger RO system is needed in order to produce an increased amount of fresh water when sufficient wind energy is available which makes the FWM system more expensive. Also, it should be mentioned that with lower $LWSP_{sev}$ values the spread in NPC becomes smaller, however the difference in cost between the motor and no-motor configuration remains significant even for $LWSP_{sev}$ values as low as 2%. It can thus be concluded that for the case study of

Johnny Cay the extended version of the FWM system is highly recommendable when the average yearly wind speeds amount to about 5 m/s. This also applies for lower water supply reliability values.

The simulation for the no-motor configuration was also run for an average yearly wind speed of 4 m/s. However, no results were obtained for water supply reliabilities of 97% and higher which is the range of importance. As observed in Figure 28 - Figure 30 the electric motor is of substantially bigger capacity compared to all other wind speed meaning that the water desalination system is to a large extent driven by electricity. Since no electric drive is available in the current FWM system design, a high fresh water supply reliability cannot be assured due to insufficient wind energy. This shows that for average wind speeds of 4 m/s the addition of an electric drive is quintessential. Rather, the FWM system should not be installed in locations with these prevailing weather conditions.

7.5 Comparison of results with different reliability indices

When designing and optimising a stand-alone renewable energy system, power reliability analysis is considered an important step in any such system design. For this purpose, different methods exist. In section 3.2.1 the most commonly used reliability indices, namely the LLP and LPSP, were introduced and explained. Assuming hourly simulations for an entire year, the calculations of the LLP involve counting the number of hours in which the system load exceeds the available generating capacity and dividing it by the total number of hours in a year. The LPSP on the other hand, is the amount of electricity that the power system is not able to supply during a year divided by the total yearly electricity demand. The $LPSP_{sev}$, which has been used as reliability index for the simulation and optimisation procedure in this thesis, differs from the traditional LPSP definition in that it includes a factor that reflects the severity of the power outages based on peak and off-peak times. The LLP is a good metric when the number of outages is of importance, whereas with the LPSP statements regarding the magnitude of the outages can be made. The $LPSP_{sev}$ includes the magnitude as well as the severity. Consequently, each reliability index provides specific information regarding the power outages, but ignores other valuable insights. These reliability indices can naturally be applied to fresh water supply in the same way.

In order to understand how the choice of the reliability index impacts the results, the simulation and optimisation procedure of the FWM system is performed for all three metrics for the case study of Johnny Cay and an average yearly wind speed of 4 m/s. Figure 34 presents the 2D Pareto fronts for the $LPSP_{sev}$, LPSP and LLP index for a 100% water supply reliability. An exponential line of best fit has been created in order to display the trend of the optimal points for each metric.

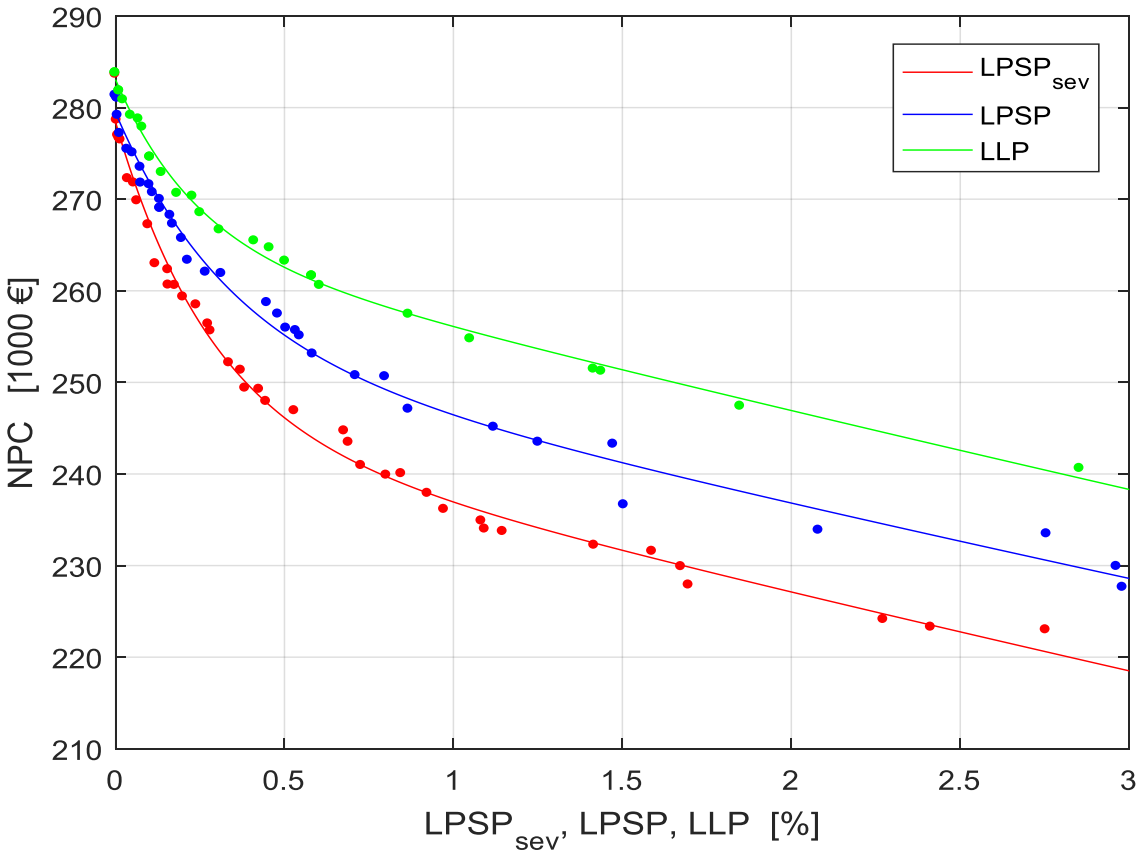

Figure 34. 2D Pareto fronts for different reliability indices and a $LWSP_{sev}$ = 0%.

The figure clearly shows that the optimal sizing results of the FWM system differ considerably based on the reliability index used for the simulation. Naturally, the difference is rather small for low electricity supply probability indices and increases for higher values. It can be observed that for all reliability values the NPC is the highest when using the LLP method, followed by the LPSP and lastly the $LPSP_{sev}$ metric. The explanation for this can be found in the magnitude and severity of the outages. If the magnitude of all FWM system outages were to be equal to the average electricity load of Johnny Cay, the results would be the same for all indices. However, since the LPSP curve is steeper compared to the LLP curve, one can conclude that the magnitude of an average outage experienced by the FWM system is lower than the average electricity demand. Furthermore, by comparing the LPSP and $LPSP_{sev}$ curve, it can also be deduced that on average, the power outages occur during off-peak times. From this it also follows that the optimal FWM systems are well-designed for the case study of Johnny Cay as the power interruptions mainly happen during off-peak times and of a magnitude lower than the average electricity demand.

In conclusion, it is important to stress that the choice of the reliability index when performing a power reliability analysis can have a great impact on the results. Consequently, the system designer should bear in mind which are the advantages and shortcomings of these indices and choose accordingly. Moreover, in order to carry out an in-depth analysis regarding the number,

magnitude and severity of the power outages and obtain extensive information on the FWM system design, a comparison of all three metrics is advisable.

7.6 Main findings and observations

Using the Pareto-based multi-objective GA method one can perform a thorough analysis of the relationship between NPC and electricity as well as fresh water supply reliabilities as numerous Pareto-optimal FWM system configurations are obtained for the decision-making process. By means of the Pareto-front, the system designer gains valuable insights into where most of the cost gains can be achieved, and thus decide on the 'best' configuration which meets the cost and/or reliability requirements of the project. The simulation and optimisation procedure has shown that for the case study of Johnny Cay, a substantial cost decrease of 25% could be achieved with lowering the electricity supply reliability to around 99% and the water supply reliability to around 99.5% compared to a 100% reliable system. For even lower reliability values, further cost gains can be obtained, which are however minor compared to the outages that would have to be accepted. If a single-objective optimisation had been performed with system reliability as a constraint, these insights would not have been visible.

The cost reduction potential is much more prominent with respect to lower electricity supply reliability values due to several reasons. Firstly, the average hourly electricity demand is about twice as high as the fresh water demand on the island, assuming an average SEC of 5.9 kWh/m^3 for running the RO plant. Secondly, storing fresh water in a tank is much more cost-efficient than storing electricity in a battery. As a consequence, the computed size of the water tank provides a water supply autonomy of about three days compared to an electricity supply autonomy of 1.5 days or lower for the battery bank. As a result, the FWM system is less prone to water supply outages.

The lower NPC for decreased system reliability values is mainly a result of a considerably smaller capacity rating of the PV system and the battery. For the optimal FWM configuration mentioned above, a nominal capacity of 28 kW for the PV system and 100 kWh for the battery bank was computed compared to 40 kW and 220 kWh, respectively, for a 100% reliable system. This amounts to a decrease in nominal size of 28% with respect to the PV system and close to 55% for the battery bank. It indicates that the 100% reliable FWM system is for most of the time oversized and does only require the additional solar and storage capacity for a small number of bad weather periods. Additionally, with reference to the great decrease in battery size of about 55%, it follows that the wind and solar resources generally complement each other well at the location under study. The rather big size of the PV system compared to the island's overall consumption can mainly be explained with the daily load distribution: most of the fresh water and electricity is consumed during the time when the PV system is in operation.

As Johnny Cay features a relatively high average yearly wind speed of 7 m/s, the sensitivity of the optimal sizing results was analysed with respect to lower wind speeds. Results indicated that the

NPC is naturally higher for average wind speeds of 5 m/s and 4 m/s compared to the reference scenario. This can mainly be attributed to a substantially bigger PV system, battery bank and for the 4 m/s scenario to the additional RO unit. Also, it was found that lowering the fresh water supply reliability did not incur any cost gains. A lower electricity supply reliability resulted in a lower NPC, however, compared to the reference scenario the gains were not as great implying that the FWM system is not as much oversized as in the case of a 100% reliable system compared to the reference scenario.

The nominal ratings of the electric motor assisting in driving the desalination plant vary substantially for different wind speeds. For the reference scenario, the electric motor size is minimal regarding all water supply reliability values. However, when compared to lower average wind speeds, the optimal ratings increase, underlining the fact that the electricity generated by the PV system is no longer mainly used for electricity demand coverage, but to a great extent also for water production. Indeed, for an average wind speed of 4 m/s and a 100% reliable FWM system, the optimal size of the electric drive amounts to about 10 kW compared to a nominal power of the HPP of 14 kW.

For all wind speed scenarios and reliability cases the optimal size of the water tank is not subject to much variability, amounting to about three days of fresh water autonomy. This result is not surprising as storing fresh water in a tank is considerably cheaper than alternatively making use of a battery bank as storage technology.

For the case study of Johnny Cay, the high SEC values of about 6 kWh/m^3 indicate that the RO plant operates in most of the cases close to its nominal power resulting in a fresh water salinity of about 170 ppm. For average wind speeds of 5 m/s and 4 m/s the SEC of the RO plant showed lower values indicating that it made better use of the variable flow strategy. However, the plant also experiences an increased number of interruptions for lower wind speeds.

When comparing the current FWM system design without electric drive for powering the RO unit with the extended design, it was found that for all reliability combinations and wind speeds the NPC is lower for the FWM system including an electric drive. This is due to a more intelligent energy use since the RO unit can also operate during low or no wind speed periods resulting in more flexibility and a higher reliability. When no electric drive is in place, a bigger RO system is needed in order to produce an increased amount of fresh water when sufficient wind energy is available which makes the FWM system more expensive. For an average wind speed of 7 m/s, the spread in NPC between the two FWM designs is only clearly visible for water supply reliabilities of 99% or higher. Afterwards, the difference becomes negligible. This downward trend is also given for a yearly average wind speed of 5 m/s, however, the difference in cost remained substantial even for low water supply reliability values. For an average yearly wind speed of 4 m/s no solutions were found by the simulation and optimisation procedure with respect to the current FWM system design. This implies that the addition of an electric drive is quintessential for the

operation of the desalination plant in case strict water supply reliability requirements are in place and in case of low average wind speed occurrence.

Finally, it should be stressed that the most commonly used power system reliability indices have their advantages and shortcomings which have to be kept in mind when performing this or similar optimisation procedures. The LLP index only refers to the number of outages that occur during a given period whereas the LPSP index refers to the magnitude of these outages. The $LPSP_{sev}$ and $LWSP_{sev}$ metric used in the framework of this thesis not only includes the magnitude of the outages but further provides information whether these occur during base, peak or off-peak times. Hence, in order to obtain valuable insights into the number, magnitude and type of the system outages, it is advisable to undertake a comparison between the different indices. Compared to the LPSP method, better results could be achieved when the severity was considered implying that on average the outages on Johnny Cay occur during off-peak times, which is preferable. Also, when comparing to the LLP index, results indicated that the average magnitude of the outages was smaller than the average yearly demand on Johnny Cay.

8

Conclusions and recommendations

The last chapter of this thesis project aims at drawing general conclusions regarding the proposed simulation and optimal sizing procedure and the results obtained for the case study of Johnny Cay. In this context, the research questions formulated in section 1.3 are answered. Finally, the main shortcomings of the model as well as the optimal sizing approach are highlighted and recommendations for further research are given.

8.1 Conclusions

In the framework of this thesis project, a procedure has been developed for optimally sizing the FWM system: a stand-alone microgrid including a hydraulic wind turbine, a PV system, various storage technologies and a water desalination plant that provides isolated communities with both electricity and fresh water. This optimal sizing procedure can be applied to any location in the world provided that its solar irradiation, wind speed, temperature, electricity and fresh water load profiles are available for performing yearly simulations by means of the FWM computer model. As financial resources are the main limiting factor for the adoption of renewable energies, the procedure simultaneously optimises the conflictive objectives, cost and system reliability, aiming at finding a trade-off between them and thus reducing its overall cost. Oversizing the system components will enhance the system cost while undersizing leads to failure of power supply. In traditional sizing approaches the system costs are minimised while important design parameters such as the reliability are implemented in the form of a constraint for which the value has to be decided beforehand by the designer. Further, the computed output is one single best system configuration along with the respective component sizes. The sizing procedure employed in this thesis, however, is found to be more comprehensive as it computes numerous Pareto-optimal FWM system configurations for a specific location and displays the relationship between cost and

reliability on a Pareto-front. Consequently, the system designer is provided with valuable and rich information for the decision-taking process and can choose and compare multiple suitable FWM system configurations from a set of alternatives based on the insights gained from the analysis. This trade-off approach is especially interesting for FWM system installations in developing countries in which the reliability requirements are rather loose which allows for more freedom in finding an optimal compromise between cost and reliability.

The optimal sizing procedure has been applied to the remote Colombian island of Johnny Cay in the Caribbean Sea with an average wind speed of 7 m/s. Results showed that the more outages are tolerated by the consumer, the greater the FWM system is undersized and hence cheaper. Indeed, there is a substantial cost decrease of 26% between sizing a system that provides 99% and 100% of the island's fresh water and electricity needs. In this case, considerably smaller PV system (28 kW vs. 40 kW) and battery bank (100 kWh vs. 220 kWh) capacities were computed compared to a 100% reliable system indicating that the latter is for most of the time oversized and only requires the additional solar and storage capacity for a small number of bad weather periods. A further reduction of the system reliability is not advisable as the implied cost gains are minor compared to the electricity and fresh water supply outages that would have to be accepted. The sensitivity analysis performed for the case study of Johnny Cay demonstrated that a cost cut as high as 26% in case of a system reliability of 99% is only possible if high average wind speeds occur. For wind speeds of 4 m/s and 5 m/s the cost decrease merely amounted to about 17%. The reason for this is mainly found in the higher portion of PV energy throughout the year due to lower wind speeds and hence the need of a bigger battery system in order to store the increased electricity produced during the day. Also, for an average yearly wind speed of 4 m/s an additional RO unit is required in order to be able to cover the fresh water needs of the island. The optimal volume of the water tank is for all Pareto-optimal solutions and wind speed scenarios not subject to much variability amounting to about three days of fresh water autonomy on the island. Storing fresh water in a tank is considerably cheaper than alternatively making use of a battery bank as storage technology and hence the simulation and optimisation procedure tends to compute an optimal water tank size which is close to its upper limit.

As with the current design of the FWM system the desalination plant can only be powered by the hydraulic wind turbine, a comparison was made between the current and extended design in which fresh water can also be produced by the PV system via an electric drive. The simulation and optimisation procedure for the case study of Johnny Cay has highlighted that the addition of the electric drive is mainly economically beneficial if water supply reliabilities close to 100% are required. Also, in case of lower average wind speeds, i.e. 4 m/s and 5 m/s, the electric motor becomes an overall quintessential component of the FWM system as otherwise cost shoot up and/or the water supply reliabilities are too low. The electric drive provides more system reliability in terms of fresh water production and decreases the dependence of the FWM system on the occurrence of high average wind speeds at the installed location.

Finally, various metrics exist for assessing the reliability of a power system where all display different information such as the yearly number, yearly magnitude and/or severity (peak/off-peak) of the outages occurred. The optimal sizing results can differ considerably depending on the employed reliability index. It is thus important for the system designer to be aware of these differences when performing this or similar optimisation procedures and accordingly choose a suitable reliability index based on the information most valuable to him. Nevertheless, as all reliability indices have their shortcomings it is advisable to perform the optimal sizing procedure with multiple indices and to compare the obtained results in order to gain overarching information regarding the number, magnitude and type of the yearly system outages.

8.2 Limitations and further research

- **Include component outages and maintenance activities:** In the framework of this thesis, system reliability only refers to outages incurred by insufficient power supply from the fluctuating renewable energy sources and the storage systems. Power systems, however, periodically experience outages due to failures of its individual components. These break-downs can become highly problematic, especially for stand-alone systems located in remote areas. Hence, it is a recommended next step to also include these types of outages in addition to considering the times when components are not in operation due to regular maintenance activities.
- **Scale-dependent cost of components:** The optimisation involves the calculation of the NPC for which average prices per unit are used for each component of the FWM system. However, the computed ratings of the FWM system components can vary substantially depending on the demand and climatic conditions as well as specific requirements of a location. It would thus be advisable to include scale-dependent cost in the simulation and optimisation procedure.
- **Integrate measured power curve of hydraulic wind turbine:** The computed output power of the wind turbine model is based on and derived from the original power curve of the Lagerwey 18/80 with the conventional electromechanical transmission system. Measurements of the new power curve with a hydraulic transmission system are currently being performed. Once this power curve is available, it should be included in the model in order to make the calculations and yearly simulations of the wind turbine more precise and thus the overall FWM system model more representative.
- **Model and operation control improvement:** The developed model includes all main components of the FWM system on which basis the power flows are computed. However, some smaller devices such as the pump for transporting the seawater to the RO unit are neglected and thus also their power requirements. Additionally, for each stop of the RO unit, the membranes should be flushed in order to avoid fouling, a process which demands for power as well as fresh water. Further, the model of the PV system does not differentiate

between direct and diffuse radiation, a distinction that becomes more important for sites located further away from the equator. Also, the dependence of the battery's efficiency and capacity on the battery SOC, the charging rate, its general history and the temperature are omitted and thus the SOC is assumed to increase and decrease linearly over time. Integrating the above mentioned components into the model, improving the level of detail of certain sub-systems and considering the respective power and fresh water requirements in the operation control would be an important next step in order to increase the reliability of the optimal sizing procedure.

- **Include energy recovery device:** The model of the RO desalination plant used for the optimal sizing procedure does not employ an energy recovery device resulting in an average SEC of 6 kWh/m^3. Energy recovery devices make use of the energy contained in the reject water exiting the RO modules at high pressures which are only slightly below those of the feed water. This pressure energy, amounting to about two thirds of the total hydraulic power originally supplied by the HPP, can be recovered and returned to the shaft of the main pump leading to an increased overall efficiency. Large-scale SWRO plants always contain energy recovery devices that have lowered the SEC to a value as low as 2.64 kW/m^3 [96]. It would thus be an important future step to add to the FWM system model the option of using such a device in order to be able to determine if the additional capital cost are worth the investment.
- **Include ROSA calculations in the model:** In order to obtain the permeate versus power input curve of the desalination plant, several simulations were run with the software ROSA. The obtained data was then included into the FWM system model in the form of a look-up table. This curve is however specific to the location under study and the RO design meaning that parameters such as the salinity level and temperature of the feed water, number and type of RO membranes or recovery factor impact the quantity and quality of fresh water production. Hence, the simulation and optimisation procedure can be applied without adaptions to locations with similar climatic conditions as the ones found in the Caribbean Sea. However, in case the climatic conditions vary substantially and/or different RO pressure vessel designs are preferred, new simulations need to be run with ROSA and the derived look-up table must then be loaded into the FWM system model in Matlab. The optimal sizing approach can potentially become more versatile and applicable if the calculations in ROSA were to be integrated into the Matlab model. This is however expected to be highly cumbersome and time-consuming.
- **Smaller time steps and simulations of several years:** The simulation and optimal sizing procedure is based on hourly time steps which neglects to a certain extent the high variability of the power production by renewable energies. Performing simulations with smaller time steps would provide more certainty on the feasibility of the computed FWM systems in reality and thus take account of the intermittent character of wind and solar resources. In addition, the calculation of a power system's reliability is typically based on simulations performed over a number of years in which yearly fluctuations with respect to demand and climatic conditions

are considered. Hence, in order to provide a more complete picture and obtain highly reliable results, the collection and usage of extensive climate and load data is recommended.

Appendix

Optimal sizing for different wind speeds

Table 14. Optimal FWM system configurations for different wind speeds with $LPSP_{sev}$ = $LWSP_{sev}$ = 0%.

	Reference	6 m/s	5 m/s	4 m/s
Costs [€]	244 626	250 558	261 100	283 642
PV [kW]	38.9	44.4	47.2	58.2
Battery [kWh]	218.4	212.2	230.9	193.4
RO unit [-]	1	1	1	2
Water tank [m^3]	47	43	40	54
Electric motor [kW]	1.5	1.5	3	9.7
Generator [kW]	8.1	8	8	5.8
Electricity dumping [% of total production]	39	40	33	31
Water dumping [% of total production]	20	14	16	31
Average TDS [ppm]	169	174	182	181
Average SEC [kWh/m^3]	5.9	5.8	5.7	5.7
°N of RO interruptions [-]	359	390	440	498

Table 15. Optimal FWM system configurations for different wind speeds with $LPSP_{sev}$ = 0% and $LWSP_{sev}$ = 1%.

	Reference	6 m/s	5 m/s	4 m/s
Costs [€]	227 352	249 586	258 210	276 770
PV [kW]	41.6	41.6	47.2	58.2
Battery [kWh]	162.2	224.6	224.6	181
RO unit [-]	1	1	1	2
Water tank [m^3]	35	40	39	49

Electric motor [kW]	1.4	1	1.7	4.8
Generator [kW]	7.7	8	7.9	6
Electricity dumping [% of total production]	41	38	34	36
Water dumping [% of total production]	20	13	14	24
Average TDS [ppm]	171	179	191	200
Average SEC [kWh/m³]	5.9	5.8	5.6	5.5
°N of RO interruptions [-]	398	399	441	508

Table 16. Optimal FWM system configurations for different wind speeds with $LPSP_{sev}$ = 1% and $LWSP_{sev}$ = 0%.

	Reference	6 m/s	5 m/s	4 m/s
Costs [€]	190 860	206 315	217 183	236 130
PV [kW]	38	38.9	42.1	50
Battery [kWh]	68.6	112.3	124.8	99.8
RO unit [-]	1	1	1	2
Water tank [m³]	42	38	38	41
Electric motor [kW]	1.3	1.2	4.1	8.6
Generator [kW]	7.5	6.7	8.5	6.9
Electricity dumping [% of total production]	36	32	31	27
Water dumping [% of total production]	20	17	13	27
Average TDS [ppm]	172	189	175	183
Average SEC [kWh/m³]	5.8	5.6	5.8	5.6

°N of RO interruptions [-]	396	379	450	543

Table 17. Optimal FWM system configurations for different wind speeds with $LPSP_{sev}$ = $LWSP_{sev}$ = 1%.

	Reference	6 m/s	5 m/s	4 m/s
Costs [€]	182 447	194 210	214 139	235 061
PV [kW]	28.3	33.6	42.3	48.5
Battery [kWh]	87.4	99.8	118.6	106.1
RO unit [-]	1	1	1	2
Water tank [m^3]	44	40	37	42
Electric motor [kW]	0.9	1.1	2.2	6.3
Generator [kW]	7.5	7.5	7.6	6.3
Electricity dumping [% of total production]	29	29	30	26
Water dumping [% of total production]	18	14	11	24
Average TDS [ppm]	164	181	184	192
Average SEC [kWh/m^3]	6	5.8	5.7	5.6
°N of RO interruptions [-]	456	389	450	540

Bibliography

[1] Al Fry, “Facts and Trends: Water,” *World Bus. Counc. Sustain. Dev.*, p. 16, 2006.

[2] EU, “ADIRA Handbook. A guide to autonomous desalination system concepts,” *Euro-Mediterranean Reg. Program. Water Manag.*, 2008.

[3] G. Bergkamp and C. W. Sadoff, “Water in a Sustainable Economy,” *State World 2008 Innov. a Sustain. Econ.*, pp. 107–122, 2008.

[4] N. Ghaffour, T. M. Missimer, and G. L. Amy, “Technical review and evaluation of the economics of water desalination: Current and future challenges for better water supply sustainability,” *Desalination*, vol. 309, pp. 197–207, 2013.

[5] E. Koutroulis and D. Kolokotsa, “Design optimization of desalination systems power-supplied by PV and W/G energy sources,” *Desalination*, vol. 258, no. 1–3, pp. 171–181, 2010.

[6] M. Isaka, “Water Desalination Using Renewable Energy - Technology Brief,” *IRENA - IEA - Etsap*, no. March, p. 24, 2012.

[7] A. Subramani, M. Badruzzaman, and J. Oppenheimer, “Energy minimization strategies and renewable energy utilization for desalination : A review,” *Water Res.*, vol. 45, no. 5, pp. 1907–1920, 2011.

[8] C. Koroneos, A. Dompros, and G. Roumbas, “Renewable energy driven desalination systems modelling,” *J. Clean. Prod.*, vol. 15, no. 5, pp. 449–464, 2007.

[9] A. D. Bagul, Z. M. Salameh, and B. Borowy, “Sizing procedure a stand-alone hybrid wind-photovoltaic system using a three-event probability density approximation,” *Sol. Energy*, vol. 56, no. 4, pp. 323–335, 1996.

[10] D. P. Clarke, Y. M. Al-abdeli, and G. Kothapalli, “Multi-objective optimisation of renewable hybrid energy systems with desalination,” *Energy*, vol. 88, pp. 457–468, 2015.

[11] Dutch Water Sector, “Solteq to build wind-RO desalination plant on Johnny Cay island, Colombia,” 2014. [Online]. Available: http://www.dutchwatersector.com/news-events/news/12204-solteq-to-build-wind-ro-desalination-plant-on-johnny-cay-island-colombia.html. [Accessed: 23-Mar-2017].

[12] R. D. Daniel Schnitzer, Deepa Shinde Lounsbury, Juan Pablo Carvallo and and D. M. K. Jay Apt, “Microgrids for Rural Electrification : A critical review of best practices based on seven case studies,” 2014.

[13] R. Kempener, O. Lavagne, D. Saygin, J. Skeer, S. Vinci, and D. Gielen, “Off-Grid Renewable Energy Systems: Status and Methodological Issues,” p. 29, 2015.

[14] B. Bhandari, K.-T. Lee, Y.-M. Cho, and S.-H. Ahn, “Optimization of Hybrid Renewable Energy Power system: A review,” *Int. J. Precis. enginnering Manuf. Technol.*, vol. 2, no. 1, pp. 99–112, 2015.

[15] W. Zhou, C. Lou, Z. Li, L. Lu, and H. Yang, “Current status of research on optimum sizing of stand-alone hybrid solar – wind power generation systems,” *Appl. Energy*, vol. 87, no. 2, pp. 380–389, 2010.

[16] A. Chauhan and R. P. Saini, “A review on Integrated Renewable Energy System based power generation for stand-alone applications: Configurations, storage options, sizing methodologies and control,” *Renew. Sustain. Energy Rev.*, vol. 38, pp. 99–120, 2014.

[17] Incell Academy, “Comparison Battery Technologies for Telecom,” Kista, Sweden.

[18] United Nations, “United Nations World Water Development Report 2016: Water and Jobs,” Paris, France, 2016.

[19] International Desalination Association, “Desalination by Numbers,” 2017. [Online]. Available: http://idadesal.org/desalination-101/desalination-by-the-numbers/. [Accessed: 30-Mar-2017].

[20] H. G. Gorchev and G. Ozolins, “WHO guidelines for drinking-water quality,” *WHO Chron.*, vol. 38, no. 3, pp. 104–108, 2011.

[21] N. Kayaalp, I. Koyuncu, and D. Akgul, “Cost analysis of seawater desalination with reverse osmosis in Turkey,” vol. 220, pp. 123–131, 2008.

[22] M. Eltawil, Z. Zhengming, and L. Yuan, “Renewable energy powered desalination systems: Technologies and economics-state of the art,” *12th Int. Water Technol. Conf.*, pp. 1–38, 2008.

[23] A. Al-Karaghouli and L. L. Kazmerski, “Energy consumption and water production cost of conventional and renewable-energy-powered desalination processes,” *Renew. Sustain. Energy Rev.*, vol. 24, pp. 6–11, 2008.

[24] M. A. Eltawil, Z. Zhengming, and L. Yuan, “A review of renewable energy technologies integrated with desalination systems,” vol. 13, pp. 2245–2262, 2009.

[25] A. Murray Thomson, “Reverse-Osmosis Desalination of Seawater Powered by Photovoltaics Without Batteries,” Loughborough University.

[26] D. E. A. Zaid, “Economic analysis of a stand-alone reverse osmosis desalination unit powered by photovoltaic for possible application in the northwest coast of Egypt,” *Desalin. Water Treat.*, vol. 54, no. 12, pp. 3211–3217, 2015.

[27] M. S. Miranda and D. Infield, “A wind-powered seawater reverse-osmosis system without batteries,” *Desalination*, vol. 153, 2002.

[28] A. A. Mbarga, L. Song, and W. R. Williams, “Integration of Renewable Energy Technologies With Desalination,” pp. 11–18, 2014.

[29] W. Arras, N. Ghaffour, and A. Hamou, “Performance evaluation of BWRO desalination plant - A case study,” *Desalination*, vol. 235, no. 1–3, pp. 170–178, 2009.

[30] I. C. Karagiannis and P. G. Soldatos, “Water desalination cost literature : review and assessment,” vol. 223, pp. 448–456, 2008.

[31] J. Salazar, F. Tadeo, and C. Prada, “Renewable Energy for Desalinization using Reverse Osmosis,” pp. 5–10, 2010.

[32] Dow Water and Process Solutions, “FILMTEC Reverse Osmosis Membranes - Technical Manual.”

[33] B. V. Lenntech, “RO pressure vessel,” 2017. [Online]. Available: http://www.lenntech.com/processes/desalination/reverse-osmosis/general/reverse-osmosis-desalination-process.htm. [Accessed: 17-Apr-2017].

[34] CONWED - Global Netting Solutions, “Spiral wound membrane elements,” 2017. [Online]. Available: http://www.conwedplastics.com/en/markets/reverse-osmosis/. [Accessed: 16-Apr-2017].

[35] J. MCDONALD, D. CHRISTOPHERSEN, and C. HOWELL, “Reduce membrane fouling with good CIP procedures,” *Ultrapure water*, vol. 21, no. March, pp. 1–3, 2004.

[36] A. Technology, “Repowering Solutions Lagerway 80kW,” 1983.

[37] wind-turbine.com, “Lagerwey turbines on sold,” 2017. [Online]. Available: https://wind-turbine.com/windkraftanlagen/hersteller/lagerwey. [Accessed: 03-Aug-2017].

[38] Management Association Information Resources, *Artificial Intelligence: Concepts, Methodologies, Tools, and Applications*. IGI Global, 2016.

[39] S. Bandyopadhyay and S. Saha, *Unsupervised classification: Similarity measures, classical and metaheuristic approaches, and applications*. Springer Berlin Heidelberg, 2013.

[40] R. K. Arora, *Optimization Algorithms and Applications*. Chapman and Hall/CRC 2015, 2015.

[41] A. Badar, B. S. Umre, and A. S. Junghare, “Study of Artificial Intelligence Optimization Techniques applied to Active Power Loss Minimization,” *IOSR J. Electr. Electron. Eng.*, vol. 2014, no. 1989, pp. 39–45, 2014.

[42] M. Fadaee and M. A. M. Radzi, “Multi-objective optimization of a stand-alone hybrid renewable energy system by using evolutionary algorithms : A review,” *Renew. Sustain. Energy Rev.*, vol. 16, no. 5, pp. 3364–3369, 2012.

[43] R. Baños, F. Manzano-Agugliaro, F. G. Montoya, C. Gil, A. Alcayde, and J. G??mez, “Optimization methods applied to renewable and sustainable energy: A review,” *Renew. Sustain. Energy Rev.*, vol. 15, no. 4, pp. 1753–1766, 2011.

[44] GIZ, “Analysis of System Stability in Developing and Emerging Countries Table of Contents,” Berlin, Germany, 2013.

[45] S. Diaf, M. Belhamel, M. Haddadi, and A. Louche, “Technical and economic assessment of hybrid photovoltaic / wind system with battery storage in Corsica island,” vol. 36, pp. 743–754, 2008.

[46] H. Yang, W. Zhou, L. Lu, and Z. Fang, “Optimal sizing method for stand-alone hybrid solar – wind system with LPSP technology by using genetic algorithm,” vol. 82, pp. 354–367, 2008.

[47] S. Diaf, G. Notton, M. Belhamel, M. Haddadi, and A. Louche, “Design and techno-economical optimization for hybrid PV / wind system under various meteorological conditions,” vol. 85, pp. 968–987, 2008.

[48] R. Belfkira, L. Zhang, and G. Barakat, “Optimal sizing study of hybrid wind/PV/diesel power generation unit,” *Sol. Energy*, vol. 85, no. 2011, pp. 100–110, 2010.

[49] J. L. Bernal-Agustín and R. Dufo-López, “Efficient design of hybrid renewable energy systems using evolutionary algorithms,” *Energy Convers. Manag.*, vol. 50, no. 3, pp. 479–489, 2009.

[50] Y. Hongxing, Z. Wei, and L. Chengzhi, “Optimal design and techno-economic analysis of a hybrid solar – wind power generation system,” vol. 86, pp. 163–169, 2009.

[51] Daming Xu, Longyun Kang, Liuchen Chang, and Binggang Cao, “Optimal sizing of standalone hybrid wind/pv power systems using genetic algorithms,” *Can. Conf. Electr. Comput. Eng. 2005.*, no. May, pp. 1722–1725, 2005.

[52] E. Koutroulis and D. Kolokotsa, “Methodology for optimal sizing of stand-alone photovoltaic / wind-generator systems using genetic algorithms,” vol. 80, pp. 1072–1088, 2006.

[53] A. Navaeefard, O. Babaee, and H. Radmanesh, “Optimal Sizing of Hybrid Systems and Economical Comparison,” *Int. J. Sustain. Energy Environ. Res.*, vol. 6, no. 1, pp. 1–8, 2017.

[54] A. Kashefi Kaviani, G. H. Riahy, and S. M. Kouhsari, “Optimal design of a reliable hydrogen-based stand-alone wind/PV generating system, considering component outages,” *Renew. Energy*, vol. 34, no. 11, pp. 2380–2390, 2009.

[55] A. Rabhi, J. Bosch, and A. Elhajjaji, “Energy Management for an Autonomous Renewable Energy System,” *Energy Procedia*, vol. 83, pp. 299–309, 2015.

[56] D. Tsuanyo, Y. Azoumah, D. Aussel, and P. Neveu, “Modeling and optimization of batteryless hybrid PV (photovoltaic)/ Diesel systems for off-grid applications,” *Energy*, vol. 86, pp. 152–163, 2015.

[57] J. Razak, K. Sopian, Y. Ali, and M. Alghoul, “Optimization of PV-wind-hydro-diesel hybrid system by minimizing excess capacity,” *Eur. J. Sci. Res.*, vol. 25, no. 4, pp. 663–671, 2009.

[58] B. Ould Bilal, V. Sambou, P. A. Ndiaye, C. M. F. Kébé, and M. Ndongo, “Multi-objective design of PV-wind-batteries hybrid systems by minimizing the annualized cost system and the loss of power supply probability (LPSP),” *Proc. IEEE Int. Conf. Ind. Technol.*, pp. 861–868, 2013.

[59] B. O. Bilal, V. Sambou, C. M. F. Kébé, P. A. Ndiaye, and M. Ndongo, “Methodology to size an optimal stand-alone PV/wind/diesel/battery system minimizing the levelized cost of energy and the CO 2 emissions,” in *Energy Procedia*, 2012, vol. 14, no. 2011, pp. 1636–1647.

[60] B. Ould Bilal, V. Sambou, P. A. Ndiaye, C. M. F. Kébé, and M. Ndongo, “Optimal design of a hybrid solar-wind-battery system using the minimization of the annualized cost system and the minimization of the loss of power supply probability (LPSP),” *Renew. Energy*, vol. 35, no. 10, pp. 2388–2390, 2010.

[61] J. L. Bernal-Agustín, R. Dufo-Lopéz, and D. M. Rivas-Ascaso, “Design of isolated hybrid systems minimizing costs and pollutant emissions,” *Renew. Energy*, vol. 31, pp. 2227–2244, 2005.

[62] R. Dufo-López and J. L. Bernal-Agustín, “Multi-objective design of PV-wind-diesel-hydrogen-battery systems,” *Renew. Energy*, vol. 33, no. 12, pp. 2559–2572, 2008.

[63] D. Abbes, A. Martinez, and G. Champenois, “Life cycle cost, embodied energy and loss of power supply probability for the optimal design of hybrid power systems,” *Math. Comput. Simul.*, vol. 98, pp. 46–62, 2014.

[64] M. Sharafi and T. Y. ELMekkawy, “Multi-objective optimal design of hybrid renewable energy systems using PSO-simulation based approach,” *Renew. Energy*, vol. 68, pp. 67–79, 2014.

[65] E. S. Mohamed and G. Papadakis, “Design , simulation and economic analysis of a stand-alone reverse osmosis desalination unit powered by wind turbines and photovoltaics,” vol. 164, pp. 87–97, 2004.

[66] D. Manolakos, G. Papadakis, D. Papantonis, and S. Kyritsis, “A simulation-optimisation programme for designing hybrid energy systems for supplying electricity and fresh water through desalination to remote areas case study: The Merssini village, Donoussa island, Aegean Sea, Greece,” *Energy*, vol. 26, no. 7, pp. 679–704, 2001.

[67] T. Ben M’Barek, K. Bourouni, and K. B. Ben Mohamed, “Optimization coupling RO desalination unit to renewable energy by genetic algorithms,” *Desalin. Water Treat.*, vol. 51, no. 7–9, pp. 1416–1428, 2013.

[68] K. Bourouni, T. B. M. Barek, and A. Al Taee, “Design and optimization of desalination reverse osmosis plants driven by renewable energies using genetic algorithms,” *Renew. Energy*, vol. 36, no. 3, pp. 936–950, 2011.

[69] A. M. Gilau and M. J. Small, “Designing cost-effective seawater reverse osmosis system under optimal energy options,” *Renew. Energy*, vol. 33, no. 4, pp. 617–630, 2008.

[70] P. M. Olabarria Gonzalez, *Constructive Engineering of Large Reverse Osmosis Desalination Plants*. Chemical Publishing Company, 2015.

[71] Hydranautics, “Design and Engineering Information,” 2001.

[72] P. Feron, “Use of Windpower in Autonomous Reverse Osmosis Seawater Desalination,” *Wind Eng.*, vol. 9, no. 3, pp. 180–199, 1985.

[73] C. Bartels, M. Hirose, S. Rybar, and R. Franks, “Optimum RO system design with high area spiral-wound elements,” *Desalin. Water Treat.*, vol. 10, pp. 21–26, 2009.

[74] Arizona State University, “SOLAR PV STAND-ALONE SYSTEMS Good Practice Guide: Small System Sizing,” Arizona.

[75] Victron Energy, “Which solar charge controller: PWM or MPPT?,” Almere, White paper, 2014.

[76] A. Lasserre-bigorry, “Vertical profiles of wind , temperature and turbulence,” 1997.

[77] I. Troen and E. Lundtang Petersen, *European Wind Atlas*, Communitie. Kopenhagen: National LaboratoryTUD - Technical University of Denmark, Roskilde: Risø, 1989.

[78] U.S. Department of Energy, “Variable Speed Pumping - A Guide to Successful Applications,” Washington, D.C., 2004.

[79] “Interview with Herre Rost van Tonningen,” 2017.

[80] R. Chenni, E. Matagne, and M. Khennane, “Study of Solar Radiation in View of Photovoltaic Systems Optimization,” vol. 2011, no. November, pp. 367–374, 2011.

[81] Power Sonic, “Power Sonic - Lead-acid battery PS-122500 data sheet.” Power Sonic.

[82] Solar-facts, “Charging and discharging lead-acid batteries.” [Online]. Available: http://www.solar-facts.com/batteries/battery-charging.php. [Accessed: 14-Aug-2017].

[83] H. R. Baghaee, “Three dimensional Pareto Optimal solution to design a hybrid stand-alone wind / PV generation system with hydrogen energy ... Three dimensional Pareto Optimal Solution to Design a Hybrid Stand-alone Wind / PV generation System with Hydrogen Energy Storage using Multi-Objective Particle Swarm Optimization,” no. December 2016, 2012.

[84] O. Abdoun, J. Abouchabaka, and C. Tajani, “Analyzing the Performance of Mutation Operators to Solve the Travelling Salesman Problem,” 2012.

[85] Matlab Mathworks, “Multiobjective Genetic Algorithm Options,” 2017. [Online]. Available: https://nl.mathworks.com/help/gads/examples/multiobjective-genetic-algorithm-options.html. [Accessed: 17-Jul-2017].

[86] K. Jaffres-Runser, J.-M. Gorce, and S. Ubeda, “Mono- and Multiobjective Formulations for theIndoor Wireless LAN Planning Problem,” New-Jersey, United States, 2007.

[87] Google, “Johnny Cay,” *Google Maps*. [Online]. Available: https://www.google.nl/maps/place/Islote+Sucre/@12.6,-81.6919107,17z/data=!3m1!4b1!4m5!3m4!1s0x8f05a8a73fe92bf5:0xa0a7a7001be99f03!8m2!3d12.6!4d-81.689722. [Accessed: 08-Jul-2017].

[88] Coralina, “PLAN DE MANEJO PARQUE NATURAL REGIONAL,” San Andrés, 2014.

[89] EEDAS, “PROYECTO IMPLEMENTACIÓN DE ALTERNATIVAS TÉCNOLOGICAS PARA LA AUTOGENERACIÓN DE ENERGIA ELECTRICA Y PRODUCCIÓN DE AGUA POTABLE EN EL PARQUE REGIONAL JOHNNY CAY, ARCHIPIELAGO DE SAN ANDRÉS, PROVIDENCIA Y SANTA CATALINA,” San José, Costa Rica, 2011.

[90] Meteotest, “Meteonorm.” Bern, Switzerland, 2017.

[91] index mundi, “Colombia Central bank discount rate,” *2017*, 2017. [Online]. Available: http://www.indexmundi.com/colombia/central_bank_discount_rate.html. [Accessed: 31-Aug-2017].

[92] R. Fu *et al.*, “U . S . Solar Photovoltaic System Cost Benchmark : Q1 2016,” 2016.

[93] SUNPOWER, “SUNPOWER E18/230 SOLAR PANEL data sheet.” San Josè, California, USA.

[94] Voltronic Power, “MPPT Solar Charge Controller - SCC-MPPT 3KW data sheet.” .

[95] The DOW Chemical Company, “ROSA - Reverse Osmosis System Analysis 9.1.” Dow Water & Process Solutions, 2016.

[96] E. Sh, G. Papadakis, E. Mathioulakis, and V. Belessiotis, “An experimental comparative study of the technical and economic performance of a small reverse osmosis desalination system equipped with an hydraulic energy recovery unit,” vol. 194, pp. 239–250, 2006.